Analysis and Modeling of Some Traffic Characteristics using Lattice Hydrodynamic Approach

A Thesis
submitted in partial fulfillment of the requirements
for the award of the degree
of

Doctor of Philosophy

in

Mathematics

by

Ramanpreet Kaur
(Registration No.: 901511006)

under the supervision of

Dr. Sapna Sharma
Associate Professor

School of Mathematics
Thapar Institute of Engineering and Technology
(Deemed to be University)
Patiala-147004 (Punjab), India

May 2019

DEDICATED

TO

THE ALMIGHTY

AND

MY PARENTS

Certificate

I hereby declare that the work which is being presented in the thesis entitled **Analysis and Modeling of Some Traffic Characteristics using Lattice Hydrodynamic Approach**, in partial fulfillment of the requirements for the award of the degree of **Doctor of Philosophy** and submitted to the institution is an authentic record of my own work carried out during the period **July 2015** to **May 2019** under the supervision of **Dr. Sapna Sharma**, Associate Professor, School of Mathematics, Thapar Institute of Engineering and Technology, Patiala.

Date: 20 May 2019

Ramanpreet Kaur.
(**Ramanpreet Kaur**)
Candidate

It is certified that the above statement made by the candidate is correct to the best of my knowledge.

Date: 20 May 2019

Dr. Sapna Sharma
Supervisor

Acknowledgements

This thesis would not have been possible without the inspiration, support and guidance of a number of wonderful individuals. I take this opportunity to express my sincere gratitude to all of them for being part of this journey and making this task possible.

First and foremost, I am extremely grateful to my supervisor **Dr. Sapna Sharma**, Associate Professor, School of Mathematics, Thapar Institute of Engineering and Technology, Patiala for her valuable guidance, consistent encouragement, understanding, and patience throughout my research work. I am thankful to **Dr. Arvind Kumar Gupta**, Associate Professor and Head, Department of Mathematics, Indian Institute of Technology, Ropar for his unconditional support during my research work. He has made himself available to clarify my doubts despite his busy schedules and I consider it as a great opportunity to work under his guidance as well and to learn from his positive disposition and research expertise.

I take this opportunity to express my deep sense of gratitude and respectful regards to Dr. Satish Kumar Sharma, Associate Professor and Head, School of Mathematics and Dr. Arvind Kumar Lal, Professor and Former Head, School of Mathematics for their continuous motivation and inspiration. I am thankful to all the members of doctoral committee Dr. Harish Garg (Assistant Professor, School of Mathematics), Dr. Parimita Roy (Assistant Professor, School of Mathematics) and Dr. Richa Babbar (Associate Professor, Civil Engineering Department) for their valuable comments and suggestions. I am highly thankful to all other faculty members of the School of Mathematics and non-teaching staff members for providing me guidance and necessary facilities for carrying out my research work.

I also extend my sincere thanks to Dr. Prakash Gopalan, Director, Thapar Institute of Engineering and Technology, Patiala, for providing me the necessary infrastructure and resources to accomplish my research work. I am thankful to Dr. Rafat Siddique, Dean of Research and Sponsored Projects, for providing me assistance required to complete my research work.

I would like to express my limitless thanks to my parents for their continuous and unparalleled love, motivation, support, faith and giving me the liberty to choose what I desired. I salute them for all the selfless love, care, pain and sacrifice they did to shape my life. I am forever indebted to my brother Akash, for being available at times

I thought that it is impossible to continue. I greatly value his contribution and support to keep things in perspective.

I sincerely admire the contribution of all my lab mates for their valuable support and timely motivation during the course of my entire study.

Above all, I pay my obeisance to Almighty to bestowed upon me good health, courage, zeal, and light.

Date: 20 May 2019.

Ramanpreet Kaur

Ramanpreet Kaur

Abstract

Mathematical models can be used to study various non-equilibrium systems that are of current interest. Among them, traffic flow is the most important one. In this light, present research contributes to the modeling and analysis of some real traffic characteristics using lattice hydrodynamic approach. Under lattice hydrodynamic approach, space is discretized in the form of lattice sites. The model is formed by the set of continuity equation and a momentum equation consisting of global variables that describe the aggregate behavior of traffic flow at each site. Traffic problems are defined by considering road design such as curved road and curved road with slope as well as driver's behavior both for one and two lane. Furthermore, the effect of heterogeneous traffic on unidirectional single lane highway is presented. The most common feature of overtaking has also been incorporated in lattice model using feedback control for one dimensional system. Moreover, the extensions are made for two dimensional system by incorporating the effect of bidirectional flow. All the models are analyzed theoretically by linear as well as nonlinear analysis and theoretical investigations are validated through numerical simulations. With the aim to investigate, how different factors affect the stability of traffic flow, models are analyzed and programming is done on MATLAB software. The effect of different parameters representing different traffic phenomena has been presented through graphs. The thesis is presented in six chapters:

In **Chapter 1** background of the proposed study followed by its need is given. Then the objective is defined along with the justification of the study. Further, the tools and techniques adopted in the study are discussed. Briefly, the scope and limitation of the study are proposed.

Chapter 2 is devoted to the problem of traffic due to road geometry. We propose an improved lattice model for curved road by including the impact of driver's characteristics on a unidirectional one lane road. Parameters representing the influence of curved road and driver's behavior are added to Nagatani's model [1]. With the aim to derive the stability conditions for the new model, linear analysis is conducted and to analyze the evolution of density waves near critical point, nonlinear analysis is performed. Phase plot in the (ρ, a) plane, presenting the neutral and coexisting curves are plotted which reflect the influence of the curved road angle and the intensity of driver's attribute on dynamics of traffic. It is found that the curved road angle negatively impact the flow stability and aggressive drivers help in overcoming the congestion. In order to

represent traffic jams in terms of density waves, kink solution is obtained by deriving mKdV equation in the neighborhood of critical point. Theoretical investigations are confirmed through numerical simulations and then the summary of results as well as future scope is given.

Chapter 3 deals with the problem of traffic on curved road with slope by incorporating driver's anticipation effect. As in real traffic situations, design of roads affect flow conditions, thus an important aspect of road designs, i.e., curved road having slope is incorporated in the lattice model. As in Chapter 2, description for curved road is given that have negative impact on stability of flow. But what if curved road also have slope? Clearly it gives rise to more serious congestion. So, the Chapter is devoted to the model for curved road with slope on two lane highway along with anticipation effect of drivers. The effects of different slopes on traffic flow phenomena are presented and are examined theoretically via linear and nonlinear analysis. Phase plot, showing the impact of different angles of slopes is presented. Simulation is performed and the results agree with the theoretical analysis. At last, the summary of results is given with possible future scope.

The influence of heterogeneous vehicles on traffic flow is explored in **Chapter 4**. All lattice models presented before deals with homogeneous traffic flow, but in real traffic situations there exists different vehicles that affect vehicular flow differently. Thus by using lattice approach, a new model is presented by considering two distinct kinds of vehicles. One type of vehicles are small and the other one are taken to be large. The model is developed by including the parameters representing the impacts of heterogeneous mix as well as optimal current difference effect for one lane road. For the purpose to check the influence of bigger and smaller vehicles on stability of flow, the model is analyzed theoretically via linear as well as nonlinear analysis. Two phase plots are presented; one for a parameter representing heterogenous mix and other represent five distinct regions corresponding to the fraction of mixed vehicles. It is shown that bigger vehicles cause congestion and smaller vehicles are liable to reduce congestion. In addition, mKdV equation representing kink antikink density waves is obtained near critical point. Then simulation is performed and the summary of results is given.

In **Chapter 5**, basic lattice model is extended by taking the passing effect using feedback control. Control theory is used and the stability of the system is checked by using Hurwitz criteria and H_∞ norm of transfer functions are obtained. The efficiency of control signal in minimizing the jamming transitions due to passing is shown through Bode plot. The results show that the control parameter helps in reducing congestion

and makes the flow stable even at higher rate of passing. In order to justify the theoretical results numerical simulation is conducted. In the end of the Chapter, conclusion of results is given.

Lattice model for bidirectional flow on a square lattice is presented in **Chapter 6**. Because in real traffic situations vehicles can move in any possible direction and the flow varies according to the route choice of drivers. Thus, the effect of bidirectional flow on a square lattice is analyzed with optimal current difference effect. Theoretical investigations are done using linear and nonlinear analysis. Results are presented by taking different fractions of cars moving in different directions. Results show that the flow will be uniform in case of an equal fraction of vehicles otherwise unequal fractions of vehicles give rise to congestion. The results also show that optimal current difference help in making the flow more stable. The results are found compatible with the characteristics of real network situations. The validity of theoretical investigations is checked through numerical simulation and the last section refers to concluding remarks.

As in the present thesis, traffic flow models describing some features of real road situations using lattice approach are presented and traffic jams are represented in terms of kink density waves. Therefore, possible future scope based on the significance of lattice approach is also given in the end.

List of Research Papers

1. **R. Kaur** and S. Sharma. Analysis of driver's characteristics on a curved road in a lattice model. *Physica A: Statistical Mechanics and its Applications*, 471:59–67, 2017. Doi.org/10.1016/j.physa.2016.11.116. **(SCI, Impact factor: 2.132)**.

2. **R. Kaur** and S. Sharma. Modeling and simulation of driver's anticipation effect in a two lane system on curved road with slope. *Physica A: Statistical Mechanics and its Applications*, 499:110–120, 2018. Doi.org/10.1016/j.physa.2017.12.101. **(SCI, Impact factor: 2.132)**.

3. **R. Kaur** and S. Sharma. Analyses of a heterogeneous lattice hydrodynamic model with low and high–sensitivity vehicles. *Physics Letters A*, 382(22):1449–1455, 2018. Doi.org/10.1016/j.physleta.2018.03.045. **(SCI, Impact factor: 1.863)**.

4. **R. Kaur** and S. Sharma. Analyses of lattice hydrodynamic model using delayed feedback control with passing. *Physica A: Statistical Mechanics and its Applications*, 510:446–455, 2018. Doi.org/10.1016/j.physa.2018.06.118. **(SCI, Impact factor: 2.132)**.

5. **R. Kaur** and S. Sharma. The effect of bidirectional traffic flow on a two dimensional network with optimal current difference. (Communicated)

Table of Contents

Acknowledgements . . . . **v**

Abstract . . . . **vii**

List of Research Papers . . . . **xi**

Table of Contents . . . . **xiii**

List of Figures . . . . **xvii**

Abbreviations/Notations . . . . **xxi**

Chapter 1 Introduction **1**

1.1 Classification of traffic flow models 2

1.1.1 Microscopic models 3

1.1.2 Macroscopic models 6

1.1.3 Mesoscopic models 10

1.2 Fundamental relation between microscopic and macroscopic variables . 10

1.2.1 Classical theory of traffic flow 11

1.2.2 Properties of fundamental relation 12

1.3 Phase transitions 12

1.4 Formation and characterization of traffic jams 13

1.5 Origin of lattice hydrodynamic model 15

1.6 Lattice hydrodynamic approach 16

1.6.1 Basic lattice model 16

Chapter 2 Theoretical investigation of driver's behavior on curved road **21**

2.1 Mathematical models 23

2.1.1 Lattice model for curved road 23

2.1.2 Lattice model for driver's behavior on curved road 24

2.2 Linear stability analysis 26

2.3 Nonlinear stability analysis 28

2.4 Numerical simulation 30

2.5 Conclusion 35

2.5.1 Outcomes: 35
2.5.2 Future scope: 36

Chapter 3 The analysis of driver's anticipation effect on slopy curved road 37
3.1 Models for curved road with slope 39
3.1.1 Car following model 39
3.1.2 Extended lattice models 40
3.1.3 Lattice model for slopy curved road 41
3.2 Effect of small amplitude perturbation 42
3.3 Effect of long wave perturbation 44
3.4 Simulation results 47
3.5 Conclusion 51

Chapter 4 Lattice model for heterogeneous traffic flow 53
4.1 Models for heterogeneous traffic flow 55
4.1.1 Car following model for heterogeneous traffic flow 55
4.1.2 New lattice model for heterogeneous traffic flow 55
4.2 Theoretical analysis of the new model 58
4.2.1 Linear stability analysis 58
4.2.2 Nonlinear stability analysis 60
4.3 Simulation 63
4.4 Summary of results 66
4.4.1 Outcomes: 66
4.4.2 Future scope: 67

Chapter 5 The effect of passing on traffic flow with delayed feedback control 69
5.1 Extended lattice model 70
5.2 Qualitative properties of the proposed model 71
5.2.1 Stability analysis using control signal 71
5.2.2 Nonlinear stability analysis 75
5.3 Discussion of results 78
5.3.1 Early time effect of feedback control 78
5.3.2 Long time effect of feedback control 82
5.4 Conclusion and future scope 86

Chapter 6 The observation of bidirectional traffic flow on two dimensional network 89

6.1 Two dimensional lattice hydrodynamic model 91
6.1.1 Lattice model for bidirectional flow 92
6.2 Linear stability analysis 94
6.2.1 Phase plots for equal fraction parameters ($C_1 = C_2$) 96
6.2.2 Phase plots for unequal fraction parameters ($C_1 \neq C_2$) 97
6.3 Nonlinear analysis 99
6.4 Numerical simulation 101
6.4.1 When fraction parameters are equal ($C_1 = C_2$) 102
6.4.2 When fraction parameters are unequal ($C_1 \neq C_2$) for ($\lambda = 0.2$) . 109
6.5 Conclusion 114

Chapter 7 Summary and future scope 117

Summary and future scope 117
7.1 Summary 117
7.2 Future scope 119

References 121

Appendix 135

List of Figures

1.1 An illustration of microscopic models. 4

1.2 An illustration of macroscopic models. 6

1.3 Patterns of density waves (a) Asymmetric kink antikink (b) Soliton density wave (c) Symmetric kink antikink 15

1.4 An illustration of lattice model. 16

2.1 The illustration of lattice model for a curved road. 23

2.2 Phase plot in (ρ, a) space with $\rho_0 = \rho_c = 0.2$, $\mu = 0.3$, $\mathbf{r} = 10$, ${k_1}^1 = 0.14$ for (a) $p = 0.2,\ 0.4,\ 0.6,\ 0.8$ (b) $\theta_j = \pi/6,\ \pi/4,\ \pi/3,\ 5\pi/12,\ \pi/2$. . . . 27

2.3 Spatiotemporal evolution of density when $a = 2.2$ and $\theta_j = \pi/4$ for (a) $p = 0.2$, (b) $p = 0.4$, (c) $p = 0.6$ and (d) $p = 0.8$. 31

2.4 Density profiles for different values of p at (a) $t = 8 \times 10^4$ sec., (b) $t = 9.99 \times 10^4 - 10^5$ sec. on lattice site 45 and (c) lattice site 70. 32

2.5 Space-time evolutions of density waves when $a = 3.5$ and $p = 0.8$ for (a) $\theta_j = \pi/12$, (b) $\theta_j = \pi/6$ and (c) $\theta_j = \pi/4$. 33

2.6 Density wave profile for different θ_j at (a) $t = 8 \times 10^4$ sec., (b) $t = 9.99 \times 10^4 - 10^5$ sec. on lattice site 45 and (c) lattice site 70. 34

3.1 The illustration of lattice model for a curved road with slope. 38

3.2 Phase plot in (ρ, a) space for different values of ϕ when $\gamma = 0.1, \alpha = 0.2, \theta_j = \pi/3$ corresponding to (a) Uphill (b) Downhill situations. . . . 43

3.3 Spatiotemporal evolution of density waves at $t = 9.9 \times 10^4$-10^5 sec. for uphill case when $\gamma = 0.1$ and $\phi = 0, \pi/90, \pi/45, \pi/30$. 48

3.4 Spatiotemporal evolution of density waves at $t = 9.9 \times 10^4$-10^5 sec. for downhill case when $\gamma = 0.1, \phi = 0, \pi/90, \pi/45, \pi/30$. 49

3.5 Density profiles for uphill case at (a) $t = 8 \times 10^4$ sec. (b) on lattice site $j = 50$ when $\gamma = 0.1,\ \phi = 0, \pi/90, \pi/45, \pi/30$. 50

3.6 Density profiles for downhill case at (a) $t = 8 \times 10^4$ sec. (b) on lattice site $j = 50$ when $\gamma = 0.1,\ \phi = 0, \pi/90, \pi/45, \pi/30$. 50

4.1 An illustration of lattice model for heterogeneous traffic flow. 54

4.2 Phase plots showing (a) phase separation curves in (ρ, a) space for $c = 0.1, 0.2, 0.3, 0.4$. (b) critical lines dividing (ρ, c) space into five distinct regions of flow for $a = 0.2$. The critical density and reaction coefficient of optimal current difference are chosen respectively as $\rho_0 = \rho_c = 0.2$, and $\lambda = 0.2$. 59
4.3 Space-time evolutions of density waves when $\lambda = 0.2, p_1 = 2.5, q = 0.5, a = 3.2$ for (a) $c = 0.1$, (b) $c = 0.2$, (c) $c = 0.3$ and (d) $c = 0.4$ respectively. 64
4.4 Density profiles corresponding to different values of fraction parameter c obtained at (a) fixed time $t = 8 \times 10^4$ sec. and lattice sites varies (b) for fixed lattice site $j = 50$ and time varies from $t = 9.99 \times 10^4 - 10^5$ sec. when $\lambda = 0.2, p_1 = 2.5, q = 0.5$. 65
4.5 Plots of density versus density difference when $\lambda = 0.2, p_1 = 2.5, q = 0.5, a = 3.2$ for (a) $c = 0.1$, (b) $c = 0.2$, (c) $c = 0.3$ and (d) $c = 0.4$ respectively. 65

5.1 Bode plot for $\zeta = 0.1, 0.3, 0.5$ when (a) $\gamma_1 = 0.01$ and (b) $\gamma_1 = 0.1$ . . . 74
5.2 Phase plot in (ρ, a) space for $\zeta = 0, 0.3, 0.5$ (a) for $\gamma_1 = 0.01$ (b) for $\gamma_1 = 0.1$. 78
5.3 Density profiles for $\zeta = 0, 0.3, 0.5$ at time $t = 1 - 200$ sec. when $\gamma_1 = 0.01$. 79
5.4 Density profiles for $\zeta = 0, 0.3, 0.5$ at time $t = 1 - 200$ sec. when $\gamma_1 = 0.1$. 80
5.5 Plots of density difference $\rho_j(t) - \rho_j(t-1)$ against $\rho_j(t)$ when $\gamma_1 = 0.1$ at time $t = 1 - 500$ sec. for $\zeta = 0$ at different sites. 81
5.6 Plots of density difference $\rho_j(t) - \rho_j(t-1)$ against $\rho_j(t)$ when $\gamma_1 = 0.1$ at time $t = 1 - 500$ sec. for $\zeta = 0.5$ at different sites. 82
5.7 Spatiotemporal evolutions of density waves for $\zeta = 0, 0.3, 0.5$ at time $t = 20100 - 20300$ sec. when $\gamma_1 = 0.01$. 83
5.8 Spatiotemporal evolutions of density waves for $\zeta = 0, 0.3, 0.5$ at time $t = 20100 - 20300$ sec. when $\gamma_1 = 0.1$. 84
5.9 Density profiles for $\zeta = 0, 0.3, 0.5$ at time $t = 20100 - 20300$ sec. when $\gamma_1 = 0.01$. 85
5.10 Density profiles for $\zeta = 0, 0.3, 0.5$ at time $t = 20100 - 20300$ sec. when $\gamma_1 = 0.1$. 86

6.1 An illustration of bidirectional flow in lattice model. 90
6.2 Phase diagram in parameter space (ρ, a) for $C_1 = C_2 = 0.1$, $C_1 = C_2 = 0.2$, $C_1 = C_2 = 0.3$, $C_1 = C_2 = 0.4$ when $\rho_0 = \rho_c = 0.2$ (a) $\lambda = 0$ (b) $\lambda = 0.2$. 96

6.3 Plots of critical points versus critical sensitivity for $C_1 = C_2 = 0.1$, $C_1 = C_2 = 0.2$, $C_1 = C_2 = 0.3$, $C_1 = C_2 = 0.4$ when $\rho_0 = \rho_c = 0.2$ (a) $\lambda = 0$ (b) $\lambda = 0.2$. 97
6.4 Phase plot in the (ρ, a) plane when $\lambda = 0.2$ and $\rho_0 = \rho_c = 0.2$ (a) when C_1 is fixed (b) when C_2 is fixed. 98
6.5 Plots of critical points versus critical sensitivity when $\lambda = 0.2$ and $\rho_0 = \rho_c = 0.2$ (a) when C_1 is fixed (b) when C_2 is fixed. 98
6.6 Traffic patterns at $t = 2 \times 10^3, a = 0.5, \lambda = 0$ for equal values of C_1 and C_2 (a) $C_1 = C_2 = 0.1$ (b) $C_1 = C_2 = 0.2$ (c) $C_1 = C_2 = 0.4$. 103
6.7 Density wave profile at $t = 15 \times 10^3, a = 0.5, \lambda = 0$ for equal values of C_1 and C_2 (a) $C_1 = C_2 = 0.1$ (b) $C_1 = C_2 = 0.2$ (c) $C_1 = C_2 = 0.4$. . 104
6.8 Phase plots of density versus density difference at $t = 15 \times 10^3 - 2 \times 10^4, a = 0.5, \lambda = 0$ for equal values of C_1 and C_2 (a) $C_1 = C_2 = 0.1$ (b) $C_1 = C_2 = 0.2$ (c) $C_1 = C_2 = 0.4$. 105
6.9 Traffic patterns at $t = 2 \times 10^3, a = 0.5, \lambda = 0.2$ for equal values of C_1 and C_2 (a) $C_1 = C_2 = 0.1$ (b) $C_1 = C_2 = 0.2$ (c) $C_1 = C_2 = 0.4$. . . . 106
6.10 Density wave profile at $t = 15 \times 10^3, a = 0.5, \lambda = 0.2$ for equal values of C_1 and C_2 (a) $C_1 = C_2 = 0.1$ (b) $C_1 = C_2 = 0.2$ (c) $C_1 = C_2 = 0.4$. . 107
6.11 Phase plots of density versus density difference at $t = 15 \times 10^3 - 2 \times 10^4, a = 0.5, \lambda = 0.2$ for equal values of C_1 and C_2 (a) $C_1 = C_2 = 0.1$ (b) $C_1 = C_2 = 0.2$ (c) $C_1 = C_2 = 0.4$. 108
6.12 Traffic patterns at $t = 2 \times 10^3, a = 0.6, \lambda = 0.2$ for fixed $C_1 = 0.1$ (a) $C_2 = 0.2$ (b) $C_2 = 0.3$ (c) $C_2 = 0.5$. 109
6.13 Density wave profile at $t = 15 \times 10^3, a = 0.6, \lambda = 0.2$ for fixed $C_1 = 0.1$ (a) $C_2 = 0.2$ (b) $C_2 = 0.3$ (c) $C_2 = 0.5$. 110
6.14 Phase plots of density versus density difference at $t = 15 \times 10^3 - 2 \times 10^4, a = 0.6, \lambda = 0.2$ for fixed $C_1 = 0.1$ (a) $C_2 = 0.2$ (b) $C_2 = 0.3$ (c) $C_2 = 0.5$. 111
6.15 Traffic patterns at $t = 2 \times 10^3, a = 0.6, \lambda = 0.2$ for fixed $C_2 = 0.1$ (a) $C_1 = 0.2$ (b) $C_1 = 0.3$ (c) $C_1 = 0.5$. 112
6.16 Density wave profile at $t = 15 \times 10^3, a = 0.6, \lambda = 0.2$ for fixed $C_2 = 0.1$ (a) $C_1 = 0.2$ (b) $C_1 = 0.3$ (c) $C_1 = 0.5$. 113
6.17 Phase plots of density versus density difference at $t = 15 \times 10^3 - 2 \times 10^4, a = 0.6, \lambda = 0.2$ for fixed $C_2 = 0.1$ (a) $C_1 = 0.2$ (b) $C_1 = 0.3$ (c) $C_1 = 0.5$. 114

Abbreviations/Notations

mKdV	Modified Korteweg-de Vries
OVM	Optimal velocity model
FVDM	Full velocity difference model
X	Space
T	Time
S	Speed of soliton density wave
L_1	Speed of kink density wave
$\mathbf{a}$	Acceleration
a	Driver's sensitivity
ρ_0	Average density
ρ	Density
ψ	Sensitivity
H	Heaviside function
v	Macroscopic velocity
V	Optimal velocity
θ	Angle of curved road
$\mathbf{r}$	Radius of curved road
p	Driver's behavior
ϕ	Angle of slope
R_1	Curvature radius
α	Coefficient of driver's anticipation
γ	Parameter for lane change
c	Fraction of small vehicles in heterogeneous traffic stream
λ	Reaction coefficient of optimal current difference effect
ζ	Control paramter
γ_1	Coefficient for passing
C	Fraction of east-bound and west-bound cars
C_1	Fraction of east-bound cars
C_2	Fraction of north-bound cars

Chapter 1

Introduction

Transportation is a key tool that helps people and goods to reach their destinations at minimum cost and in the shortest possible time. The whole process is followed by the steps of defining goals and objectives, identifying problems and developing plans. Nowadays, the increasing vehicular traffic not only damages the environment but also slowing down economic growth. In transport policy, planning, and engineering, traffic forecasts are therefore used to calculate infrastructure capacity, e.g., how many lanes should be there on a road or bridge and to evaluate the impacts related to environment (air and noise pollution). Furthermore, transport forecasts are an attempt to evaluate the proportion of vehicles and people using particular facility related to future transport infrastructure. For the task of estimating the capacity of road infrastructure, transportation engineers apply the comprehensive approach in order to inspect the existing alternatives and their impacts on the transportation system to influence advantageous results.

Due to urbanization, roadways needs to get redesigned for better traffic containment and management to mitigate traffic congestion. Nowadays, the strategy has been caricatured as 'predicting and providing' rule, i.e., to predict future transport demand and provide an efficient network, usually by building an efficient road network. However, the thought has been devoted to the analysis of the fundamental mechanisms which operate to control the movement of traffic. For that, several interesting theoretical approaches to the characterization of these mechanisms have been developed.

Historically, the field of transport engineering starts becoming a practical discipline when researchers from various fields start solving particular traffic problems. Nowadays, the developing area of study known as traffic flow theory which explains the properties of traffic based on mathematical and statistical ideas [2, 3]. During this highly active period, mathematics established itself as a solid basis for theoretical analysis of traffic phenomena. Based on the theoretical analysis, a transportation engineer is able to answer: when do traffic jams emerge, when the queuing takes place, how long will the traffic queues be, how long they spread in space and time and how much time the traffic jams will take to get resolved. In addition, strategies adopted to expand roads and to measure traffic can affect functioning of traffic either directly or indirectly by influencing driving behavior.

The field evolved further by the emergence of technology; the engineers follow more control oriented methods as a means of reducing congestion at intersections, e.g., adaptive traffic control system (ATCS). Nowadays, the field has been embraced by the industry called intelligent transportation system (ITS), covering nearly all aspects of the transportation community. The theory of traffic require the knowledge of the fundamental characteristics and gives an accurate description of queue formation and evolution [4] of traffic jams. Because traffic congestion show discontinuities thus there exists a correspondence between traffic congestion and shock waves [5, 6]. Traffic flow theories can be seen as the foundation of traffic science and are aimed at providing an understanding of phenomena associated with the movement of individual vehicles along a highway as they interact with neighboring vehicles.

1.1 Classification of traffic flow models

Phenomena of traffic flow is highly complex and nonlinear, and is influenced by different factors: driver-vehicle combinations (driver's characteristics like age, gender etc. and vehicle characteristics, small or large), traffic conditions (different speeds and densities), state of infrastructure (design and conditions of road) and impacts of external situations (weather and driving rules). Therefore, to capture the essential features present in real traffic situations; traffic flow models can be categorize as: continuous or discrete, analytical or simulation, deterministic or stochastic etc.

- Stochastic models use random elements to describe aspects of the traffic flow which are unknown, immeasurable, impossible to model. For example, different drivers can react in a different way in the same situation.
- Deterministic models are based on an exact relationship without any randomness. The formulation of car following models can be done in both ways (deterministic or stochastic) as the reaction time of drivers can be defined as a constant or random variable.

The most general categorization of traffic models follow the 'level of detail'. This categorization can be operationalized by taking into account the distinct traffic entities and their level of description in the respective models. Various researchers tried to categorize these models based on various factors as enumerated below:

1.1.1 Microscopic models

Microscopic models define traffic flow as a set of individual vehicles by providing a detailed description of the individual speeds, positions, and accelerations using ordinary differential equations. Vehicle's velocity and position define the state of the system as dependent variables of the time variable. The characteristic of the individual vehicle is modeled by combination of two conditional equations: One is temporal derivative of position $x_n(t)$ of n^{th} vehicle at t time which is equal to speed:

$$\dot{x}_n(t) = u_n(t), \tag{1.1.1}$$

and the second is temporal derivative of its velocity $u_n(t)$ at time t which is equal to its acceleration $\mathbf{a}_n(t)$:

$$\dot{u}_n(t) = \mathbf{a}_n(t). \tag{1.1.2}$$

Basic variables that represent the microscopic models are: headway, space and speed.

Variable	Symbol	Unit
Headway	h	sec
Space	s_1	m
Speed	u	m/sec

Table 1.1: Microscopic variables [2]

The distance between following and leading vehicles can be defined as net space headway (or gap) and the gross space headway is the distance in which the length of the vehicle (following) is also included, i.e., the distance from the rear bumper of the leader ($(n+1)^{th}$ vehicle) to the rear bumper of the follower (n^{th} vehicle). Likewise, net time headway can be defined as the time taken by the follower (with its front bumper) to arrive at the location of the rear bumper of the leader. Moreover, if the time taken by the vehicle to cover the distance of vehicle length is also included then it is called the gross time headway (or headway). Speed can be determined by the amount of distance covered by the vehicle in a unit of time. Generally, by headway and spacing we mean gross values. The length of the vehicle remain unchanged so, gross or net space headway is same. On the contrary, the variation in gross and net time headway difference is due to the speed of the vehicle.

Car following models come into the category of micro models. Microscopic models are useful [3] for the following applications:

- Visualization of interactions among different participants in traffic (cars, trucks, buses, cyclists etc.).
- Describing human driving behavior, e.g., different driving styles.
- Modeling how single vehicle affects traffic, e.g., vehicle-vehicle and infrastructure-vehicle communication.

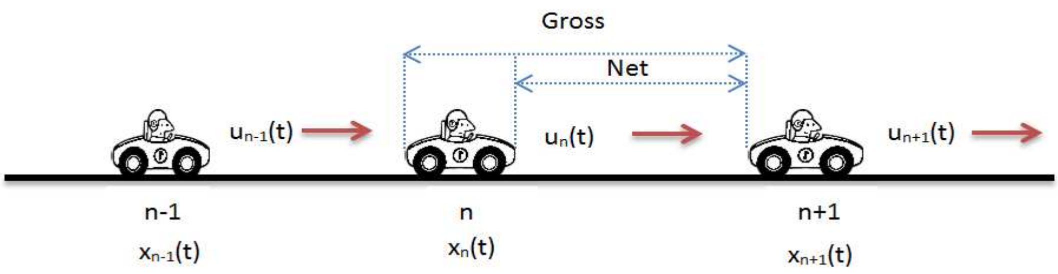

Figure 1.1: An illustration of microscopic models.

1.1.1.1 Car following models

Car following models follow the assumption that the motion of every individual vehicle depend on the distance and velocity difference to the ahead vehicle [7]. Car following theories [8–10] follow the Newton's laws of motion. In mechanics, acceleration is a form of response to the stimulus that the particle receives in terms of force. This force is the combination of the external forces and the forces resulting by the interaction of the particle with other particles in the system [11]. Therefore in the traffic stream, by accelerating or decelerating the vehicle, driver responds to the surrounding traffic conditions. The difference of speeds among leading and following vehicles as well as the distance headway work as a stimulus to the driver. General formulation of car following models is described by the following equation:

$$\mathbf{a}_n = G(u_n, \Delta x_n, \Delta u_n), \tag{1.1.3}$$

where G denotes the stimulus gained by vehicle n. Different categorizations of car following models exist; among them, the models developed at general motors research laboratories come under the category of GHR models [12–16]. The basic philosophy of GHR type models is that the follower (n^{th} vehicle) responds to the non-zero relative speed between itself and the leading vehicle ($(n+1)^{th}$ vehicle) by accelerating or decelerating its own speed. The relative speed behaves like a stimulus to the follower;

and the acceleration or deceleration of the follower caused by the stimulus is vehicle's response. The degree to which a given stimulus affects the response, is a function of the distance headway among the follower and leader and the speed of the follower. Mathematical formulation of the GHR type models is:

$$\mathbf{a}_n(t+\tau) = \Big\{\frac{W(\kappa,\chi)(u_n(t+\tau))^{\chi}}{(x_{n+1}(t)-x_n(t))^{\kappa}}\Big\}(u_{n+1}(t)-u_n(t)), \tag{1.1.4}$$

where κ and χ are the exponents and the dimensions of the constant $W(\kappa,\chi)$ are dependent on them. The sensitivity is represented by the term under braces and the term inside the brackets represent stimulus. Some other models [17–21] are also special case of general motors model.

Optimal velocity models (OVM) [22–25] follow the assumption that each vehicle has an optimal velocity depending upon its distance from the preceding vehicle. The difference between the actual velocity $u_n(t)$ and the optimal velocity V determines the acceleration of n^{th} vehicle. General formulation of these models is given below:

$$\mathbf{a}_n(t) = a[V(\Delta x_n(t-\tau)) - u_n(t-\tau)] + \psi\Delta u_n(t)H(-\Delta u_n(t)). \tag{1.1.5}$$

OVM developed by Bando et al. [22, 23] is a well known micro model due to its capability in analyzing numerous features of traffic flow, i.e., traffic congestion and its variation and the development of stop-start waves.

Many extended versions of microscopic optimal velocity models have been developed by taking realistic features into account [26–33]. Recently, by taking the effect of lateral gap in the micro model; the characteristics of electric vehicles are analyzed in transportation cyber-physical system [34]. Jin et al. [35] investigated the nonlinear density waves in a modified car following model by considering memory and jerk. By taking into account the characteristics of curved and straight roads, the control signal has been investigated using car following model [36]. An extended micro model taking the variable safety distance and time delay effect has been constructed based on the classical car following theory [37]. By taking multiple preceding car's speed differences as well as the difference between headway and safety distance into account, a modified control signal has been presented from the viewpoint of feedback control method. An extended car following model accounting for cooperation driving system with vehicle's velocity uncertainty is proposed following the full velocity difference model [38]. Latest advancements in car following models considering the human behavior are presented in review paper [39]. In addition, review on optimal velocity models is also presented [40].

1.1.2 Macroscopic models

In order to define traffic flow, macroscopic models utilize the aggregate quantities, i.e., the description of traffic flow is analogously to gases or liquids in motion. Therefore, these models are sometimes called 'hydrodynamic models'. In these models, traffic flow is characterized by locally aggregated quantities (ρ, q, v), i.e., density, flow, and average velocity associated with flux relation. The independent variables are location x and time t corresponding to which these aggregated quantities vary. Let us assume a small section $[x, x+dx)$ of road. Then the density is the number of vehicles passing through a point per unit length at an instant t. Flow is the number of vehicles passing through a point per unit time. There are two different ways to measure velocity: space mean velocity and time mean velocity. When velocity is measured by keeping space as reference then it refers to the space mean velocity; on the other side when time is kept as reference then it refers to time mean velocity. Time mean velocity is the average of local velocities of all vehicles crossing a point x during the time interval $[t, t+dt)$:

$$v(x,t) = \frac{1}{n}\sum_{i=1}^{n} v_i, \tag{1.1.6}$$

where v_i denotes local velocity of i^{th} vehicle and the number of vehicles is denoted by n. Space mean velocity of local velocity distribution is defined by its harmonic mean:

$$v(x,t) = \frac{n}{\sum_{i=1}^{n} \frac{1}{v_i}}, \tag{1.1.7}$$

All three variables (ρ, v, q) are related by the relation $q = \rho v$.

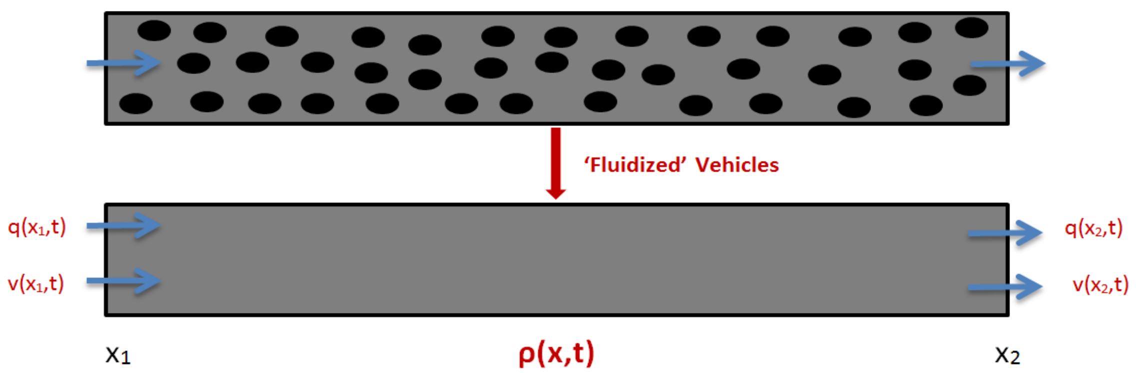

Figure 1.2: An illustration of macroscopic models.

Variable	Symbol	Unit
Flow	$q(x,t)$	veh/hr
Density	$\rho(x,t)$	veh/km
Average speed	$v(x,t)$	km/hr

Table 1.2: Macroscopic variables [2]

Therefore, macroscopic models can explain the phenomena in aggregate terms, such as the evolution of jammed regions or the speed of traffic wave propagation. The behavior of aggregate quantities in continuous traffic flow is modeled by two conditional equations. The first is the continuity equation, which assures the conservation of mass and the second one is an equation of motion which assures the conservation of momentum. Furthermore, macroscopic models are useful [3] if:

- Macroscopic quantities are of particular interest.
- Simulation time is more due to large system of equations.
- Available data come from heterogeneous sources and is inconsistent.
- Describe major properties of traffic flow, i.e., queue formation and shock waves.

Continuum models are an example of macroscopic models which can be further divided into two categories: First-order continuum models and second-order continuum models.

First-order continuum model

Lighthill, Whitham [41] and Richards [42] in 1950′s proposed LWR (Lighthill- Whitham-Richards) model which is the first-order continuum traffic flow model. It models traffic flow as continuum similar to fluid and is governed by two main postulates:

- Number of vehicles remain conserved.
- The average velocity is a function of density under equilibrium conditions.

LWR model explains the traffic flow dynamics using fundamental variables and the continuity equation of the model is given by:

$$\partial_t \rho + \partial_x(\rho v) = 0. \tag{1.1.8}$$

The on and off ramp flows are not considered here. By considering the velocity-density relationship $v = V(\rho)$, the model acquires nonlinear scalar conservation equation:

$$\partial_t \rho + \partial_x(\rho V(\rho)) = 0, \tag{1.1.9}$$

$V(\rho)$ in (1.1.9) denotes equilibrium velocity function and having the following properties:

- $V(\rho)$ is strictly decreasing in $\rho \in (0, \rho_{\max})$.
- The maximum and minimum velocities are $V(0) = V_{\max}$ and $V(\rho_{\max}) = 0$ respectively.
- If $q_e(\rho) = \rho V(\rho)$ and $q_e^{''}(\rho) < 0$, then the LWR model is analogous to the Burger's equation and is characterized by nonlinear waves, known as shocks and rarefaction. These shocks or rarefaction waves arise from an increase or decrease in density downstream.

Limitations

- One of the basic assumptions regarding velocity in the LWR model is its dependence solely on density. The demerit for this assumption is that when such speed-density functions are used the traffic will be in equilibrium, i.e., given a specific density the velocity will be fixed. Moreover, the model does not recognize the desired velocity distribution over vehicles. The model, therefore, can not describe the observed behavior in light traffic.
- It fails to model two important traffic phenomena: stop-start waves caused by instability in traffic flow and forward propagation of disturbances in heavy traffic.
- The model has no inertial effects, which means that the vehicles instantly adjust their speeds. It does not contain any diffusive terms that can model the driver's ability to look forward and to adjust in changing conditions.
- Produces discontinuous solutions regardless of initial conditions being smooth.

Higher-order continuum model

By keeping the idea of first-order continuum model, higher-order continuum models follow the assumption that the velocity is not a function of density alone, but also of its gradient ρ_x and higher ordered terms ρ_{xx}, i.e., diffusion.

$$v = V(\rho, \rho_t, \rho_x, \rho_{xx}, ...), \tag{1.1.10}$$

which means that the drivers not only adjust their speed according to local traffic situations but as per the situations ahead. In order to improve the LWR model [41,42], a different approach has been adopted by developing speed evolution equation that allows non-equilibrium states (ρ, v) to deviate from the equilibrium curve $(\rho, V(\rho))$. Its general formulation is:

$$\dot{v} = v_t + \underbrace{vv_x}_{Convection} = \underbrace{\frac{V(\rho) - v}{\tau}}_{Reaction} - \underbrace{\frac{1}{\rho}P_x + \frac{\eta}{\rho}v_{xx}}_{Anticipation}, \tag{1.1.11}$$

where the total time derivative of v is the sum of two terms, actual velocity v_t and $Convection$ term vv_x that describes the variations in average velocity caused by inflowing vehicles with different velocities. *Reaction* term explains the driver's tendency to achieve the desired velocity. Driver's anticipation behavior corresponding to changing traffic conditions ahead is represented by the *Anticipation* term. The local anticipation behavior of drivers is described by the pressure term P_x and the term v_{xx} denotes diffusion describing higher order tendencies of drivers. If the pressure term takes the value $P = \rho {c_0}^2$ and $\eta = 0$ then Payne's model [43] can be recovered which is the first higher-order model in traffic flow theory. Payne's model [43] originates from the following equation:

$$u(x(t + \tau), t + \tau) = u(\rho(x + s_1), t). \tag{1.1.12}$$

Additionally, Phillips [44] choose $P = \rho {\sigma_1}'(\rho)$, Kuhne [45], Kuhne and Michalopoulos [46] and Kerner and Konhäuser [47] choose $P = \rho {c_0}^2$ and $\eta = \eta_0$. More serious problem present in Payne's model as pointed out by Daganzo [48] is that the characteristic speed travels faster than vehicles. This means that the vehicles from behind can influence vehicles in front, which violates the anisotropic property of traffic flow. Moreover, Payne's model is found to be diffusive because diffusion travels both ways. Payne's model can produce negative travel speeds ('wrong way travel') under certain circumstances. So as to remove the deficiencies of Payne's model, as pointed out by Daganzo, modified models were presented [49, 50] and a review is also presented [51]. After that many extensions were proposed for continuum models by adding realistic factors such as two lane [52, 53], heterogeneous traffic [54], interruption probability [55], traffic jerk [56,57], driver's memory effect [58], timid and aggressive attributes of drivers [59]. Recently, a modified continuum model [60] is proposed following the full velocity difference model that consider the effect of driver's anticipation. Furthermore, by considering the multiple optimal velocity functions with probabilities, new macro model [61] is developed. Recently, the optimal velocity difference effect is analyzed by Fan et al. [62] in an extended continuum model. In addition, a novel continuum model is presented [63] by considering the electronic throttle (ET) dynamics to capture the behavior of vehicles in traffic flow.

1.1.3 Mesoscopic models

Mesoscopic models follow the properties of the family of micro and macro models. Mesoscopic models describe comprehensive behavior of vehicles using probability distributions but with special considerations for microscopic characteristics (i.e., driving behavior etc.). Gas kinetic models and continuum gas kinetic models come into the category of mesoscopic models. The gas kinetic models describe traffic phenomena in terms of reduced phase-space density (PSD) $\tilde{\rho}(x, v, t)$ as a mesoscopic generalization of macroscopic density $\rho(x, t)$. Let us consider a road segment $[x, x + dx)$, then the reduced PSD is the expected number of vehicles moving with velocity $[v, v + dv)$ on this segment equals $\tilde{\rho}(x, v, t)dxdv$. Following equation was given by Prigogine and Herman [64]:

$$\partial_t \tilde{\rho} + v\partial_x \tilde{\rho} = (\partial_t \tilde{\rho})_{acc} + (\partial_t \tilde{\rho})_{int}, \tag{1.1.13}$$

where the term $(\partial_t \tilde{\rho})_{acc}$ represents the changes due to acceleration in order to achieve desired velocity and $(\partial_t \tilde{\rho})_{int}$ denotes changes resulted by vehicular interactions.

1.2 Fundamental relation between microscopic and macroscopic variables

In microscopic view, there exists a fundamental relationship among three fundamental variables: headway (h), spacing (s_1) and speed (u) [2]. The headway times the speed results to spacing. The relationship between microscopic variables can be expressed in the following form:

$$s_1 = hu. \tag{1.2.1}$$

Microscopic	Macroscopic
h	$q = \frac{1}{h}$
s_1	$\rho = \frac{1}{s_1}$
u	$v = \frac{1}{u}$
$s_1 = hu$	$q = \rho v$

Table 1.3: Relationship among micro-macro variables

This relationship has a macroscopic equivalent as headways and spacings have macroscopic counterparts. After reordering (1.2.1):

$$\frac{1}{h} = \frac{1}{s_1} u. \tag{1.2.2}$$

By using $q = \frac{1}{h}$ and $\rho = \frac{1}{s_1}$, (1.2.2) results to:

$$q = \rho v. \tag{1.2.3}$$

Thus the flow q is proportional with both v and ρ.

1.2.1 Classical theory of traffic flow

Traffic models follow the assumption that there exists a space-velocity relationship. This relation was firstly studied by Greenshields [65] and is called the fundamental relation. However, it is also possible to express fundamental relation using macroscopic variables: density (ρ), flow (q) and velocity (v). Some classical speed-density and speed-flow relationships are given in the following table:

Model	Speed-density function	Speed-flow funcion
Greenshields [65]	$\rho = \rho_{\max}\left(1 - \frac{v}{V_{\max}}\right)^{\frac{1}{\beta}} (\beta > 0)$	$q = \rho_{\max} v \left(1 - \frac{v}{V_{\max}}\right)^{\frac{1}{\beta}}$
Greenberg [66]	$\rho = \rho_{\max} \exp\left(-\frac{v}{V_{\max}}\right)$	$q = \rho_{\max} v \exp\left(-\frac{v}{V_{\max}}\right)$
Underwood [67]	$\rho = \rho_{\max}\left(\delta_1 \ln\left(\frac{V_{\max}}{v}\right)\right)^{\frac{1}{\beta}} (\delta_1 > 0)$	$q = \rho_{\max} v \left(\delta_1 \ln\left(\frac{V_{\max}}{v}\right)\right)^{\frac{1}{\delta_1}}$

Table 1.4: Classical speed-density and speed-flow relationships [68]

1.2.2 Properties of fundamental relation

Castillo et al. [69] proposed the following properties of a sound fundamental relation:

- The range of values of equilibrium velocity is from zero to $V_{\max}$, i.e., free flow speed.
- The density ranges from zero to jam density, i.e., maximum value $\rho_{\max}$.
- At the extreme density values the velocities are $V(0) = V_{\max}$ and $V(\rho_{\max}) = 0$.
- At the extreme density values the values of flow are $q(0) = q(\rho_{\max}) = 0$.
- At the extreme density values, maximum velocity and congestion wave velocity are the slopes of the fundamental relation given as: $V_{\max} = \frac{dq}{d\rho(0)}$ and $w = \frac{dq}{d\rho(\rho_{\max})}$.
- The fundamental relation is strictly concave: $\frac{d^2q}{d\rho^2} < 0$ for almost all $\rho \in [0, \rho_{\max}]$.

1.3 Phase transitions

By 'phase transition' we mean the change of physical state in a given substance, for example, liquid$\longleftrightarrow$vapor. It has been shown in [70] that the traffic may exhibit two distinct phases:

- **Free flow phase:** Free flow phase refers to the conditions under which all vehicles can achieve an optimal level of velocity.
- **Congested phase:** Congested phase can be defined as a phase of traffic under which the vehicle's velocity remains below the minimum achievable velocity in free flow, i.e., the velocity is associated with the limit point.

Mathematically, it can be represented by conservation laws in following form:

$$\begin{cases} \partial_t(U) + \partial_x(F(U)) = 0, \quad t \in [0, \infty), \quad U \in \Omega, \quad \Omega \subseteq \mathbb{R}^n, \\ U(0, x) = U_0(x), \quad x \in \mathbb{R}^n, \quad F : \Omega \to \mathbb{R}^n \quad \text{smooth}, \end{cases} \tag{1.3.1}$$

where U represents an unknown vector of the conserved variables and flux function is denoted by F. The system is strictly hyperbolic and the solution of these equations may develop discontinuities in finite time. In presence of phase transitions, Ω is the disjoint union of two (or more) sets, called phases.

$$\Omega = \Omega_1 \cup \Omega_2. \tag{1.3.2}$$

A phase transition is a jump discontinuity between states belonging to different phases, solution of the above system (1.3.1) can be constructed with the following form of initial data:

$$U_0(x) = \begin{cases} U_L, & \text{if } \ x < 0, \\ U_R, & \text{if } \ x > 0. \end{cases} \tag{1.3.3}$$

1.4 Formation and characterization of traffic jams

It is well known that a uniform flow equilibrium exists for low density of traffic where vehicles follow one another at the same speed, whereas oscillations may occur when traffic becomes more dense. One of the typical oscillations is the stop and go wave, when the speed breaks down and vehicles get densely packed on a highway segment. The congested regime of finite length is enclosed by two fronts traveling at the same speed: a stop front in which vehicles enter the congested region and a go front in which vehicles leave the congested state. The term 'phantom jams' can be used for these waves resulted in spontaneous fluctuations. By examining a number of aerial photos of a multi-lane road, direct empirical evidence was presented for the formation of spontaneous jams in [71]. In addition, an experiment was conducted [72] on a circular road without bottleneck by taking 22 equally spaced vehicles into account. Initially, all vehicles are distributed homogeneously and move with the same velocity. A small fluctuation in the homogeneous flow grows larger and resulted as a jam cluster which propagates backward like a single pulse density wave with the same speed as that of jam. In order to boost up the experimental evidence, Nakayama et al. [73] conducted an experiment on a circular road. For that, vehicles were distributed homogeneously on the road and were running with the same velocity. After 10 minutes traffic jam emerged spontaneously on road. Based upon the analysis, it was confirmed that for the density higher than the critical level, a small amplitude disturbance in uniform flow generated localized regions of high density. Jamming states which emerge in vehicular traffic and then die out are called stable when density is low. But flow becomes unstable when density rise above the jam density and the disturbance amplifies in time resulting in terms of propagating density waves. Theoretical and empirical evidence [72, 74, 75] shows that traffic congestion appears in the form of density waves. Among them, continuum models characterize traffic in the form of density and velocity fields by using partial differential equations. Currently, macroscopic models use hyperbolic partial differential equations. In order to represent traffic jams in the form of density waves, nonlinear wave equations have been proposed. In traffic flow theory, Burger's, KdV and mKdV equations have been presented as the typical ones.

Through numerical solution of the hydrodynamic models, a single pulse density wave was observed by Kerner and Konhäuser [47] (as shown in Fig. 1.3(a)). KdV equation was derived by Kurtze and Hong [75] from the hydrodynamic model using nonlinear analysis method. KdV equation consist of the nonlinear and dispersive terms and explains the long waves spreading in dispersive media whose amplitude is small but finite. KdV equation is given by:

$$\frac{\partial R}{\partial T} - \frac{\partial^3 R}{\partial X^3} + 2R\frac{\partial R}{\partial X} = 0, \tag{1.4.1}$$

where the variable X is for space and T is time variable. The term $\frac{\partial R}{\partial T}$ describes the time evolution of the wave propagating in one direction. Moreover, the nonlinear term $R\frac{\partial R}{\partial X}$ accounts for steepening of the wave and the term $\frac{\partial^3 R}{\partial X^3}$ represents the linear dispersion describing the spreading of wave. The solution of KdV equation is:

$$R(X,T) = S\text{sech}^2\Big(\sqrt{\frac{S}{12}}\Big(X - \frac{ST}{3}\Big)\Big), \tag{1.4.2}$$

where S is the amplitude of density wave. It was concluded that both single pulse density wave and soliton are same and can be obtained by solution of KdV equation (Fig. 1.3(b)).

However, shape of density wave in Fig. 1.3(a) is not consistent with that in Fig. 1.3(b). It was assumed that the single pulse density wave is not 'soliton' but is similar to the asymmetric kink antikink density wave. In addition, mKdV equation was obtained by Komatsu and Sasa [76] and showed that the solution of mKdV equation gives density wave of kink antikink form (Fig. 1.3(c)). Analytical solution and simulation results were compared which confirmed that the phantom traffic jams come out in terms of symmetric kink antikink wave. Following equation represent the mKdV equation:

$$\frac{\partial R}{\partial T} - \frac{\partial^3 R}{\partial X^3} + \frac{\partial R^3}{\partial X} = 0, \tag{1.4.3}$$

and its solution (see Appendix) is:

$$R(X,T) = \sqrt{2L_1}\tanh\Big(\sqrt{\frac{L_1}{2}}(X - 2L_1 T)\Big) \tag{1.4.4}$$

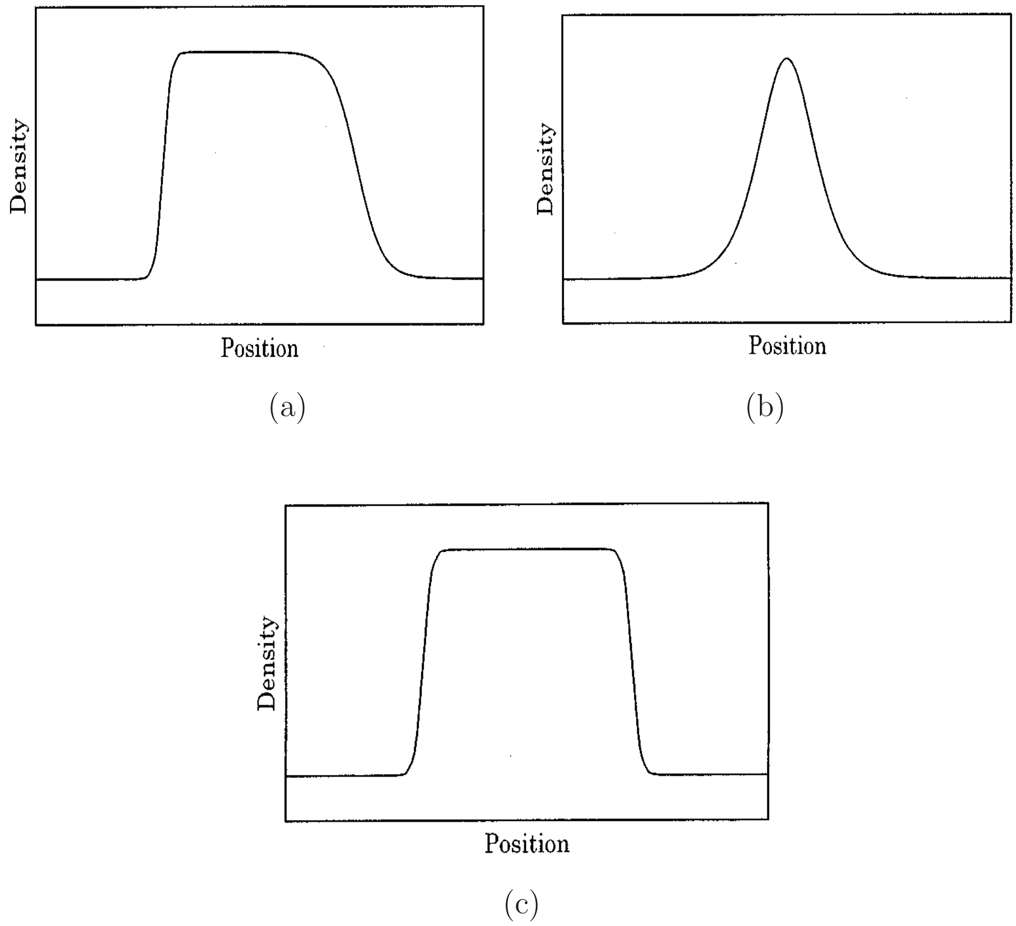

Figure 1.3: Patterns of density waves (a) Asymmetric kink antikink (b) Soliton density wave (c) Symmetric kink antikink

1.5 Origin of lattice hydrodynamic model

As discussed in previous sections, both microscopic and macroscopic models play a major role in analyzing the properties of real traffic networks. Microscopic models describe small details of traffic while macroscopic models are based on aggregate quantities. Macro models are suitable for large scale systems and their calibration is simple relatively to micro models. But the major drawback of macro models is the loss of small details as they cannot correctly describe microscopic details and impacts.

Due to the complexity of the partial differential equations of hydrodynamic models, it was very difficult to derive the mKdV equation through nonlinear analysis. Also, it was not easy to get the evolution equation from the analytical method, which can describe the traffic jam phase transitions. Thus, in order to fulfill the need to describe traffic at both micro and macro level arise.

In order to represent traffic jams in terms of density waves and to analyze the jamming transitions lattice model was proposed. The different wave equations: Burger's, KdV and mKdV; describe the density waves that appear in three distinct regions: the stable traffic region out of the coexisting curves, metastable region existing between the stability curves (neutral and coexisting), and the unstable region within the coexisting curves, respectively.

1.6 Lattice hydrodynamic approach

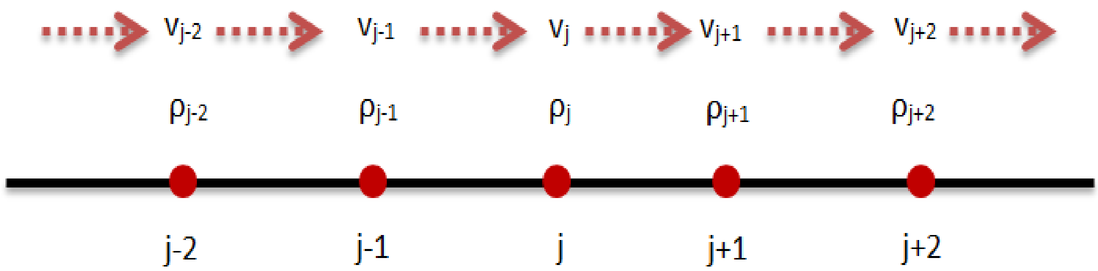

Figure 1.4: An illustration of lattice model.

Lattice model is the combination of both microscopic models [22, 23] and macroscopic hydrodynamic models [43, 77]. It analyzes the jamming transitions and separation of traffic flow phases as well as explains the evolution of traffic jams in terms of kink density waves. The concept of discrete lattice is introduced to characterize the density wave profile. The model is formed by the set of continuity equation and a momentum equation consisting of global variables and explain the aggregate properties of traffic flow. Space is discretized in the form of lattice sites and governing system of equations is derived at each site based on higher-order continuum models.

1.6.1 Basic lattice model

By considering a unidirectional road of length L without entrance or exit, Nagatani [1] proposed following continuity equation connecting the local average density $\rho(x,t)$ to local average speed $v(x,t)$:

$$\partial_t(\rho) + \partial_x(\rho v) = 0. \tag{1.6.1}$$

The local speed follows the evolution equation similar to Navier-Stokes equation with some features different from hydrodynamic models. The simplified version is:

$$\partial_t(\rho v) = a\rho_0 V(\rho(x+\delta)) - a\rho v, \tag{1.6.2}$$

in the above equation, the local density at position $x+\delta$ is denoted by $\rho(x+\delta)$, ρ_0 is average density, driver sensitivity is denoted by a which is inverse of delay time τ, i.e., $a = \frac{1}{\tau}$. Average headway is represented by δ that is related to average density ρ_0 by $\delta = \frac{1}{\rho_0}$. Local density $\rho(x+\delta)$ is inverse of headway $h(x,t)$. The basic idea behind the evolution equation is that the driver adjusts his running behavior by observing the density ahead $\rho(x+\delta)$ or observed headway $h(x,t)$. The term in right hand side of (1.6.2) indicates the tendency of traffic flow ρv to adjust to average flow $\rho_0 V(\rho(x+\delta))$ at a given density. $\rho_0 V(\rho(x+\delta))$ represents the optimal flow or current. One can observe from equation (1.6.2) that the flow is determined by both the local density $\rho(x,t)$ at position x as well as the density ahead $\rho(x+\delta)$ at position $x+\delta$. Parameters of the model are normalized such that $0 \le \rho(x) < 1$ and $0 \le v(\rho) \le V_{\max}$ [78]. Following table shows the units of important parameters:

Parameter	Unit
Density (ρ)	$veh/site$
Velocity (v)	$site/sec$
Sensitivity (a)	$(sec)^{-1}$
Delay time (τ)($\tau = \frac{1}{a}$)	sec

Table 1.5: Parameters and units of lattice model

Further, the continuity equation is improved with dimensionless space by considering $x^* = \frac{x}{\delta}$, and then replacing x^* by x following models are obtained:

$$\text{Model B}_1\text{:}\begin{cases} \partial_t(\rho) + \rho_0\partial_x(\rho v) = 0, & (1.6.3) \\ \partial_t(\rho v) = a\rho_0 V(\rho(x+1)) - a\rho v, & (1.6.4) \end{cases}$$

$$\text{Model B}_2\text{:}\begin{cases} \partial_t(\rho_j) + \rho_0(\rho_j v_j - \rho_{j-1}v_{j-1}) = 0, & (1.6.5) \\ \partial_t(\rho_j v_j) = a\rho_0 V(\rho_{j+1}) - a\rho_j v_j. & (1.6.6) \end{cases}$$

Model B_2 represent the lattice form of model B_1 where j is indicated as j^{th} site on one dimensional lattice, the density and velocity at j^{th} site are represented by ρ_j and v_j.

Optimal velocity function (as given in [22]) is described by $V(\cdot)$:

$$V(\rho_j(t)) = \frac{V_{\max}}{2}\Big[\tanh\Big(\frac{2}{\rho_0} - \frac{\rho_j(t)}{\rho_0^2} - \frac{1}{\rho_c}\Big) + \tanh\Big(\frac{1}{\rho_c}\Big)\Big], \tag{1.6.7}$$

where the inverse of safety distance is described by critical density ρ_c. By eliminating speed v from equations (1.6.3) and (1.6.4) ((1.6.5) and (1.6.6)) density equations for the models B_1 and B_2 are given by:

$$\begin{cases} \text{Model B}_1: \quad \partial_t{}^2(\rho) + a\partial_t(\rho) + a{\rho_0}^2\partial_x V(\rho(x+1)) = 0, & (1.6.8) \\ \text{Model B}_2: \quad \partial_t{}^2(\rho_j) + a\partial_t(\rho_j) + a{\rho_0}^2(V(\rho_{j+1}) - V(\rho_j)) = 0, & (1.6.9) \end{cases}$$

these density equations can be used to obtain the density waves with the help of initial and boundary conditions.

The stability conditions for the model are obtained through linear stability analysis. For which, initially uniform steady-state solution $(\rho_0, V(\rho_0))$ is considered, i.e., the vehicles are considered to move with uniform density and optimal velocity at each site. Then a linear perturbation is applied to the homogeneous density and is expanded in terms of Fourier modes. Then, the stability condition is derived that divide the entire phase plane ((ρ, a) plane) in two distinct regions stable and unstable by neutral stability curve. General form of neutral stability conditions for models B_1 and B_2 is:

$$a = Q_1(\rho_0, V^{'}). \tag{1.6.10}$$

Generally, the dynamics of traffic flow is highly complex and nonlinear which varies instantly when vehicles enter or exit the jamming situations. As explained in the previous section when jamming situations arise then traffic comes out in terms of density waves. Thus, in order to check the behavior of traffic near critical point; nonlinear analysis is performed using long wavelength expansion method and mKdV equation is derived. Solution of mKdV equation represents traffic jams in terms of kink density waves. Coexisting curves has been obtained with the help of nonlinear analysis dividing the stable region into two regions: stable and metastable region. The long wavelength perturbation grows or decays in the metastable region while the small amplitude disturbance die out in stable and metastable regions.

Because of its simplified nature lattice models got attention of researchers and many extended versions were presented by incorporating many realistic factors, such as lane changing [79–82], passing [83–85], optimal current difference effect [86–89], driver's behavior [81, 84, 87, 90–92], memory effect [93], feedback control [94–98], backward looking effect [99], forward looking effect [100], interruption probability [101–103] etc.

As in real traffic situations, roads are not always straight, a road may be curved or it may have slope; thus by incorporating the effect of road design, lattice model was further extended for curved road [104–106] both for one lane as well as two lane. The effect of passing was also investigated for curved road [107]. Recently, control theory has been applied to the lattice model for curved road [108]. In real traffic conditions there exists some external means as well, due to which freely flowing traffic get interrupted, e.g., bottlenecks, that causes serious congestion. Therefore, lattice model has been extended by incorporating the effect of bottleneck as well as on and off ramp effect [109–111] etc. As in real traffic situations, vehicular flow consists of different vehicles such as car, bus, truck, bicycle etc. and every vehicle affects the flow in its own way by having distinct properties. Thus, the effect of heterogeneous traffic mix has been incorporated in the basic lattice model [112]. Lattice model is further improved by Zhao et al. [113] by considering the effect of historical current integration in a continuous time interval and analyzed the influence of continuous historical current information on traffic stability.

Due to the simplicity in describing the traffic situations realistically, lattice models are widely used and analyzed. Theoretical investigations have made easy by linear and nonlinear analysis which helps to capture the realistic features found in traffic dynamics. Therefore, present thesis is motivated by the importance of lattice approach through which some of traffic characteristics are modeled and analyzed.

Chapter 2

Theoretical investigation of driver's behavior on curved road

Due to the huge rise in automobiles in the past few decades, jamming states of traffic has become a typical issue in modern society. Congestion on roads has the ability to adversely affect the natural environment and people's health and give rise to security risks for drivers. Therefore, to solve the problem of congestion and to provide the passengers a safe atmosphere on roadways, numerous mathematical theories came into existence.

Generally speaking, these theories characterize the dynamical system of traffic flow by utilizing statistical approach or by defining it in terms of fluid flow or hydrodynamic flow. Under the latter one, flow of traffic is regarded as compressible fluid having a certain density or concentration and a certain velocity. These analyses follow the conservation laws to present the traffic flow phenomena which assumes an empirical relation between the flow and concentration.

Following the above analysis with the aim to reduce jamming states of traffic, variety of mathematical models came into existence such as car following models [8–10, 25, 114], cellular automata models [115, 116], continuum models [117–119], hydrodynamic models [120, 121]. In Chapter 1, basic background of all these models have been discussed in detail. Among all, macroscopic hydrodynamic models are found more realistic in describing traffic flow characteristics.

Lattice model proposed by Nagatani [1] as discussed in Chapter 1, got much attention of researchers due to its capability in describing traffic jams in terms of nonlinear density waves. Following the work of Nagatani [1], many extended versions of lattice model were presented by considering important factors [79,80,86,87,99,122–124].

In real traffic flow, different driver's characteristics would affect the phenomena differ-

The content of this chapter has been published in Physica A: Statistical Mechanics and its Applications, 471: 59-67, (2017).

ently. Generally, drivers can be differentiated into three categories: timid, aggressive and normal. Aggressive drivers always overestimate the downstream density as they always try to maintain a close headway with the preceding vehicle. Aggressive and skillful drivers anticipate future traffic conditions quickly and adjust their own velocity. For aggressive drivers, their perceived optimal velocity is smaller than the actual optimal velocity due to the fact that the optimal velocity function is monotonically decreasing function. On the contrary, timid drivers always try to move by keeping a large gap with the vehicle ahead and underestimate the downstream density using a larger optimal velocity to adjust the vehicle's motion.

Thus to analyze the role of drivers, many studies are carried out which describe various aspects related to driver's behavior, i.e., driver's perception ability and attribution [125–129]. In this direction, the anticipation effect of individual behavior, driver's delay effect [81, 87, 90–92] are studied. In recent past, lattice model examining the impact of timid and aggressive drivers on two lane system is presented by Sharma [82]. Additionally, the domination of driver's characteristics on dynamics of vehicular traffic with respect to overtaking/passing is analyzed [84] in a single lane system.

It is widely known that traffic flow is a mechanical process in which interaction between different vehicles and drivers take place but road infrastructure, i.e., the formation of roads and quality of roads also play their part. If we talk about the formation of roads then there exist roads having different shapes, i.e., a road may be curved, it may have a slope, multi-lane roads, one way roads etc. According to the formation of roads, traffic phenomena is different, for example, in real traffic networks there exists a difference between straight road and curved road. The reason behind it is that while running on a curved road, movement of vehicle is affected by the centripetal force. This leads to an irregular traffic flow which is more complicated as compared to the flow on straight roads.

Some studies describing the influence of conditions of road [130] on dynamics of traffic flow have also been carried out by utilizing car following approach [131, 132] and macroscopic approach [133]. Following the idea of describing the traffic states on particular shape of road, Ros et al. [134] provides a valuable insight into how congestion can be reduced at sags by means of traffic management measures using in-car systems. While moving on a curved road, traffic turns into an unstable state frequently. To overcome this traffic state Cao and Shi [104] developed a novel lattice model for curved road by analyzing the effects of friction coefficient as well as the radius of curvature in the basic lattice model [1]. In addition, length of the curved road also matters as if the length of curve is long the flow will be more unstable. Thus, Zhou and Shi [105] extended the lattice model by including the effects of radian and angle of curved road. Further, Zhou et al. [106] extended the lattice model for curved road to two lane network by taking the lane changing effect.

It is well examined both experimentally and theoretically that the driver's behavior significantly affect the stability of flow on a straight road. As the drivers behave differently when they move on curved road, therefore it will be more adequate to analyze the effect of different drivers on a road having curved shape. Though the above discussed models for curved road considered the effect of road characteristics, but none of them is able to explain the impact of driver's characteristics on vehicular flow moving on curved road as they do not consider the driver's behavior. Thus in the present Chapter, the main motivation behind the proposed model is to develop a new lattice model for curved road by incorporating the driver's characteristics and investigate their effect.

The Chapter is organized in 5 sections: Section 2.1 refers to the model formulated by introducing driver's behavior, friction coefficient, radius of curvature and angle of the curved road. In the next section 2.2, linear stability analysis is used and stability conditions are derived. The propagation behavior of traffic jams has been described in section 2.3 by using nonlinear analysis. In section 2.4, simulation results are discussed and finally in section 2.5, conclusion and future scope is given.

2.1 Mathematical models

2.1.1 Lattice model for curved road

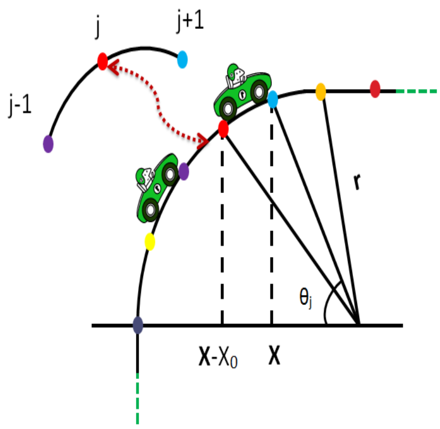

Figure 2.1: The illustration of lattice model for a curved road.

The basic lattice model considers the situation of single lane straight road but as mentioned in Chapter 1, real traffic situations consists of roads having bends or curves. Thus by taking into account the situation of a curved road, the effects of radius of curved road and friction coefficient are examined by Cao and Shi [104]. In real traffic conditions (as shown in Fig. 2.1) while moving on curved road, centripetal force $f = \mu mg$ consisting of μ (friction coefficient), m (mass of vehicle) and g (gravity due to acceleration), acts on the running vehicles. Let us consider the total length of the curved section be $\mathbf{X} = \mathbf{r}\theta$, where $\mathbf{r}$ and θ are the radius and central angle of the curved road section, respectively. By defining the relationship among arc and central angle of the curved road, i.e., $\mathbf{X}_j(t) = \mathbf{r}\theta_j(t)$ and $\Delta\mathbf{X}_j(t) = \mathbf{r}\Delta\theta_j(t)$, the optimal velocity function takes the following form:

$$V\Big(\frac{1}{\mathbf{r}\Delta\theta_j(t)}\Big) = \frac{\mathbf{r}\omega_{\max}}{2}\Big[\tanh\Big(\mathbf{r}\Delta\theta_j(t) - \frac{1}{\rho_c}\Big) + \tanh\Big(\frac{1}{\rho_c}\Big)\Big], \tag{2.1.1}$$

where $\omega_{\max}$ is the maximum angular velocity. According to Newton's second law, $m{\omega^2}_{\max}\mathbf{r} = \mu mg$, we have $\omega_{\max} = \sqrt{\frac{\mu g}{\mathbf{r}}}$ and $\Delta\mathbf{X}_j(t) = \mathbf{r}\Delta\theta_j(t) = \frac{1}{\rho_j(t)}, h_c = \frac{1}{\rho_c}$. Therefore, the above optimal velocity function (2.1.1) indicates that increasing radius of curved road and friction coefficient leads to increasing ideal maximum velocity $V_{\max} = \sqrt{\mu g\mathbf{r}}$. Due to the complexity of driving on curved road section, drivers move their vehicle at low speed thus the real maximum velocity is far less than the ideal maximum velocity. So, by introducing a modified coefficient ${k_1}^1 (0 < {k_1}^1 \leq 1)$ of the maximum velocity, the optimal velocity function takes the following form [104]:

$$V(\rho_j(t)) = \frac{{k_1}^1\sqrt{\mu g\mathbf{r}}}{2}\Big[\tanh\Big(\frac{2}{\rho_0} - \frac{\rho_j(t)}{\rho_0^2} - \frac{1}{\rho_c}\Big) + \tanh\Big(\frac{1}{\rho_c}\Big)\Big]. \tag{2.1.2}$$

2.1.2 Lattice model for driver's behavior on curved road

Further, the above model was modified by Zhou and Shi [105] by introducing the influence of radian of curved road. The distance $y = \sqrt{(\mathbf{r})^2 - (\mathbf{X} - \mathbf{r})^2}$ denotes the characteristics of the curved road, where the curvature radius of curved road is represented by $\mathbf{r}$. The lattice spacing between the site j and $j-1$ is:

$$l = \int_{X-X_0}^{X} \sqrt{1 + y'^2}dx = \frac{X_0}{\sin\theta_j}, \tag{2.1.3}$$

where the radian of curved road at j^{th} site is denoted by θ_j. The modified lattice spacing of the curved road can be used to compute the average headway on curved road in relation to the average headway on a straight road ($\frac{1}{\rho_0}$). Therefore, the basic lattice model of Nagatani [1] is modified for curved road and is given as:

$$\partial_t(\rho_j) + \frac{\rho_0}{\sin\theta_j}(\rho_j v_j - \rho_{j-1}v_{j-1}) = 0, \tag{2.1.4}$$

$$\partial_t(\rho_j v_j) = a\Big[\frac{\rho_0}{\sin\theta_j}V(\rho_{j+1}) - \rho_j v_j\Big]. \tag{2.1.5}$$

There exists different factors which influence the flow of traffic and among them, one and most important factor is the behavior of drivers. On the behalf of different driver's characteristics namely aggressive, normal and timid, drivers observe inter-vehicular spacing differently. Aggressive (timid) drivers overestimate (underestimate) downstream density as compared to normal drivers. The effect of driver's behavior is included in a modified evolution equation by Sharma [82] by incorporating a factor p that reflects the influence of driver's characteristics with the consideration of anticipation effect on traffic system as:

$$\rho_j(t+\tau)v_j(t+\tau) = \rho_0[pV(\rho_{j+1}(t+\alpha\tau)) + (1-p)V(\rho_{j+1}(t-\alpha\tau))]. \tag{2.1.6}$$

We further modified the above evolution equation (2.1.6) to incorporate the influence of driver's behavior on curved road and write it in fully discrete form as:

$$\rho_j(t+\tau)v_j(t+\tau) = \frac{\rho_0}{\sin\theta_j}[pV(\rho_{j+1}(t+\alpha\tau)) + (1-p)V(\rho_{j+1}(t-\alpha\tau))], \tag{2.1.7}$$

where as mentioned above, ρ_0 is average density on straight road and $\frac{1}{\sin\theta_j}$ is the factor for curved road. The parameter α is the coefficient of driver's anticipation effect (DAE) corresponding to driver's behavior. Parameter $0 \leq p \leq 1$ denotes the intensity of influence of driver's behavior in traffic stream. Larger value of p corresponds to aggressive driver's characteristics while smaller values of p represent timid driver's characteristics. With the help of Taylor series expansion and ignoring higher order terms in (2.1.7), we obtained:

$$\rho_j(t+\tau)v_j(t+\tau) = \frac{\rho_0}{\sin\theta_j}[V(\rho_{j+1}(t)) + (2p-1)(\alpha\tau)V'(\rho_{j+1}(t))\partial_t(\rho_{j+1}(t))]. \tag{2.1.8}$$

Eliminating speed v_j from (2.1.4) and (2.1.8), the density evolution equation is obtained as:

$$\begin{aligned}\rho_j(t+2\tau) - \rho_j(t+\tau) + \frac{\tau\rho_0^2}{\sin^2\theta_j}[V(\rho_{j+1}(t)) - V(\rho_j(t))] + \frac{\tau\rho_0^2}{\sin^2\theta_j}\\ (2p-1)\alpha[V'(\rho_{j+1}(t))\tilde{\Delta}\rho_{j+1}(t) - V'(\rho_j(t))\tilde{\Delta}\rho_j(t)] = 0,\end{aligned} \tag{2.1.9}$$

where $\tilde{\Delta}\rho_j(t) = \rho_j(t+\tau) - \rho_j(t)$.

The proposed model reduces to the model for curved road [105] when the parameters α and p takes the values $\alpha = 0$ and $p = 0$ or $p = 1$.

2.2 Linear stability analysis

We check the impact of driver's characteristics on the jamming transitions of traffic flow on a curved road through linear stability analysis. Suppose the vehicles are moving on curved road with uniform density ρ_0 and equilibrium velocity $V(\rho_0)$. Hence, the solution of uniform steady-state is:

$$\rho_j(t) = \rho_0, \quad v_j(t) = V(\rho_0). \tag{2.2.1}$$

Now, we gave a small deviation in terms of $y_j(t)$ to the uniform steady-state solution at j^{th} site and got the perturbed density as follows:

$$\rho_j(t) = \rho_0 + y_j(t). \tag{2.2.2}$$

Inserting the above perturbed density profile (2.2.2) and using (2.2.1) into (2.1.9) and linearizing the equation for $y_j(t)$, we obtained:

$$y_j(t+2\tau)-y_j(t+\tau)+\frac{\tau\rho_0^2}{\sin^2\theta_j}V'(\rho_0)\Delta y_j(t)+\frac{\tau\rho_0^2}{\sin^2\theta_j}(2p-1)\alpha V'(\rho_0)\tilde{\Delta}(\Delta y_j(t)) = 0, \tag{2.2.3}$$

where $V'(\rho_0)$ represents the derivative of $V(\rho)$ at point $\rho = \rho_0$. Assuming the deviation as $y_j(t) = \mathrm{e}^{(ikj+zt)}$ which results:

$$e^{2z\tau} - e^{z\tau} + \frac{\tau\rho_0^2}{\sin^2\theta_j}V'(\rho_0)(e^{ik}-1) + \frac{\tau\rho_0^2}{\sin^2\theta_j}(2p-1)\alpha V'(\rho_0)(e^{z\tau}-1)(\mathrm{e}^{ik}-1) = 0. \tag{2.2.4}$$

Putting $z = z_1(ik) + z_2(ik)^2.....$ into (2.2.4), the coefficients of (ik) and $(ik)^2$ are obtained as:

$$z_1 = -\frac{\rho_0^2}{\sin^2\theta_j}V'(\rho_0), \tag{2.2.5}$$

$$z_2 = -\frac{3}{2}\tau\Big[\frac{\rho_0^4}{\sin^4\theta_j}V'^2(\rho_0)\Big] - \frac{\rho_0^2 V'(\rho_0)}{2\sin^2\theta_j} + \frac{\rho_0^4\tau}{\sin^4\theta_j}(2p-1)\alpha V'^2(\rho_0). \tag{2.2.6}$$

If $z_2 > 0$, then homogenous steady-state flow becomes stable and if $z_2 < 0$ then it leads to unstable state. Therefore, the stability condition for the homogeneous flow is:

$$\tau < \frac{\sin^2\theta_j}{(-3 + 2(2p-1)\alpha)(\rho_0^2 V'(\rho_0))}, \tag{2.2.7}$$

the neutral stability criterion is given by:

$$\tau = \frac{\sin^2\theta_j}{(-3 + 2(2p-1)\alpha)(\rho_0^2 V'(\rho_0))}. \tag{2.2.8}$$

For $\alpha = 0$ and $\theta_j = \pi/2$, the above stability criteria recover the results of basic lattice model [1] and when $\alpha = 0$ and $p = 0.5$ the model reduces to the one discussed in [105]. It can be easily depicted from equation (2.2.8) that driver's behavior and the parameters representing the characteristics of curved road, significantly affect the stability of the traffic flow.

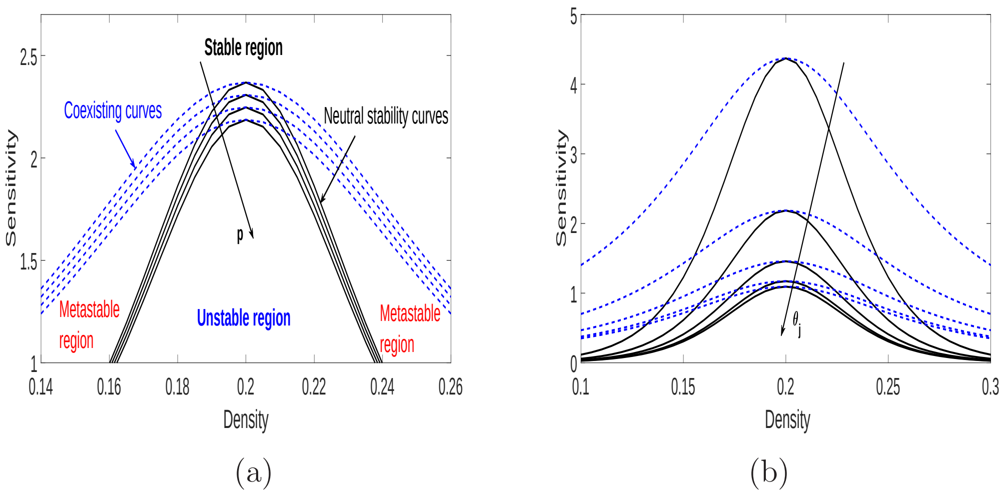

Figure 2.2: Phase plot in (ρ, a) space with $\rho_0 = \rho_c = 0.2$, $\mu = 0.3$, $\mathbf{r} = 10$, ${k_1}^1 = 0.14$ for (a) $p = 0.2,\ 0.4,\ 0.6,\ 0.8$ (b) $\theta_j = \pi/6,\ \pi/4,\ \pi/3,\ 5\pi/12,\ \pi/2$.

The neutral stability curves in (ρ, a) plane are displayed using black curves for different values of p in Fig. 2.2(a) and for θ_j in Fig. 2.2(b). From Fig. 2.2(a) it is clear that the apex of each curve (ρ_c, a_c) decreases with increasing value of p. The pattern shows that with increasing value of p, stable region increases. As mentioned in the previous section that larger values of p denote more aggressive drivers in the traffic stream and by nature, they drive fast leading to less congestion and the flow becomes stable. The case of timid drivers can be explained in a similar fashion.

The black curves in Fig. 2.2(b) represents the neutral stability curves for different values of θ_j, i.e., $\theta_j = \pi/6,\ \pi/4,\ \pi/3,\ 5\pi/12,\ \pi/2$. The pattern shows that for increasing values of θ_j, the stable region increases. Which can be described by the fact that if the curve of road is more then there will be more congestion. Due to an increase in the angle, the bend of curved road reduces which forces the drivers to increase their speed and the flow becomes more stable. Moreover, for particular value $\theta_j = \pi/2$, the curved road becomes straight and the maximum stable region can be achieved.

2.3 Nonlinear stability analysis

We examine the evolution properties of traffic congestion around the critical point (ρ_c, a_c) on coarse-grained scale by applying reduction perturbation method. The slow variables X and T for $0 < \epsilon \leq 1$ are described by:

$$X = \epsilon(j + bt), \quad T = \epsilon^3(t), \tag{2.3.1}$$

the constant term b in (2.3.1) needs to be obtained. Let the density ρ_j at j^{th} site satisfy the equation:

$$\rho_j(t) = \rho_c + \epsilon R(X, T). \tag{2.3.2}$$

By putting the slow variables X and T defined in (2.3.1) and the perturbed density profile (2.3.2), expand (2.1.9) with the help of Taylor series expansion up to fifth-order of ϵ, the resulting nonlinear equation is obtained as under:

$$\begin{aligned}\epsilon^2 k_1 \partial_X R + \epsilon^3 k_2 \partial_X^2 R + \epsilon^4(\partial_T R + k_3 \partial_X^3 R + k_4 \partial_X R^3) + \epsilon^5(k_5 \partial_T \partial_X R \\ + k_6 \partial_X^4 R + k_7 \partial_X^2 R^3) = 0.\end{aligned} \tag{2.3.3}$$

Table 2.1 gives the values of $k_i (i = 1, 2, 3, ..., 7)$, $V' = \frac{dV(\rho)}{d\rho}\Big|_{\rho=\rho_c} = -\frac{A_1}{\rho_0^2}$ and $V''' = \frac{d^3V(\rho)}{d\rho^3}\Big|_{\rho=\rho_c} = \frac{2A_1}{\rho_0^6}$, $A_1 = \frac{{k_1}^1\sqrt{\mu g \mathbf{r}}}{2}$. Let us take the value of τ near (ρ_c, a_c) as:

$$\tau = \tau_c(\epsilon^2 + 1). \tag{2.3.4}$$

By utilizing the constant $b = \frac{-\rho_c^2 V'}{\sin^2\theta_j}$ and removing the terms of ϵ having second and third-order, we get:

$$\epsilon^4(\partial_T R - g_1 \partial_X^3 R + g_2 \partial_X R^3) + \epsilon^5(g_3 \partial_X^2 R + g_4 \partial_X^4 R + g_5 \partial_X^2 R^3) = 0, \tag{2.3.5}$$

the values of ${g_i}'s (i = 1, 2, ..., 5)$ are given in Table 2.2. Following transformations are adopted to convert (2.3.5) into standard mKdV equation:

$$T' = g_1 T, \quad R = \sqrt{\frac{g_1}{g_2}} R', \tag{2.3.6}$$

The coefficients k_i of the model	
k_1	$b+\frac{\rho_c^2 V'}{\sin^2\theta_j}$
k_2	$\frac{3}{2}b^2\tau+\frac{\rho_c^2 V'}{\sin^2\theta_j}\left[\frac{1}{2}+(2p-1)\alpha b\tau\right]$
k_3	$\frac{7}{6}b^3\tau^2+\frac{\rho_c^2 V'}{6\sin^2\theta_j}\left[1+3(2p-1)\alpha b\tau(1+b\tau)\right]$
k_4	$\frac{\rho_c^2 V'''}{6\sin^2\theta_j}$
k_5	$3b\tau+\frac{\rho_c^2 V'}{\sin^2\theta_j}(2p-1)\alpha\tau$
k_6	$\frac{5}{8}b^4\tau^3+\frac{\rho_c^2 V'}{24\sin^2\theta_j}\left[1+(2p-1)\alpha b\tau(4+6b\tau+4b^2\tau^2)\right]$
k_7	$\frac{\rho_c^2 V'''}{12\sin^2\theta_j}$

Table 2.1: The coefficients k_i of the model

The coefficients g_i of the model	
g_1	$-\frac{7}{6}b^3{\tau_c}^2-\frac{\rho_c^2 V'}{\sin^2\theta_j}\left[\frac{1}{6}+\frac{1}{2}(2p-1)\alpha b\tau_c(1+b\tau_c)\right]$
g_2	$\frac{\rho_c^2 V'''}{6\sin^2\theta_j}$
g_3	$\frac{3}{2}b^2\tau_c+\frac{\rho_c^2 V'}{\sin^2\theta_j}(2p-1)\alpha b\tau_c$
g_4	$\frac{\rho_c^2 V'}{24\sin^2\theta_j}\left[1+(2p-1)\alpha b\tau_c(4+6b\tau_c+4b^2{\tau_c}^2)\right]+\frac{5}{8}b^4{\tau_c}^3$ $+\left[3b+\frac{\rho_c^2 V'}{\sin^2\theta_j}(2p-1)\alpha\right]\tau_c g_1$
g_5	$-\left[3b+\frac{\rho_c^2 V'}{\sin^2\theta_j}(2p-1)\alpha\right]g_2\tau_c+\frac{\rho_c^2 V'''}{12\sin^2\theta_j}$

Table 2.2: The coefficients g_i of the model

So, the formation of equation (2.3.5) into standard mKdV equation is given below:

$$\partial_{T'}R^{'}-\partial_X^3 R^{'}+\partial_X R^{'3}+\epsilon M[R^{'}]=0, \tag{2.3.7}$$

where $M[R'] = \frac{1}{g_1}[g_3\partial_X^2 R' + g_4\partial_X^4 R' + \frac{g_1 g_5}{g_2}\partial_X^2 R'^3]$. For getting the solution of standard mKdV equation, higher-order terms of ϵ are ignored from (2.3.7) which results:

$$R_0'(X, T') = \sqrt{L_1}\,\tanh\Big(\sqrt{\frac{L_1}{2}}(X - L_1 T')\Big), \tag{2.3.8}$$

where the propagation velocity L_1 is computed as:

$$L_1 = \frac{5g_2 g_3}{2g_2 g_4 - 3g_1 g_5}, \tag{2.3.9}$$

by solving the following necessary criterion:

$$(R_0', M[R_0']) \equiv \int_{-\infty}^{\infty} dX R_0' M[R_0'] = 0, \tag{2.3.10}$$

when $M[R_0'] = M[R']$. Finally, the kink solution is determined:

$$\rho_j = \rho_c + \epsilon\sqrt{\frac{g_1 L_1}{g_2}}\tanh\Big(\sqrt{\frac{L_1}{2}}(X - L_1 g_1 T)\Big), \tag{2.3.11}$$

where $\epsilon^2 = \Big(\frac{a_c}{a} - 1\Big)$ and the amplitude a_m of the solution take the value:

$$a_m = \sqrt{\frac{g_1}{g_2}\epsilon^2 L_1}.$$

The coexisting phase consisting of the free flow and jammed phase is represented by the kink antikink solution (2.3.11) described by $\rho_j = \rho_c \pm a_m$ in (ρ, a) space. Dotted curves in blue color (coexisting curves) and solid black curves (neutral stability curves) both split the whole space into three distinct regions (see Fig. 2.2(a)-(b)): the stable region which is above the coexisting curves, metastable region in between the coexisting curves and neutral stability curves and the unstable region comes under the neutral stability curves. It is clear from the figures that the apex of each curve lower down with increasing values of p and θ_j which means that aggressive drivers and bigger value of the angle of the curved road affect positively the flow stability.

2.4 Numerical simulation

With the aim to examine the capability of the new model in explaining the influence of driver's behavior on traffic flow dynamics over a curved road and to test the validity of theoretical findings, simulation is performed in this section for the extended model. Periodic boundary condition is applied and the initial condition is adopted as:

$$\rho_j(1) = \rho_j(0) = \begin{cases} \rho_0; & j \neq \frac{N}{2}, \frac{N}{2} - 1 \\ \rho_0 - \sigma; & j = \frac{N}{2} \\ \rho_0 + \sigma; & j = \frac{N}{2} - 1, \end{cases} \tag{2.4.1}$$

where the initial disturbance $\sigma = 0.05$, total number of lattice sites $N = 100$, maximum time $t = 10^5$ sec., and the other parameters are chosen as $\rho_0 = \rho_c = 0.2, \mu = 0.3,\ \mathbf{r} = 10,\ g = 10,\ {k_1}^1 = 0.14,\ \alpha = 0.1$.

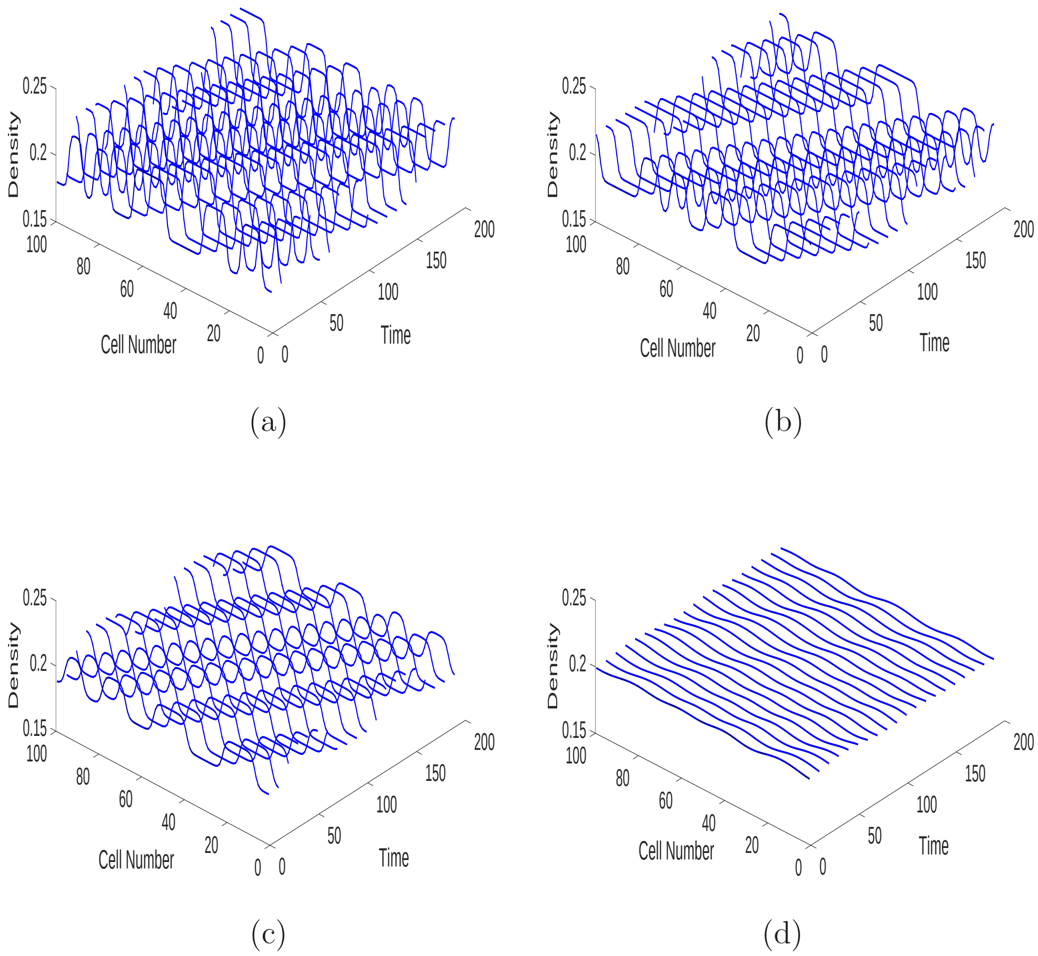

Figure 2.3: Spatiotemporal evolution of density when $a = 2.2$ and $\theta_j = \pi/4$ for (a) $p = 0.2$, (b) $p = 0.4$, (c) $p = 0.6$ and (d) $p = 0.8$.

Fig. 2.3 shows the influence of parameter p on space-time evolution of density obtained from the simulation after sufficiently long time $t = 9.9 \times 10^4 - 10^5$ sec. for fixed value of θ_j. It is observed from Fig. 2.3(a)-2.3(c) that the flow is in unstable state as the stability condition is not fulfilled and the initial homogeneous flow will turn into traffic jam under a small perturbation. The kink antikink soliton of the mKdV equation, obtained from the

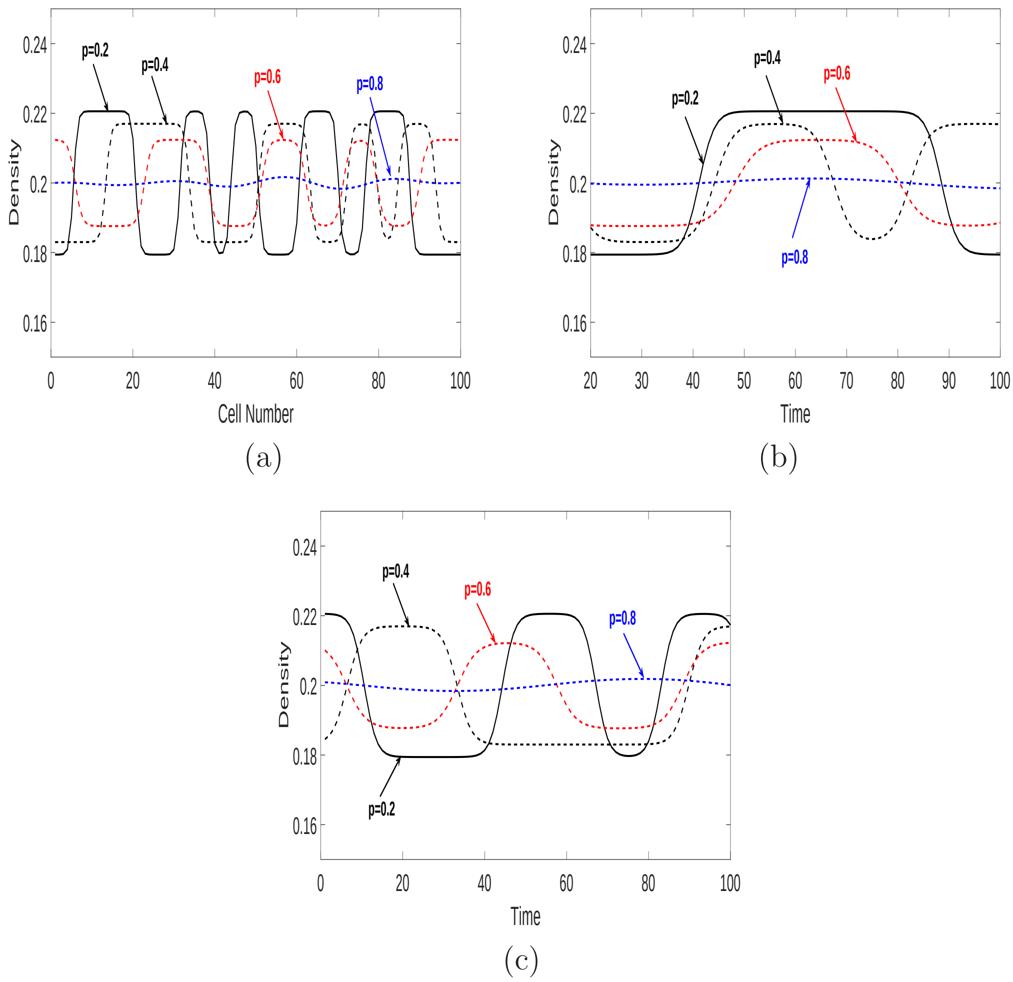

Figure 2.4: Density profiles for different values of p at (a) $t = 8 \times 10^4$ sec., (b) $t = 9.99 \times 10^4 - 10^5$ sec. on lattice site 45 and (c) lattice site 70.

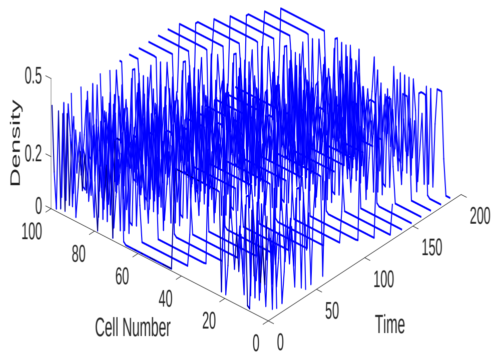

(a)

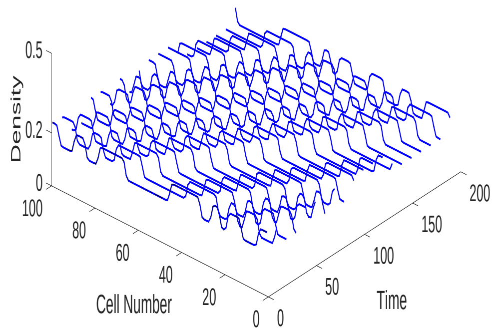

(b)

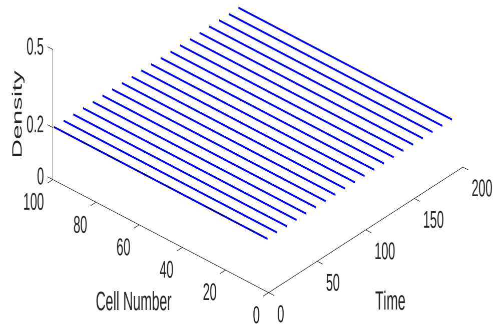

(c)

Figure 2.5: Space-time evolutions of density waves when $a = 3.5$ and $p = 0.8$ for (a) $\theta_j = \pi/12$, (b) $\theta_j = \pi/6$ and (c) $\theta_j = \pi/4$.

nonlinear analysis in section 2.3, express the propagation behavior of the traffic congestion. However, in Fig. 2.3(d) the density wave is uniform and the traffic is smooth over the whole space with the same sensitivity for higher value of p. This indicates that the aggressive driver's behavior can prevent the evolution of traffic congestion and improve the stability of flow over the curved road.

Fig. 2.4(a) describes the density profile for different values of p at fixed time $t = 8 \times 10^4$ sec. and Fig. 2.4(b)-2.4(c) at time $t = 9.99 \times 10^4 - 10^5$ sec. for fixed lattice sites 45 and 70, respectively, corresponding to the panel of Fig. 2.3. By analyzing Fig. 2.4, one can observe that the amplitude of the stop and go waves reduce slowly and finally becomes uniform with increasing values of parameter p. In particular, it can be said that aggressive drivers having positive effects on reducing traffic congestion over a curved road. All these results are consistent with the theoretical analysis discussed in previous sections.

Now, we analyzed the effect of radian of the curved road on traffic dynamics. Fig. 2.5(a)-

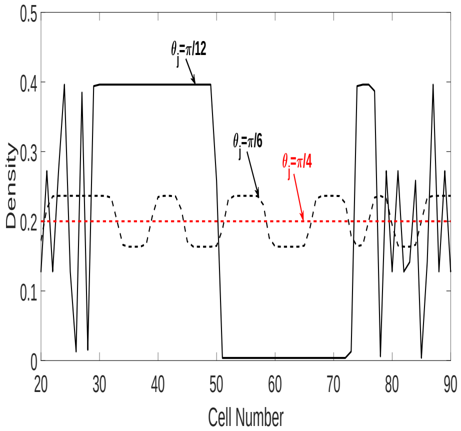

(a)

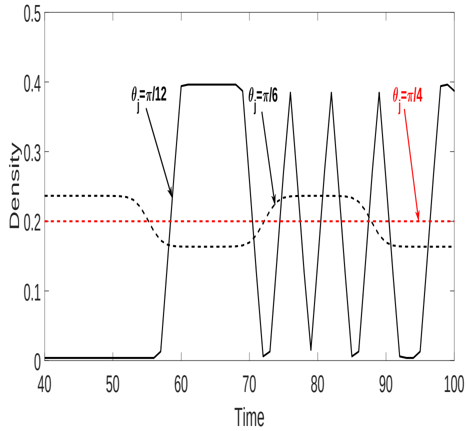

(b)

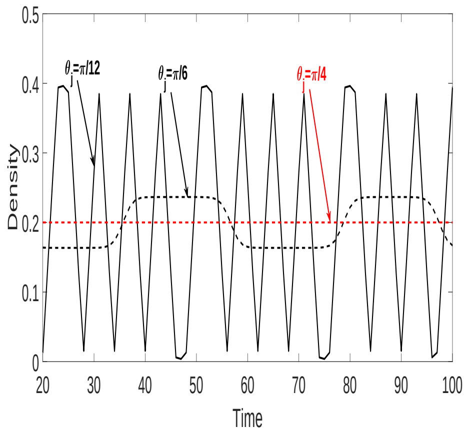

(c)

Figure 2.6: Density wave profile for different θ_j at (a) $t = 8 \times 10^4$ sec., (b) $t = 9.99 \times 10^4 - 10^5$ sec. on lattice site 45 and (c) lattice site 70.

2.5(c) represent the spatiotemporal evolution of density computed from simulation after $t = 9.9 \times 10^4 - 10^5$ sec. time steps with fixed p for distinct values of parameter θ_j. The figures show that at initial level, kink antikink soliton occurs propagating in backward direction for smaller values of θ_j. The initial small amplitude disturbance in the steady-state flow develop into jammed flow characterized by kink antikink density waves when the condition of stability is not fulfilled. However, kink antikink density waves disappear gradually and the traffic flow becomes stable for $\theta_j = \pi/4$. It is worth to mention here that the larger value of $\theta_j = \pi/2$ represents the characteristics of the straight road.

Fig. 2.6 (a) describe the density profiles for different θ_j at time $t = 8 \times 10^4$ sec. with respect to the panel of Fig. 2.5. Fig. 2.6(a) shows that a density wave in kink antikink shape appears for small values of θ_j. The results reveal the situation of stop-start density waves in traffic stream. The stop and go density waves die out gradually and finally develops into homogeneous flow with increasing θ_j. The density profiles at time $t = 9.99 \times 10^4 - 10^5$ sec. for fixed lattice sites, 45 and 70 is also shown in Fig. 2.6(b)-2.6(c), respectively. These results ensure that the radian of curved road significantly affect the dynamic process of traffic flow. As θ_j increases and curved road approaches to straight road, the traffic becomes stable against the small disturbance. The results of simulation are compatible with the theoretical results which validate the fact that traffic flow characteristics on curved road are more complex as compared to the straight road. Thus, conclusion of the overall findings is that both the driver's behavior and road characteristics impact significantly the dynamics of traffic flow on a unidirectional one lane road.

2.5 Conclusion

2.5.1 Outcomes:

- To examine the influence of two major aspects of real traffic problems, i.e., driver's behavior and geometric design of road, basic lattice model is extended by considering the impact of driver's characteristics and curved road on traffic flow.
- Theoretical observations regarding the effect of driver's behavior and radian of curved road on traffic dynamics are made through linear and nonlinear analysis.
- In order to represent traffic jam in terms of kink density waves, mKdV equation is obtained close to critical point by nonlinear analysis.
- Effect of important parameters p and curved road angle θ_j are examined and results are compared in the density-sensitivity phase plane. Increase in both aggressive driver's characteristics and radian of the curved road enhances the stability in the flow.

- For small radian of curved road when traffic will be in an unstable state, aggressive driver's characteristics can help in reducing the traffic congestion.

2.5.2 Future scope:

- The newly developed model is suitable to analyze the influence of curved road on traffic dynamics yet the model can be extended to examine the influence of many crucial phenomena present in real traffic such as passing, lane changing etc.
- It can also be utilized to explore the impact of other significant characteristics of traffic dynamics such as energy and fuel consumption etc.
- Experimental investigations should be performed to verify the theoretical predictions.

Chapter 3

The analysis of driver's anticipation effect on slopy curved road

Nonlinear vehicular flow is becoming highly complex and congested as there are million of vehicles interacting with each other and affect the overall movement of traffic. Over congestion on roads sometimes become the reason of accidents and environmental pollution which adversely affect the quality of human life. As traffic flow is a dynamical process occurring in both space and time, therefore the spatiotemporal patterns exhibited by vehicular traffic are complex similar to the system. Congested state of traffic can be defined as a state where average vehicular velocity is below the minimum possible average velocity in free flow. Thus, traffic jams can be categorized into two types: spontaneous jams which propagates backward as stop-start waves and stationary jams that arises due to sudden deceleration or interruption at any segment of road.

To analyze the complex nature behind traffic jams and to control it effectively, variety of models came into existence [11, 25, 114–121, 135]. Pipes [17] developed classical car following model in early $1950'$s. Following the classical approach, many advanced car following models were proposed by Edie [136], Newell [137], Gazis [16]. The classical theory was further improved by the development of optimal velocity model (OVM) [22] as described in Chapter 1. Further, generalized force model (GFM) [24] was introduced to overcome the deficiency of unrealistic deceleration and too high acceleration present in OVM. Later, full velocity difference model (FVDM) [25] was proposed to overcome the fault present in GFM which was unable to analyze the influence of delay time and the kinematic wave velocity on the density wave.

As discussed in Chapter 1 lattice hydrodynamic model, by combining the properties of microscopic and continuum models, was developed and later many extensions were proposed [79, 86–89, 99, 122–124, 138–140]. Modeling of traffic features address human behavior indirectly. As the principal goal of every driver is to arrive at his destination at earliest possible time by guiding his vehicle in a safe manner. Therefore, the task of achieving driver's goal is based on action which can be classified into perception, judgement, decision, and con-

The content of this chapter has been published in Physica A: Statistical Mechanics and its Applications, 499: 110-120, (2018).

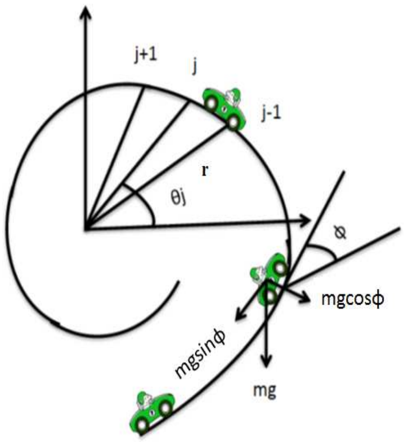

Figure 3.1: The illustration of lattice model for a curved road with slope.

trol. The category of control consists of the actions of acceleration and control of steering. To perform the steering task the driver tries to choose a reference point to regulate the misalignment or divergence of vehicle. The acceleration control consists of identifying velocity and/or spacing differences and taking actions to avoid harmful conditions. Therefore, several traffic flow models, as discussed in Chapter 2, introduce parameters describing various characteristics of drivers; most importantly, driver's anticipation effect [81, 84, 87, 90–92, 141] in the driver-vehicle system.

The major reason behind traffic jams is the slowdown sections that may exist due to the bottleneck region, accidental area, residential area, curved road section or section of road having a slope. Traffic situations based on the geometrical design of roads is totally different from that on straight roads. Therefore, the research for various forms of roads is the prevailing issue. In this direction, the effects of curved road on traffic flow were described as explained in Chapter 2. In addition, Li et al. [142] and He et al. [143] developed a new optimal velocity model (OVM) and examined the effect slope with and without gravity respectively. After that Komada et al. [144] analyzed the effect of gravitational force by taking into account different slopes on curved road. Lan et al. [145] developed a cellular automaton model to examine the slope effects. Further, Zhu and Yu [146] studied the characteristics of traffic flow by taking into account the brake distance as a function of slope and investigate its properties. Chen et al. [147] presented an extended model by taking into account the slope effects. Following this series, Zhu and Zhang [148] presented novel lattice model by examining the effect of slope and the solitary density waves in the metastable region were reproduced. Gupta et al. [149] presented lattice hydrodynamic model on a gradient road with different slopes by incorporating the effect of optimal current difference. Recently, Meng and Yan [150] presented car following model by using control theory and analyzed the effects of curved road with slope on traffic dynamics on a single channel. All the above mentioned models incorporate some realistic features of traffic flow but they can not be utilized to analyze the traffic behavior on a two lane curved road having some slope when lane changing is allowed. Present Chapter is an attempt to develop a realistic lattice model for a curved road with slope by incorporating the driver's anticipation effect.

Organization of the chapter is followed by 5 sections: Section 3.1 is devoted to discuss an improved lattice model by incorporating the anticipation effect of drivers on a slopy curved road. The stability conditions are derived using linear and nonlinear stability analysis in section 3.2 and 3.3, respectively. Numerical simulation is performed and the result discussion is done in section 3.4. At last, the conclusion of results is given in section 3.5.

3.1 Models for curved road with slope

3.1.1 Car following model

Recently, Meng and Yan [150] presented car following model by following the FVDM [25] and analyzed the effects of curved road with slope as well as the effects of curvature radius and friction coefficient. Let us assume the vehicles are moving on curved road with slope as shown in Fig. 3.1. Two types of forces work on the vehicles, one is a gravitational force and the other is the centripetal force. A horizontal and a vertical force of amplitude $mg\sin\phi$, $mg\cos\phi$ acts upon the running vehicle. Moreover, a central force of magnitude $\mu mg\cos\phi$ work upon the vehicle where m is mass and g is gravity acceleration. Let us consider the section of slopy curved road of length $\mathbf{X} = R_1\theta$ where R_1 is the curvature radius and θ is the angle of the curved road. The radius of curvature R_1 is formulated by the relation $R_1 = \frac{\mathbf{r}}{\cos\phi}$. Traffic flow model for curved road with slope based on FVDM is:

$$R_1\ddot{\theta}_n(t) = a(V(R_1\Delta\theta_n(t)) - R_1\dot{\theta}_n(t)) + \lambda_1\Delta\dot{\theta}_n(t), \tag{3.1.1}$$

where $R_1\theta_n(t)$ is the position of n^{th} vehicle at time t, $R_1\Delta\theta_n(t) = R_1\theta_{n+1}(t) - R_1\theta_n(t)$ is the arc headway of vehicle n at time t, $a = \frac{1}{\tau}$ is the sensitivity of driver, τ is the delay time, λ_1 is the sensitivity coefficient of a driver to the velocity difference, $R_1\dot{\theta}_n(t)$ and $R_1\ddot{\theta}_n(t)$ are respectively the velocity and acceleration of the n^{th} vehicle. Following the properties of optimal velocity function given in [22], following function is chosen for curved road with slope:

$$V(R_1\Delta\theta_n(t)) = \frac{R_1\omega_{\max} \mp V_{g,\max}}{2}[\tanh(R_1\Delta\theta_n(t) - h_c(\phi)) + \tanh(h_c(\phi))], \tag{3.1.2}$$

where $\omega_{\max}$ denotes maximum angular velocity and $h_c(\phi)$ is the safe arc distance given by the following relation:

$$h_c(\phi) = h_c(1 \mp \beta\sin(\phi)), \tag{3.1.3}$$

where h_c denotes the safety distance on straight road and β is a constant chosen equal to 1. $h_c(\phi)$ is modeled with the idea that as the slope increases, the brake distance decreases for uphill position and when moving towards downhill situation the brake distance increases with increasing slope. Based on the centripetal force formula we have $m\omega_{\max}^2 R_1 = \mu mg\cos\phi$ for which:

$$\omega_{\max} = \sqrt{\frac{\mu g\cos\phi}{R_1}}. \tag{3.1.4}$$

$V_{g,\max}$ in equation (3.1.2) is maximal reduced or enhanced velocity corresponding to uphill and downhill situations, respectively. The formulation of $V_{g,\max}$ is given by:

$$V_{g,\max} = \frac{mg\sin\phi}{\mu_1}, \tag{3.1.5}$$

where μ_1 is the longitudinal friction coefficient. For the sake of simplicity we take $\frac{mg}{\mu_1} = 1$, thus $V_{g,\max} = \sin\phi$. In traffic problems, the maximum angular velocity is less than the theoretic values. So, parameter ${k_2}^1 (0 < {k_2}^1 \leq 1)$ is chosen and by putting (3.1.4) and (3.1.5) in (3.1.2) optimal velocity function can be rewritten as:

$$V(R_1\Delta\theta_n(t)) = \frac{{k_2}^1\sqrt{\mu g R_1\cos\phi} \mp \sin\phi}{2}[\tanh(R_1\Delta\theta_n(t) - h_c(\phi)) + \tanh(h_c(\phi))]. \tag{3.1.6}$$

3.1.2 Extended lattice models

Lattice version of hydrodynamic models advised by Nagatani [1], as discussed in Chapter 1, explain the characteristics of unidirectional one lane road. But the given model was unable to explain the common lane changing behavior in multi lane traffic flow. Thus to capture the realistic features of traffic using lattice model, Nagatani extended it for two lane system [79] by considering the lane change effect into continuity equation while evolution equation remains unaltered.

$$\partial_t\rho_j + \rho_0(\rho_j v_j - \rho_{j-1}v_{j-1}) = \gamma|{\rho_0}^2 V'(\rho_0)|(\rho_{j+1} - 2\rho_j + \rho_{j-1}), \tag{3.1.7}$$

where γ represent the lane changing parameter and ρ_j represent the combined average local density at j^{th} site and $\rho_j v_j$ is termed as local flow at j^{th} site under two lane system. The choice of the proportionality constant $\gamma|{\rho_0}^2 V'(\rho_0)|$ is made so that it becomes dimensionless.

Further, lattice model was developed for curved road by Cao and Shi [104] by introducing new optimal velocity function (as discussed in Chapter 2) and many extended versions [105, 106, 151] also came into existence by incorporating important parameters describing features of real traffic situations. Traffic situations not only deals with vehicle-vehicle interaction or vehicle-road interaction but it deals with driver's interaction as well. Because there exist different drivers and their perception ability varies in different traffic situations. With the purpose to capture the role of different drivers in the dynamic process many studies are carried out [81, 82, 84, 90–92, 125, 127–129, 141]. In this sequence, considering anticipation effect of drivers with respect to the optimal current difference, lattice model was improved for two lane highway by Sharma [87] and the evolution equation for the new model is given by:

$$\partial_t(\rho_j v_j) = a\rho_0 V(\rho_{j+1}(t+\alpha\tau)) - a\rho_j v_j + a\lambda\rho_0\big(V_{j+2}(t+\alpha\tau) - V_{j+1}(t+\alpha\tau)\big), \qquad (3.1.8)$$

where τ is the total delay time taken by the driver to respond and by vehicle for actual movement, parameter α describe anticipation effect of driver's behavior, and the reaction coefficient of optimal current difference at $j+1^{th}$ site is λ.

Furthermore, as it is well known that actual traffic situations deal with some special road design elements, i.e., horizontal and vertical curves, lane width, curve radius etc. The driving task on these particular roads is different as well as complex. Therefore, by considering the slope effect as a special case of geometrical design of roadways Zhu and Zhang [148] presented novel lattice model for gradient highway. Thus, an improved optimal velocity function for a straight road with slope was presented as follows:

$$V(\rho_j(t), \phi) = \frac{V_{\max} \mp V_{g,\max}}{2}\Big[\tanh\Big(\frac{1}{\rho_j(t)} - \frac{1}{\rho_c(\phi)}\Big) + \tanh\Big(\frac{1}{\rho_c(\phi)}\Big)\Big], \qquad (3.1.9)$$

where $V_{\max}$ is maximum velocity on road section without slope. '$\mp$' corresponds to uphill and downhill positions of gradient highway.

3.1.3 Lattice model for slopy curved road

By using above idea of car following model proposed by Meng and Yan [150], evolution equation for the proposed model describing the motion of vehicles on two lane curved road with slope by incorporating driver's anticipation effect is given below:

$$\partial_t\rho_j + \frac{\rho_0}{\sin\theta_j}(\rho_j v_j - \rho_{j-1}v_{j-1}) = \gamma\frac{|\rho_0{}^2 V'(\rho_0, \phi)|}{\sin^2\theta_j}(\rho_{j+1} - 2\rho_j + \rho_{j-1}), \qquad (3.1.10)$$

$$\partial_t(\rho_j v_j) = a\Big[\frac{\rho_0}{\sin\theta_j}V\big(\rho_{j+1}(t+\alpha\tau), \phi\big) - \rho_j v_j\Big], \qquad (3.1.11)$$

where θ_j represents the angle for curved road at j^{th} site (Fig. 3.1). It is notable that the larger value of anticipation parameter α represents efficient drivers. The evolution equation of the following form can be obtained by using Taylor series expansion and ignoring higher ordered terms:

$$\rho_j(t+\tau)v_j(t+\tau) = \frac{\rho_0}{\sin\theta_j}\Big[V(\rho_{j+1},\phi) + \alpha\tau V'(\rho_{j+1},\phi)\partial_t(\rho_{j+1})\Big]. \tag{3.1.12}$$

Formation of $V(\cdot)$ for the proposed model is:

$$V(\rho_j(t),\phi) = \frac{{k_2}^1\sqrt{\mu g R_1 \cos\phi} \mp \sin\phi}{2}\Big[\tanh\Big(\frac{2}{\rho_0} - \frac{\rho_j(t)}{{\rho_0}^2} - \frac{1}{\rho_c}\Big) + \tanh\Big(\frac{1}{\rho_c}\Big)\Big]. \tag{3.1.13}$$

The reason behind the consideration of optimal velocity function is the symmetry of density as given in Ref. [79]. The density equation by using (3.1.10) and (3.1.12) of the present model is given by:

$$\begin{aligned} &\rho_j(t+2\tau) - \rho_j(t+\tau) + \frac{\tau{\rho_0}^2}{\sin^2\theta_j}\Big(V(\rho_{j+1},\phi) - V(\rho_j,\phi)\Big) + \frac{\tau{\rho_0}^2}{\sin^2\theta_j}\alpha \\ &\Big(V'(\rho_{j+1},\phi)\tilde{\Delta}(\rho_{j+1}) - V'(\rho_j,\phi)\tilde{\Delta}(\rho_j)\Big) - \tau\gamma\frac{|{\rho_0}^2 V'(\rho_0,\phi)|}{\sin^2\theta_j}\Delta^2\rho_{j-1}(t+\tau) = 0, \end{aligned} \tag{3.1.14}$$

where $\Delta^2\rho_{j-1}(t+\tau) = \rho_{j+1}(t+\tau) - 2\rho_j(t+\tau) + \rho_{j-1}(t+\tau)$
$\tilde{\Delta}\rho_j(t) = \rho_j(t+\tau) - \rho_j(t)$.

3.2 Effect of small amplitude perturbation

In order to find out the conditions of stability, linear stability analysis is conducted. We suppose that the vehicles are moving on curved road having slope with fixed density ρ_0 and constant velocity $V(\rho_0,\phi)$. Hence, the steady-state solution for uniform flow is:

$$\rho_j(t) = \rho_0, \quad v_j(t) = V(\rho_0,\phi). \tag{3.2.1}$$

Let us consider a small perturbation in terms of $y_j(t)$ to the above steady-state solution which leads to:

$$\rho_j(t) = \rho_0 + y_j(t). \tag{3.2.2}$$

using the above perturbed density profile into equation (3.1.14) and linearizing it we obtain:

$$\begin{aligned} &y_j(t+2\tau) - y_j(t+\tau) + \frac{\tau{\rho_0}^2}{\sin^2\theta_j}V'(\rho_0,\phi)\big(y_{j+1}(t) - y_j(t)\big) + \frac{\tau{\rho_0}^2\alpha}{\sin^2\theta_j}V'(\rho_0,\phi) \\ &\big(\tilde{\Delta}(\Delta y_j(t))\big) - \tau\gamma\frac{|{\rho_0}^2V'(\rho_0,\phi)|}{\sin^2\theta_j}\big(y_{j+1}(t+\tau) - 2y_j(t+\tau) + y_{j-1}(t+\tau)\big) = 0. \end{aligned} \tag{3.2.3}$$

Substituting $y_j(t) = \mathrm{e}^{(ikj+zt)}$ in (3.2.3) gives:

$$e^{2z\tau} - e^{z\tau} + \frac{\tau{\rho_0}^2}{\sin^2\theta_j}V'(\rho_0,\phi)(e^{ik}-1) + \frac{\tau{\rho_0}^2\alpha}{\sin^2\theta_j}(e^{z\tau}-1)(e^{ik}-1)V'(\rho_0,\phi) \qquad (3.2.4)$$
$$-\tau\gamma\frac{|{\rho_0}^2V'(\rho_0,\phi)|}{\sin^2\theta_j}(e^{ik+z\tau} - 2e^{z\tau} + e^{z\tau-ik}) = 0.$$

Inserting $z = z_1(ik) + z_2(ik)^2 + ...$ in equation (3.2.4), and comparing the coefficient (ik) with first and second-order terms, we get:

$$z_1 = \frac{-{\rho_0}^2}{\sin^2\theta_j}V'(\rho_0,\phi), \qquad (3.2.5)$$
$$z_2 = -\frac{3}{2}\tau{z_1}^2 - \frac{{\rho_0}^2}{2\sin^2\theta_j}V'(\rho_0,\phi) + \alpha\tau\frac{{\rho_0}^4}{\sin^4\theta_j}V'^2(\rho_0,\phi) + \gamma\frac{|{\rho_0}^2V'(\rho_0,\phi)|}{\sin^2\theta_j}, \qquad (3.2.6)$$

when $z_2 < 0$ then the uniform steady-state leads to unstable state. For $z_2 > 0$, the homogeneous flow achieve stable state against a long-wavelength perturbation. Therefore, the homogeneous traffic flow is unstable if:

$$\tau > -\frac{(1+2\gamma)\sin^2\theta_j}{(3-2\alpha){\rho_0}^2V'(\rho_0,\phi)}. \qquad (3.2.7)$$

and the neutral stability criterion is:

$$\tau = -\frac{(1+2\gamma)\sin^2\theta_j}{(3-2\alpha){\rho_0}^2V'(\rho_0,\phi)}, \qquad (3.2.8)$$

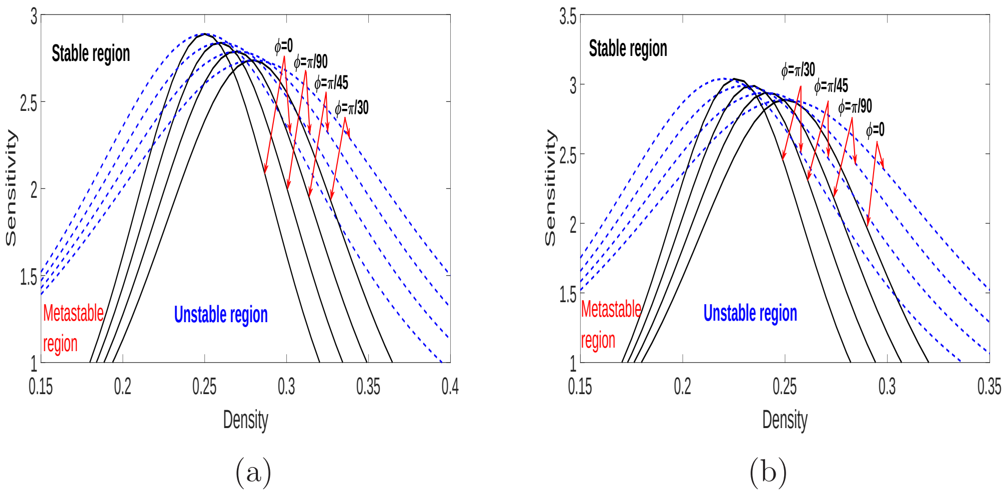

Figure 3.2: Phase plot in (ρ, a) space for different values of ϕ when $\gamma = 0.1, \alpha = 0.2, \theta_j = \pi/3$ corresponding to (a) Uphill (b) Downhill situations.

Fig. 3.2 describe different regions of flow in the parameter space (ρ, a) for varying slope angle

ϕ when vehicles are moving on a curved road with slope under two lane system. The black solid curves represent the neutral stability curves obtained by linear analysis. The region over the neutral stability curves is stable and the region under the curves is unstable. We consider the situation when lane change occurs that is $\gamma = 0.1$ corresponding to uphill and downhill situations. The critical point (ρ_c, a_c) is represented by the apex of each curve and one can observe that the stability condition is fulfilled when $\tau < \tau_c$ where $\tau_c = \frac{1}{a_c}$. From Fig. 3.2 (a)-(b) it is clear that for uphill case, apex of each curve decreases with increasing value of ϕ that leads to the enhancement of stable region with increasing values of ϕ. On the other hand for downhill position, stable region reduces corresponding to higher values of ϕ. Specifically, we notice the variation in the stability of traffic with respect to the slope in different situations (uphill or downhill). The reason behind it is that while moving towards uphill direction of road, velocity of vehicles remain slow; while moving towards downhill position, vehicles move with higher velocity and the jamming of vehicles become more than uphill case.

3.3 Effect of long wave perturbation

When vehicular density exceed some critical value then the homogeneous traffic flow loses its stability with respect to the long-wavelength perturbation. So, we investigate the evolution characteristics of traffic density describing the collective motion of vehicles on a coarse-grained scale through reduction perturbation technique. To examine the behavior of system close to the critical point (ρ_c, a_c), the slow variables X and T for $0 < \epsilon \leq 1$, are described by:

$$X = \epsilon(j + bt), \quad T = \epsilon^3(t), \tag{3.3.1}$$

where constant term b needs to be obtained. Consider $\rho_j(t)$ satisfy the following equation:

$$\rho_j(t) = \rho_c + \epsilon R(X, T), \tag{3.3.2}$$

thus we expand the density equation (3.1.14) by using previously defined slow variables in (3.3.1) and the perturbed density (3.3.2) with the help of Taylor series expansion up to fifth-order of ϵ, and a nonlinear equation is obtained as:

$$\begin{aligned} \epsilon^2 k_1 \partial_X R + \epsilon^3 k_2 \partial_X^2 R + \epsilon^4(\partial_T R + k_3 \partial_X^3 R + k_4 \partial_X R^3) + \epsilon^5(k_5 \partial_T \partial_X R \\ + k_6 \partial_X^4 R + k_7 \partial_X^2 R^3) = 0. \end{aligned} \tag{3.3.3}$$

Table 3.1 gives the coefficient values $k_i (i = 1, 2, 3, ..., 7)$, and $V'(\rho_j, \phi) = \frac{\partial V(\rho,\phi)}{\partial \rho}\Big|_{\rho=\rho_c} = -\frac{A_2}{\rho_0^2}$ and $V'''(\rho_j, \phi) = \frac{\partial^3 V(\rho,\phi)}{\partial \rho^3}\Big|_{\rho=\rho_c} = \frac{2A_2}{\rho_0^6}$ for $A_2 = \frac{{k_2}^1\sqrt{\mu g R_1 \cos(\phi) \mp \sin(\phi)}}{2}$.

The value of τ close to the critical point (ρ_c, a_c) is chosen as:

$$\tau = \tau_c(\epsilon^2 + 1), \tag{3.3.4}$$

by taking constant value $b = \frac{-\rho_c^2 V'}{\sin^2\theta_j}$ and removing the terms containing second and third-order of ϵ in equation (3.3.3), we obtain:

$$\epsilon^4(\partial_T R - g_1 \partial_X^3 R + g_2 \partial_X R^3) + \epsilon^5(g_3 \partial_X^2 R + g_4 \partial_X^4 R + g_5 \partial_X^2 R^3) = 0, \tag{3.3.5}$$

where values in Table 3.2 represent coefficients $g_i (i = 1, 2, ..., 5)$. Using the following transformation, equation (3.3.5) can be converted into standard mKdV equation:

$$T^{'} = g_1 T, \quad R = \sqrt{\frac{g_1}{g_2}} R^{'}. \tag{3.3.6}$$

The coefficients k_i of the model	
k_1	$b + \frac{\rho_c^2 V'}{\sin^2\theta_j}$
k_2	$\frac{3b^2\tau}{2} + \frac{\rho_c^2 V'}{\sin^2\theta_j}\left[\frac{1}{2} + \alpha b\tau + \gamma\right]$
k_3	$\frac{7}{6}b^3\tau^2 + \frac{\rho_c^2 V'}{\sin^2\theta_j}\left[\frac{1}{6} + \frac{\alpha}{2}(b\tau + b^2\tau^2) + \gamma b\tau\right]$
k_4	$\frac{\rho_c^2 V'''}{6\sin^2\theta_j}$
k_5	$3b\tau + \frac{\rho_c^2 V'}{\sin^2\theta_j}\alpha\tau$
k_6	$\frac{5b^4\tau^3}{8} + \frac{\rho_c^2 V'}{6\sin^2\theta_j}[\frac{1}{4} + \alpha(b\tau + \frac{3}{2}b^2\tau^2 + b^3\tau^3) + \frac{\gamma}{2}(1 + 6b^2\tau^2)]$
k_7	$\frac{\rho_c^2 V'''}{12\sin^2\theta_j}$

Table 3.1: The coefficients k_i of the model

Thus, the equation (3.3.5) takes the following form:

$$\partial_{T'} R^{'} - \partial_X^3 R^{'} + \partial_X R^{'3} + \epsilon M[R^{'}] = 0, \tag{3.3.7}$$

where $M[R^{'}] = \frac{1}{g_1}[g_3 \partial_X^2 R^{'} + g_4 \partial_X^4 R^{'} + \frac{g_1 g_5}{g_2} \partial_X^2 R^{'3}]$. After ignoring correction term $O(\epsilon)$ from

(3.3.7), we get the solution of the standard mKdV equation as:

$$R_0'(X,T') = \sqrt{L_1}\tanh\Big(\sqrt{\frac{L_1}{2}}(X - L_1T')\Big), \tag{3.3.8}$$

where the propagation velocity is denoted by L_1 and is computed by solving the following necessary condition:

$$(R_0', M[R_0']) \equiv \int_{-\infty}^{\infty} dX R_0' M[R_0'] = 0, \tag{3.3.9}$$

with $M[R_0'] = M[R']$. After solving equation (3.3.9), the selected value of L_1 is:

$$L_1 = \frac{5g_2g_3}{2g_2g_4 - 3g_1g_5}. \tag{3.3.10}$$

The coefficients g_i of the model	
g_1	$\frac{-7b^3\tau_c{}^2}{6} - \frac{\rho_c^2 V'}{\sin^2\theta_j}[\frac{1}{6} + \frac{1}{2}\alpha(b\tau_c + b^2\tau_c{}^2) + \gamma b\tau_c]$
g_2	$\frac{\rho_c^2 V'''}{6\sin^2\theta_j}$
g_3	$\frac{3}{2}b^2\tau_c + \frac{\rho_c^2 V'}{\sin^2\theta_j}\alpha b\tau_c$
g_4	$g_1(3-\alpha)\frac{(1+2\gamma)}{(3-2\alpha)} + \frac{5}{8}b^4\tau_c^3 + \frac{\rho_c^2 V'}{6\sin^2\theta_j}$ $[\frac{1}{4} + \frac{\gamma}{2}(1 + 6b^2\tau_c{}^2) + \alpha(b\tau_c + b^3\tau_c{}^3 + \frac{3}{2}b^2\tau_c{}^2)]$
g_5	$-g_2(3-\alpha)\frac{(1+2\gamma)}{(3-2\alpha)} + \frac{\rho_c^2 V'''}{12\sin^2\theta_j}$

Table 3.2: The coefficients g_i of the model

Finally, the kink solution is described by:

$$\rho_j = \rho_c + \epsilon\sqrt{\frac{g_1L_1}{g_2}}\tanh\Big(\sqrt{\frac{L_1}{2}}(X - L_1g_1T)\Big), \tag{3.3.11}$$

where $\epsilon^2 = \left(\frac{a_c}{a} - 1\right)$ and the amplitude A_m of the density is:

$$A_m = \sqrt{\frac{g_1}{g_2}\epsilon^2 L_1}$$

The kink antikink solution (3.3.11) of mKdV equation (3.3.7) described by $\rho_j = \rho_c \pm A_m$

represents the coexisting phase including uniform flow phase as well as jammed phase in (ρ, a) phase plane. For distinct values of ϕ, coexisting curves (blue dotted curves) obtained through nonlinear analysis, are shown in Fig. 3.2(a)-(b) for lane change case. It can be observed from these figures that with respective variation in slope the stability region also varies corresponding to uphill and downhill situations. Particularly, the flow of traffic on a slopy curved road reveals complications in driving comparatively to straight road but the higher rate of driver's anticipation helps in reducing traffic jams when lane change is allowed.

3.4 Simulation results

To investigate the reliability of theoretical results obtained via linear as well as nonlinear analysis, simulation is performed. A small amplitude disturbance is given to the steady-state flow and stability conditions are obtained by equation (3.2.8) which are consistent with Fig. 3.2. Contrary to the homogeneous state of flow when stability condition (3.2.8) is not satisfied then the perturbation expands over a period of time and the traffic turns into an inhomogeneous state. Thus, the typical profile of inhomogeneous flow is investigated by adopting periodic boundary conditions and the initial condition are:

$$\rho_j(1) = \rho_j(0) = \begin{cases} \rho_0; \quad j \neq \frac{N}{2}, \frac{N}{2}+1 \\ \rho_0 - \sigma; \quad j = \frac{N}{2} \\ \rho_0 + \sigma; \quad j = \frac{N}{2}+1, \end{cases} \tag{3.4.1}$$

where the initial disturbance $\sigma = 0.1$, total number of lattice sites are $N = 100$, maximum time $t = 10^5$ sec., $\rho_0 = \rho_c = 0.25$, $\mu = 0.25$, $\mathbf{r} = 10$, $g = 10$, ${k_2}^1 = 0.4$, $\alpha = 0.2$, $\theta_j = \pi/3$ and the sensitivity parameter takes the values $a = 2.7$ and $a = 2.8$ for uphill and downhill situations, respectively.

Fig. 3.3 and Fig. 3.4 shows the spatiotemporal evolution of density waves in the unstable region corresponding to Fig. 3.2 for different values of ϕ after sufficiently long time $t = 9.9 \times 10^4 - 10^5$ sec. both for uphill and downhill cases, when lane change occurs. From Fig. 3.3(a)-3.3(d) and 3.4(a)-3.4(d) one can observe that the perturbation at initial stage leads to density waves of kink antikink form for both cases. Results show that for both situations when the angle of slope is increasing the number of stop-start density waves is decreasing. On the other side, the amplitude of density waves start decreasing and free flow region turns wide in an uphill case. But the condition varies for downhill situation as the amplitude of kink waves is rising. The results indicate that the suppression of traffic jams is due to the increasing slope in an uphill situation. On the contrary, jams arise in case of downhill situation .

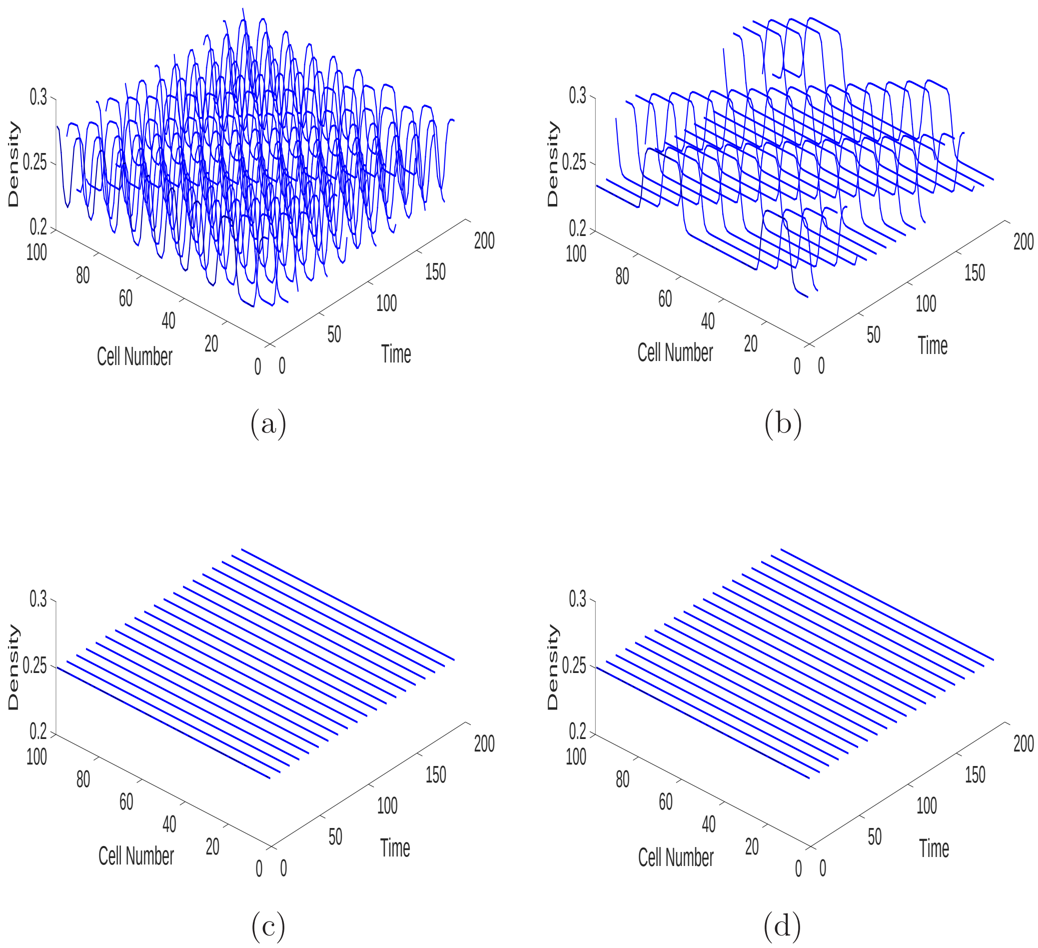

Figure 3.3: Spatiotemporal evolution of density waves at $t = 9.9 \times 10^4$-10^5 sec. for uphill case when $\gamma = 0.1$ and $\phi = 0, \pi/90, \pi/45, \pi/30$.

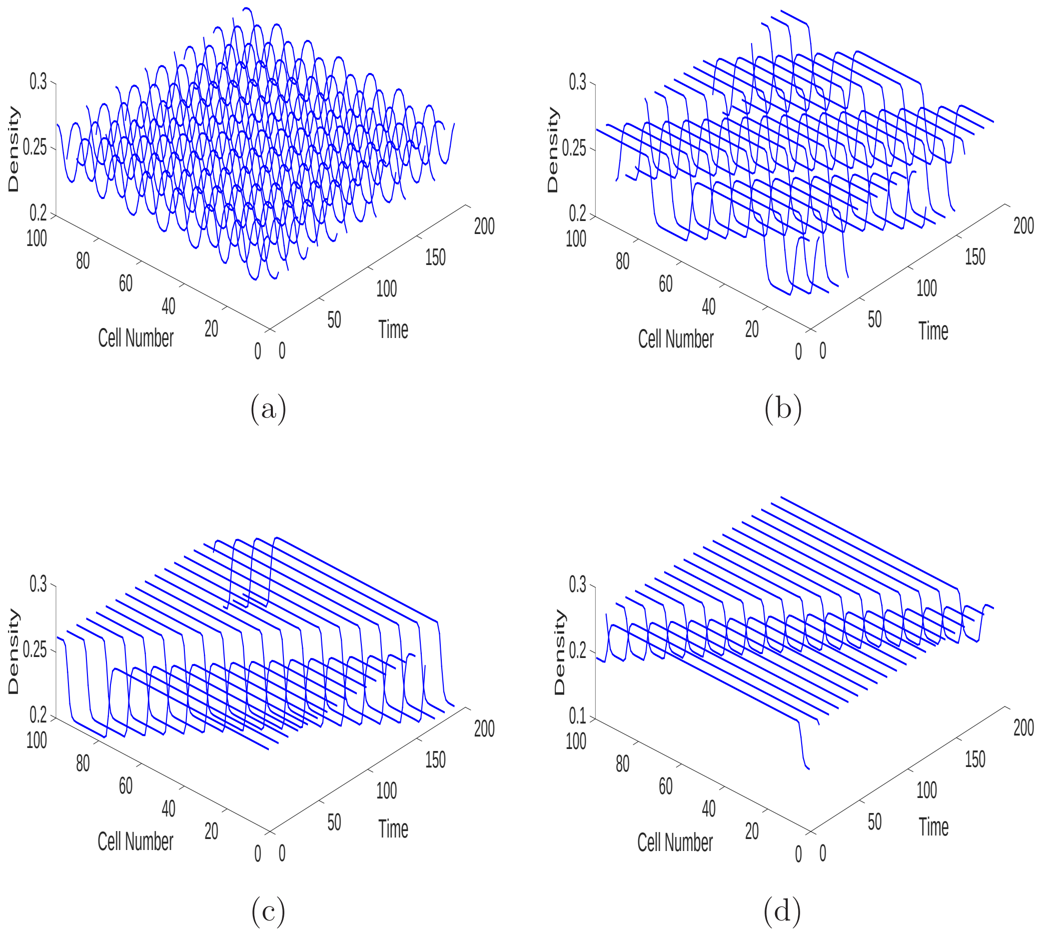

Figure 3.4: Spatiotemporal evolution of density waves at $t = 9.9 \times 10^4$-10^5 sec. for downhill case when $\gamma = 0.1, \phi = 0, \pi/90, \pi/45, \pi/30$.

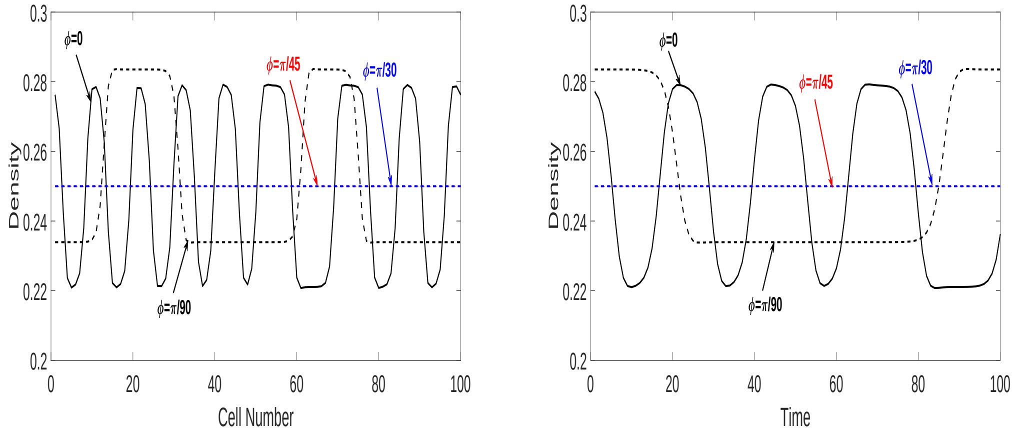

(a) (b)

Figure 3.5: Density profiles for uphill case at (a) $t = 8 \times 10^4$ sec. (b) on lattice site $j = 50$ when $\gamma = 0.1,\ \phi = 0, \pi/90, \pi/45, \pi/30$.

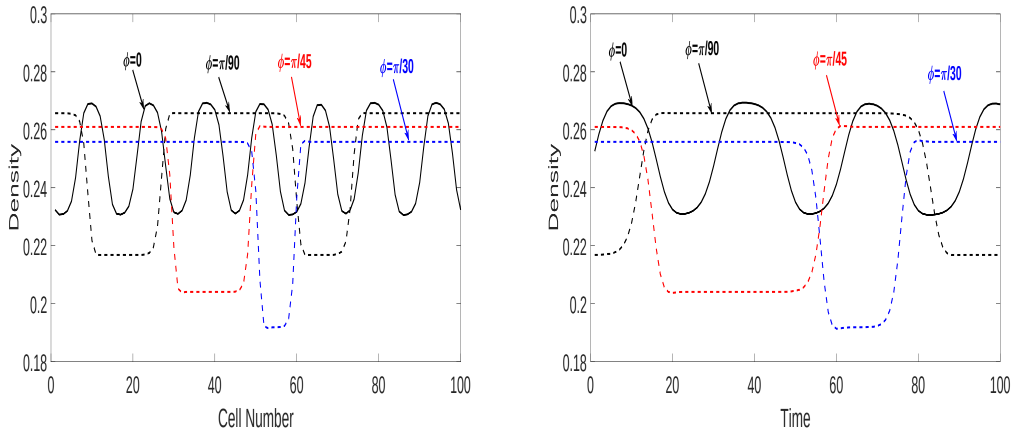

(a) (b)

Figure 3.6: Density profiles for downhill case at (a) $t = 8 \times 10^4$ sec. (b) on lattice site $j = 50$ when $\gamma = 0.1,\ \phi = 0, \pi/90, \pi/45, \pi/30$.

Fig. 3.5(a) and Fig. 3.6(a) shows the density profiles for distinct values of ϕ when $\gamma = 0.1$ at fixed time $t = 8 \times 10^4$ sec.. Fig. 3.5(b) and 3.6(b) shows the density profile with respect to time $t = 9.99 \times 10^4 - 10^5$ sec. on 50^{th} site. On comparing the figures we found that the number of stop-start waves decreases for both uphill and downhill cases with an increase in slope. Moreover, the stability region increases as the amplitude of kink antikink density wave is weakened due to increase in slope when moving towards uphill situation. On the other side for downhill situation amplitude of density waves start rising with an increasing slope which is consistent with theoretical results.

Hence, we can conclude that the vehicular traffic shows complexity in nature when it deals with curved road with slope. But the complexity can be controlled through anticipation and lane changing parameters.

3.5 Conclusion

Traffic flow phenomena for two lane curved road with slope is analyzed by using lattice hydrodynamic approach with respect to the effect of driver's anticipation. Stability conditions are obtained using linear analysis and the behavior of traffic under congestion is studied through nonlinear analysis. Traffic under the congested region comes out by revealing kink antikink density waves represented by the solution of mKdV equation resulting from nonlinear analysis. Simulations under the hypothetical test conditions are performed to verify the theoretical findings. It is concluded that the slope of curved road has a remarkable impact on the flow stability on two lane highway. Though the newly developed model appropriately reproduce the features of real traffic phenomena on a curved road with slope by explaining the effects of slope on traffic dynamics, yet the model has the following limitations:

- Vehicles are considered as homogeneous entity.
- Overtaking is restricted in the present model.
- Many important factors in traffic flow such as interruption effect [103] and delayed-feedback effect [95] etc. are not considered.
- The validity of the model should be checked through some experimental data.

Chapter 4

Lattice model for heterogeneous traffic flow

Traffic networks consisting of highways, streets, traffic control devices and various kind of vehicles provide a convenient atmosphere for passengers. The problem of traffic jams with respect to the increasing strength of automobile has become one of the challenging issues for scientists and researchers even with the development of technology and road infrastructure. To reduce jamming states, modeling of traffic plays significant role to reproduce and to forecast the complex mechanism and investigate its properties. A notable aspect of the applicability of the models is their ability to replicate the undesirable phenomena called traffic congestion. For a model, critical model parameters or traffic conditions need to be established that lead to a stable response to disturbances. In a certain density range, many traffic models become unstable due to delays in adapting to changing traffic conditions. Therefore, to avoid undesirable situations a notable amount of traffic models ranging from micro to macro level [1,11,25,114,117–121,131,132] have been produced to study the complex traffic phenomena of self-driven non-equilibrium system of interacting particles.

Among all these approaches, the lattice hydrodynamic (LH) model [1] (as discussed in Chapter 1) is one of the simplest and well known traffic model which collaborates the merits of macroscopic and microscopic models. Afterwards, the approach has been widely referred and extended by considering a series of realistic factors influencing traffic conditions [79–82, 86, 87, 99, 122, 124, 151, 152].

In reality, traffic system either of a whole city or a highway contains a mixture of a variety of vehicles. Homogeneous traffic refers to the state of traffic consisting of similar type of vehicles following lane discipline. Moreover, traffic consisting of motorized and non-motorized two wheelers and three wheelers together with other vehicles without following lane rules, is defined as heterogeneous traffic (see Fig. 4.1). The vehicle heterogeneity in traffic stream is a significant if not dominant factor in modeling highway traffic flow operations accurately. For example, high percentages of big vehicles may induce congestion at relatively lower volumes, and hence dissimilar network traffic conditions may result than with low percentages. Moreover, the ratio of small vehicles in the city traffic stream may vary considerably from highway traffic.

The content of this chapter has been published in Physics Letters A, 382 (22): 1449-1455, (2018).

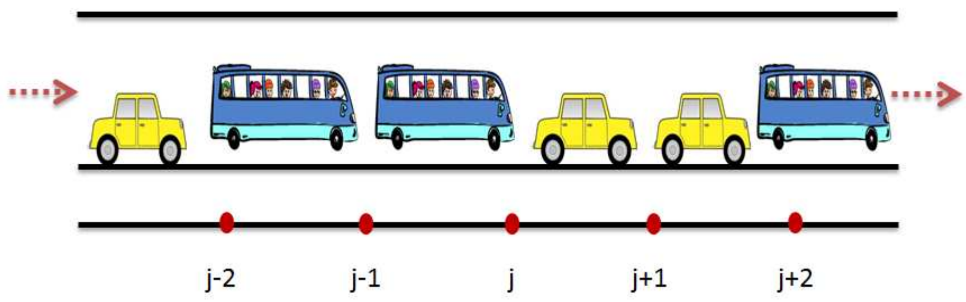

Figure 4.1: An illustration of lattice model for heterogeneous traffic flow.

To explore the influence of heterogeneous traffic, some efforts have been made to extend the macro as well as micro models. LWR model [41] was extended to discuss about driver's heterogeneity [153]. The extension was made by taking into account the driver's heterogeneity based on speed choices. Many extensions were also made at macro level to study the behavior of heterogeneous traffic [154, 155]. Recently, AWR model [49] is extended by Mohan and Ramadurai [54] to generalize the higher order continuum models for heterogeneous traffic flow by using the concept of area occupancy. The micro models in which the main focus is on car following behavior [156, 157] provide another way to include the heterogeneity of traffic and analyze its effect on traffic flow dynamics. Tang et al. [156] studied the fundamental diagram and jam density of heterogeneous traffic consisting of bus and car under three different conditions: (I) without any restriction (II) under the action of traffic control policy that restrains some private cars (III) using bus to replace the private cars restrained by traffic control policy. Mason and Woods [157] studied the behavior of multispecies car following model both on circular as well as straight roads. It was found that in the limit of long roads with a large number of cars, the linear stability criteria for circular and straight roads were same. Also, having high enough concentration of trucks in a population of cars, the system as a whole could be asymptotically unstable, i.e, trucks can cause jams. Recently, a new car following model [158] is developed composed of low and high-sensitivity vehicles. It has been analyzed that the neutral stability curves divide the headway space into five distinct regions. The effect of percentage of low-sensitivity vehicles on stability of mixed traffic has been analyzed.

Because of its capability in describing the jamming transitions in the form of kink density waves, lattice hydrodynamic approach is suitable to investigate the role of heterogeneity in flow of traffic. But the focus of previously discussed lattice models was mainly on homogeneous traffic phenomena for single lane road and/or multi lane highways. These models were unable to completely describe the features of heterogeneous traffic flow on roads, since they do not consider different heterogeneous factors of traffic, for example, heterogeneity of vehicle and/or driver's heterogeneity etc.

Present Chapter is an attempt to develop a simple lattice hydrodynamic model to incorporate a distribution of heterogeneous vehicles in section 4.1, and show by means of theoretical investigation that the resulting model, though simple in nature, is efficient to capture the influence of heterogeneous vehicles on the stability of flow in section 4.2. Simulation is performed in section 4.3 in order to confirm the analytical results and finally, in section 4.4 summary of results is provided.

4.1 Models for heterogeneous traffic flow

4.1.1 Car following model for heterogeneous traffic flow

Car following model [158] based on FVDM, focus on the modeling of heterogeneous traffic with low and high-sensitivity vehicles. The distinguishing features of each vehicle types are sensitivities. The generalized full velocity difference model considering two types of vehicles with reaction time delay is given as follows:

$$\dot{u}_n(t) = a_1\Big[\frac{V_{\max}}{2}\Big(\tanh(\Delta x_n(t-\tau)-h_c)+\tanh(h_c)\Big)-u_n(t)\Big]+K_1\Delta u(t), \tag{4.1.1}$$

which refers to vehicles with low-sensitivity with percentage c.

$$\dot{u}_n(t) = a_2\Big[\frac{V_{\max}}{2}\Big(\tanh(\Delta x_n(t-\tau)-h_c)+\tanh(h_c)\Big)-u_n(t)\Big]+K_2\Delta u(t), \tag{4.1.2}$$

which refers to vehicles with high-sensitivity with percentage $(1-c)$. a_1 and K_1 are the sensitivities for low-sensitivity vehicles, a_2 and K_2 are the sensitivities for high-sensitivity vehicles. τ is reaction time of driver. It is assumed that $a_1 < a_2$ and $K_1 < K_2$ and the percentage c of low-sensitivity vehicles satisfy the condition $0 \leq c \leq 1$. By adjusting the coefficient c, one can consider any portion of heterogeneous traffic flow composed of low and high-sensitivity vehicles. Vehicle motion is formulated by the acceleration function of its vehicle type.

4.1.2 New lattice model for heterogeneous traffic flow

Basic lattice hydrodynamic model, as discussed in Chapter 1, was proposed by Nagatani [1] for unidirectional single lane road. The fundamental idea behind lattice model is that the optimal current regulate the traffic current with a delay time. Later, the lattice model was extended by including the effect of optimal current difference that significantly affect the multi lane traffic flow system [86]. In the improved lattice model by Peng [86], continuity equation is same as (3.1.7) and the evolution equation (1.6.6) is modified to include the optimal current difference effect (OCDE) between two forward sites and is given by:

$$\partial_t(\rho_j v_j) = a\rho_0 V(\rho_{j+1}) - a\rho_j v_j + a\lambda\rho_0[V(\rho_{j+2}) - V(\rho_{j+1})], \tag{4.1.3}$$

where the last term represents the OCDE on $j+1^{th}$ site at time t and the parameter λ corresponds to the optimal current difference effect.

The above model has been found to have greater stability as compared to Nagatani's model. But this model can not be used to examine the features of heterogeneous traffic because it considers the traffic to be homogeneous.

In general, traffic stream comprises of many different types of vehicles starting from very small to large. In this chapter, our purpose is to model the behavior characteristics of heterogeneous traffic involving two types of vehicles small and large. The distinguishing features of both types of vehicles refer to the sensitivities. First type (small) of vehicles are assumed to have high-sensitivity as compared to second type (large) of vehicles. By keeping this in view, new heterogeneous lattice hydrodynamic model is proposed for both types of vehicles. The traffic is considered as unidirectional because both types of vehicles will move in the same direction. Hence, the continuity equations remain intact (same as (1.6.5)) for both type of vehicles at site j and are given by:

$$\partial_t(\rho_{1,j}) + \rho_0(\rho_{1,j}v_{1,j} - \rho_{1,j-1}v_{1,j-1}) = 0, \tag{4.1.4}$$

$$\partial_t(\rho_{2,j}) + \rho_0(\rho_{2,j}v_{2,j} - \rho_{2,j-1}v_{2,j-1}) = 0, \tag{4.1.5}$$

where $\rho_{1,j}$ ($\rho_{2,j}$) and $v_{1,j}$ ($v_{2,j}$) denotes the local density and velocity of first type (second type) vehicles at j^{th} site at any time t, respectively. Further, the modifications are made to the evolution equations for each type to include the effect of delay which is inversely proportional to the sensitivity. Assuming $a_1 = \frac{1}{\tau_1}$ and $a_2 = \frac{1}{\tau_2}$ be the sensitivities of small and large vehicles, respectively. We propose new evolution equations for each type in heterogeneous traffic stream as follows:

$$\partial_t(\rho_{1,j}v_{1,j}) = a_1\rho_0 cV(\rho_{j+1}) - a_1\rho_{1,j}v_{1,j} + a_1\rho_0 c\lambda[V(\rho_{j+2}) - V(\rho_{j+1})], \tag{4.1.6}$$

$$\begin{aligned}\partial_t(\rho_{2,j}v_{2,j}) = {} & a_2\rho_0(1-c)V(\rho_{j+1}) - a_2\rho_{2,j}v_{2,j} + a_2\rho_0(1-c)\lambda[V(\rho_{j+2}) \\ & - V(\rho_{j+1})],\end{aligned} \tag{4.1.7}$$

where c ($0 \leq c \leq 1$) denotes the fraction of small vehicles while $(1-c)$ denotes the fraction of large vehicles in heterogeneous traffic. Note that the interaction will take place between both type of vehicles and the presence of one will affect the other. This has been incorporated via optimal velocity function which is the function of total density in the evolution equation for both types of vehicles. Combining (4.1.4) with (4.1.6), the density evolution equation for first type of vehicle is obtained as:

$$\begin{aligned}\rho_{1,j}(t+2\tau_1) - \rho_{1,j}(t+\tau_1) + \tau_1 c\rho_0^2[V(\rho_{j+1}) - V(\rho_j)] + \tau_1\lambda c\rho_0^2 \\ [V(\rho_{j+2}) - 2V(\rho_{j+1}) + V(\rho_j)] = 0.\end{aligned} \tag{4.1.8}$$

Similarly, the density equation for second type of vehicles is given as:

$$\begin{aligned}\rho_{2,j}(t+2\tau_2) - &\rho_{2,j}(t+\tau_2) + \tau_2(1-c)\rho_0^2[V(\rho_{j+1}) - V(\rho_j)] \\ &+ \tau_2\lambda(1-c)\rho_0^2[V(\rho_{j+2}) - 2V(\rho_{j+1}) + V(\rho_j)] = 0.\end{aligned} \tag{4.1.9}$$

Because the major aim of the present model is to explain the characteristics of mixed traffic as a whole instead of describing it for different vehicles. In order to fulfill the purpose, we need to get density equation for combined traffic. Therefore, by adding equations (4.1.8) and (4.1.9) we obtain:

$$\begin{aligned}[\rho_{1,j}(t+2\tau_1) + \rho_{2,j}((t+2\tau_1) + (K-1)2\tau_1)] - [\rho_{1,j}(t+\tau_1) + \rho_{2,j}((t+\tau_1) \\ + (K-1)\tau_1)] + {\rho_0}^2(\tau_1 c + (1-c)\tau_2)[V(\rho_{j+1}) - V(\rho_j)] \\ + \lambda{\rho_0}^2(\tau_1 c + (1-c)\tau_2)[V(\rho_{j+2}) - 2V(\rho_{j+1}) + V(\rho_j)] = 0,\end{aligned} \tag{4.1.10}$$

constant K in the above equation is very small number and we are choosing $\tau_2 = K\tau_1$ because the time delay corresponding to bigger vehicles is more than that of small vehicles. Now the increasing value of parameter K leads to increased delay time corresponding to less-sensitive vehicles which results that the density change rate is zero. Thus, after applying Taylor series to the terms containing K and ignoring higher-ordered derivative terms the density equation of heterogeneous flow is obtained as:

$$\begin{aligned}\rho_j(t+2\tau) - \rho_j(t+\tau) + &\tau_1{\rho_0}^2(c + K(1-c))[V(\rho_{j+1}) - V(\rho_j)] + \tau_1\lambda{\rho_0}^2 \\ &(c + K(1-c))[V(\rho_{j+2}) - 2V(\rho_{j+1}) + V(\rho_j)] = 0,\end{aligned} \tag{4.1.11}$$

where the sensitivity parameters are adopted as $a_1 = p_1 a$ and $a_2 = qa$, where p_1 and q are the constants. After rewriting the equation (4.1.11) for total density of heterogeneous flow, the extended heterogeneous LH model for two types of vehicles with different sensitivities is obtained as follows:

$$\begin{aligned}\rho_j(t+2\tau) - \rho_j(t+\tau) + A{\rho_0}^2\tau[V(\rho_{j+1}) - V(\rho_j)] + B{\rho_0}^2\tau[V(\rho_{j+2}) \\ - 2V(\rho_{j+1}) + V(\rho_j)] = 0,\end{aligned} \tag{4.1.12}$$

where $A = \left[\frac{c}{p_1} + \frac{(1-c)}{q}\right]$ and $B = A\lambda$, the delay time τ represent the time consumed by the traffic current to achieve the state of optimal current. Here, $\rho_j = \rho_{1,j} + \rho_{2,j}$ denotes the total density of both types of vehicles at site j. Since an individual's response is reflected by the sensitivity to outside influences; sensitivities in our model are basically chosen as directly proportional to each other. Without loss of generality, $a_1 > a_2$ is taken which in turn implies

$p_1 > q$. Note that we can choose any section of the heterogeneous traffic flow including the vehicles with low and high-sensitivities by adjusting the coefficient c. The value of $V(\cdot)$ is adopted same as provided in [79].

The density evolution equation (4.1.12) can be used to analyze the density waves in a heterogeneous traffic with two types of vehicles. Moreover for $c = 0$ or $c = 1$, the proposed model with $p_1 = q = 1$ and $\lambda = 0$ reduces to homogeneous case of Nagatani's model [1].

4.2 Theoretical analysis of the new model

4.2.1 Linear stability analysis

The impact of heterogeneous traffic on the jamming transitions of traffic flow on a unidirectional single lane road is examined via linear stability analysis. Initially, the traffic is assumed to move with uniform density ρ_0 and optimal velocity $V(\rho_0)$, then the uniform steady-state solution for (4.1.12) is:

$$\rho_j(t) = \rho_0, \quad v_j(t) = V(\rho_0). \tag{4.2.1}$$

After perturbing the uniform density at j^{th} site in terms of $y_j(t)$ results:

$$\rho_j(t) = \rho_0 + y_j(t). \tag{4.2.2}$$

Inserting the above perturbed density profile (4.2.2) into (4.1.12) and by linearizing the equation for $y_j(t)$, we get:

$$\begin{aligned} y_j(t+2\tau) - y_j(t+\tau) + A\tau{\rho_0}^2 V'(\rho_0)[y_{j+1}(t) - y_j(t)] + \tau B{\rho_0}^2 V'(\rho_0) \\ [y_{j+2}(t) - 2y_{j+1}(t) + y_j(t)] = 0. \end{aligned} \tag{4.2.3}$$

The derivative of the optimal velocity function $V(\rho)$ is represented by $V'(\rho_0)$ at point $\rho = \rho_0$. By applying Taylor series expansion to (4.2.3) and assuming the deviation as $y_j(t) = \exp(ikj + zt)$, the eq. (4.2.3) becomes:

$$\mathrm{e}^{2z\tau} - \mathrm{e}^{z\tau} + \tau{\rho_0}^2 V'(\rho_0)\big(A(e^{ik} - 1) + B(e^{2ik} - 2e^{ik} + 1)\big) = 0. \tag{4.2.4}$$

Putting $z = z_1(ik) + z_2(ik)^2.....$ into (4.2.4), the coefficients (ik) and $(ik)^2$ are obtained as:

$$z_1 = -A{\rho_0}^2 V'(\rho_0). \tag{4.2.5}$$

$$z_2 = -\frac{3}{2}\tau {z_1}^2 - \Big[\frac{A+2B}{2}\Big]{\rho_0}^2 V'(\rho_0). \tag{4.2.6}$$

If the inequality $z_2 < 0$ holds against the small amplitude perturbation then it leads to the unstable state in uniform steady-state, on the other side it becomes stable if $z_2 > 0$. Thus, the condition for the steady-state of heterogeneous traffic flow to be unstable is given by:

$$a < -\frac{3A^2(\rho_0^2 V'(\rho_0))}{A+2B}. \tag{4.2.7}$$

The neutral stability condition for small amplitude disturbances is given as:

$$a = -\frac{3A^2(\rho_0^2 V'(\rho_0))}{A+2B}, \tag{4.2.8}$$

after putting $B = A\lambda$ the neutral stability condition (4.2.8) is given by:

$$a = -\frac{3A(\rho_0^2 V'(\rho_0))}{1+2\lambda}. \tag{4.2.9}$$

Equation (4.2.9) clearly shows that the reaction coefficient of optimal current difference and fraction of small/large vehicles considerably impact the stabilization/destabilization of heterogeneous traffic stream.

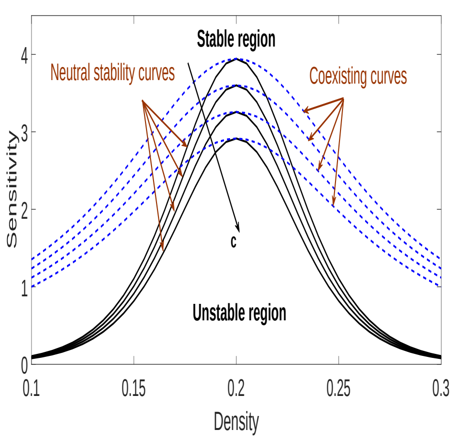

(a)

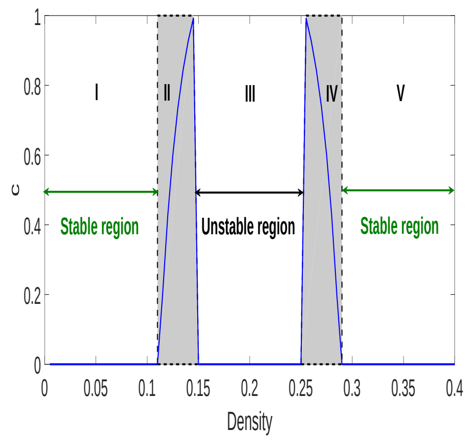

(b)

Figure 4.2: Phase plots showing (a) phase separation curves in (ρ, a) space for $c = 0.1, 0.2, 0.3, 0.4$. (b) critical lines dividing (ρ, c) space into five distinct regions of flow for $a = 0.2$. The critical density and reaction coefficient of optimal current difference are chosen respectively as $\rho_0 = \rho_c = 0.2$, and $\lambda = 0.2$.

Fig. 4.2(a) gives the coexisting curves (blue dotted curves) along with neutral stability curves (black solid curves) in (ρ, a) plane. The neutral and coexisting curves split the phase space (ρ, a) into three distinct regions. The apex of both neutral stability and coexisting curves matches at the critical point (ρ_c, a_c) for all values of c. One can observe from Fig. 4.2(a) that the apex of each curve lower down with an increase in fraction parameter c. This indicates that the traffic system gets more stable with an increase in the proportion of high-sensitivity vehicles in the traffic stream. Which is true because under the jamming conditions in real traffic situations, smaller vehicles with high-sensitivity try to accommodate themselves by using lateral spaces as compared to larger vehicles with low-sensitivity to overcome the congestion.

Further, to explain the effect of fraction of high-sensitivity vehicles on critical phase transition curves, Fig. 4.2(b) shows the phase diagram for density versus c for the model when $\lambda = 0.2$, $p_1 = 2.5$ and $q = 0.5$. The critical line is represented by the blue solid line which separates the stable and unstable region obtained from equation (4.2.9). The curve divides the whole space into five distinct regions.

Region I ($0 < \rho \leq 0.11$) and Region V ($\rho \geq 0.29$) represents the low density and high density regions, respectively, where the heterogeneous flow always remain stable for each value of fraction coefficient c. It indicates that whatever value the number of low or high-sensitivity vehicles can take, the stability remains unaffected. The stability of traffic flow in the Regions II ($0.11 < \rho \leq 0.15$) and Region IV ($0.25 < \rho \leq 0.29$) is sensitive to the fraction of small and large vehicles in the traffic stream. In these regions, higher amount of high-sensitivity vehicles refers to the stability of flow. Region III ($0.15 < \rho \leq 0.25$) shows the unbalanced state of traffic flow for each value of the fraction parameter c. The steady-state flow of traffic will evolve into an unstable stop and go density waves spreading in the backward direction.

4.2.2 Nonlinear stability analysis

When the flow is affected largely by some external forces then the density of vehicles start rising in an irregular manner leading to traffic jams in the form of nonlinear density waves. In order to check the varying nature of mixed flow near the critical point (ρ_c, a_c) as well as the impact of heterogeneous traffic on the development of traffic jams on coarse-grained scales, reductive perturbation technique is adopted. For that, space variable X and time variable T for $0 < \epsilon \leq 1$ are considered as follows:

$$X = \epsilon(j + bt), \quad T = \epsilon^3(t), \tag{4.2.10}$$

where the constant term b needs to be obtained. Let ρ_j satisfy the following equation:

$$\rho_j(t) = \rho_c + \epsilon R(X, T). \tag{4.2.11}$$

Taylor series expansion is used to expand equation (4.1.12), by putting (4.2.10) and (4.2.11), up to fifth-order of ϵ and the nonlinear equation is obtained as follows:

$$\begin{aligned}\epsilon^2 k_1 \partial_X R + \epsilon^3 k_2 \partial_X^2 R + \epsilon^4(\partial_T R + k_3 \partial_X^3 R + k_4 \partial_X R^3) + \epsilon^5(k_5 \partial_T \partial_X R \\ + k_6 \partial_X^4 R + k_7 \partial_X^2 R^3) = 0.\end{aligned} \tag{4.2.12}$$

The coefficients k_i of the model	
k_1	$b + A{\rho_c}^2 V'$
k_2	$\frac{3b^2\tau}{2} + (\frac{A+2B}{2})\rho_c^2 V'$
k_3	$\frac{7}{6}b^3\tau^2 + (\frac{A+6B}{6})\rho_c^2 V'$
k_4	$\frac{A\rho_c^2 V'''}{6}$
k_5	$3b\tau$
k_6	$\frac{5b^4\tau^3}{8} + (\frac{A}{24} + \frac{7B}{12}){\rho_c}^2 V'$
k_7	$\left(\frac{A}{12} + \frac{B}{6}\right){\rho_c}^2 V'''$

Table 4.1: The coefficients k_i of the model

Table 4.1 shows the coefficients $k_i (i = 1, 2, 3, ..., 7)$, $V' = \frac{\partial V(\rho)}{\partial \rho}\Big|_{\rho=\rho_c}$ and $V''' = \frac{\partial^3 V(\rho)}{\partial \rho^3}\Big|_{\rho=\rho_c}$. The value of τ close to the critical point (ρ_c, a_c) is chosen by:

$$\tau = \tau_c(\epsilon^2 + 1). \tag{4.2.13}$$

By substituting the constant value $b = -A{\rho_c}^2 V'$, the terms of ϵ having second and third-order completely vanished and we get:

$$\epsilon^4(\partial_T R - g_1 \partial_X^3 R + g_2 \partial_X R^3) + \epsilon^5(g_3 \partial_X^2 R + g_4 \partial_X^4 R + g_5 \partial_X^2 R^3) = 0. \tag{4.2.14}$$

Table 4.2 shows coefficients of $g_i (i = 1, 2, ..., 5)$. Eq. (4.2.14) can be transformed to mKdV equation by using following transformation.

$$T' = g_1 T, \quad R = \sqrt{\frac{g_1}{g_2}} R'. \tag{4.2.15}$$

The coefficients g_i of the model	
g_1	$-\frac{7b^3\tau_c{}^2}{6} - (\frac{A+6B}{6})\rho_c{}^2V'$
g_2	$\frac{A\rho_c^2V'''}{6}$
g_3	$\frac{3b^2\tau_c}{2}$
g_4	$\frac{15b^4\tau_c{}^3}{24} + (\frac{A}{24} + \frac{7B}{12})\rho_c{}^2V' + 3b\tau_c g_1$
g_5	$\left(\frac{A}{12} + \frac{B}{6}\right)\rho_c^2V''' - 3b\tau_c g_2$

Table 4.2: The coefficients g_i of the model

So, resulting equation (4.2.14) is given as follows:

$$\partial_{T'} R' - \partial_X^3 R' + \partial_X R'^3 + \epsilon M[R'] = 0, \tag{4.2.16}$$

where $M[R'] = \frac{1}{g_1}[g_3\partial_X^2 R' + g_4\partial_X^4 R' + \frac{g_1 g_5}{g_2}\partial_X^2 R'^3]$. By ignoring correction term $O(\epsilon)$ from (4.2.16), the solution of standard mKdV equation is:

$$R_0'(X, T') = \sqrt{L_1}\ \tanh\Big(\sqrt{\frac{L_1}{2}}(X - L_1 T')\Big). \tag{4.2.17}$$

Here, to represent the kink antikink density waves, the propagation velocity is denoted by L_1 and is obtained by solving the condition given below:

$$(R_0', M[R_0']) \equiv \int_{-\infty}^{\infty} dX R_0' M[R_0'] = 0, \tag{4.2.18}$$

with $M[R_0'] = M[R']$. From (4.2.18), the suitable choice of L_1 is obtained as

$$L_1 = \frac{5g_2 g_3}{2g_2 g_4 - 3g_1 g_5}. \tag{4.2.19}$$

Hence, the solution representing the kink antikink wave is given as under

$$\rho_j = \rho_c + \epsilon\sqrt{\frac{g_1 L_1}{g_2}}\tanh\Big(\sqrt{\frac{L_1}{2}}(X - L_1 g_1 T)\Big), \tag{4.2.20}$$

where $\epsilon^2 = \left(\frac{a_c}{a} - 1\right)$.

The kink antikink soliton solution (4.2.20) computed from the mKdV equation shows the coexisting phase composed of freely flowing as well as jammed phase in (ρ, a) space, described by $\rho_j = \rho_c \pm \epsilon\sqrt{\frac{g_1 L_1}{g_2}}$. The neutral stability curves (solid curves) obtained from linear analysis and the coexisting curves (dotted curves) acquired by nonlinear analysis in Fig. 4.2 (a) split the phase plot in three distinct regions: the no jam region is represented by the space above coexisting curves while the unstable region is represented by the space below the neutral stability curves. Thirdly, the metastable region exists between the neutral and coexisting curves. It is seen that the apex of each coexisting curve lower down corresponding to parameter c which indicates a higher rate of stability of heterogeneous flow.

4.3 Simulation

Simulation is performed for the purpose to explore the competency and rationality of theoretical results of the new model in explaining the properties of heterogeneous traffic on a single lane road. We choose the periodic boundary conditions and the selection of initial condition is given below:

$$\rho_j(1) = \rho_j(0) = \begin{cases} \rho_0; & j \neq \frac{N}{2}, \frac{N}{2} - 1 \\ \rho_0 - \sigma; & j = \frac{N}{2} \\ \rho_0 + \sigma; & j = \frac{N}{2} - 1, \end{cases} \tag{4.3.1}$$

where the system size is assumed as 100 lattice site and the other parameters are taken as $\sigma = 0.05$, $a = 3.2$, $\rho_0 = \rho_c = 0.2$, $V_{\max} = 2.0$, and $\lambda = 0.2$. Fig. 4.3 shows the simulation results of spatiotemporal evolutions of density waves and represents the effect of the parameter c on traffic stream at stationary state for $9.9 \times 10^4 - 10^5$ sec. time steps for $a = 3.2$. It is observed from Fig. 4.3(a)-4.3(c) that the kink antikink waves propagating in backward direction arise corresponding to the initial perturbation. Lower values of c lead to congested flow under small perturbation because the condition for the flow to be stable is not fulfilled. The kink antikink solution of mKdV equation (4.2.20) obtained from nonlinear stability analysis in section 4.2 represents the propagation behavior of traffic jam. For higher values of c, the stability criteria hold and the small amplitude disturbance to the uniform flow vanishes completely and stop-start density waves dissolve gradually in Fig. 4.3(d). As natural evidence of both theoretical as well as simulation results, one can claim that vehicles having high-sensitivity are much more efficient than vehicles having low-sensitivity in overcoming the congestion. It is also clear from Fig. 4.3(a)-4.3(d) that higher amount of smaller vehicles in traffic stream can help in suppressing traffic jams.

Fig. 4.4(a)-4.4(b) describe, respectively, the density profiles at fixed time $t = 8 \times 10^4$ sec. and site $j = 50$ for different values of c analogous to the panel of Fig. 4.3. One can observe from Fig. 4.4(a) that, corresponding to increasing values of c the number of kink antikink waves gradually decreases in the mixed traffic. Moreover, with increasing value of parameter c, the amplitude of density waves lower down and the free flow region spread over the whole space (see Fig. 4.4(a) & 4.4(b)). Further, the traffic jam vanishes completely and flow turns into a uniform state at $c = 0.4$. This validates the theoretical findings that in mixed traffic, vehicles with higher-sensitivity help in overcoming the jams which refer to the stability of flow.

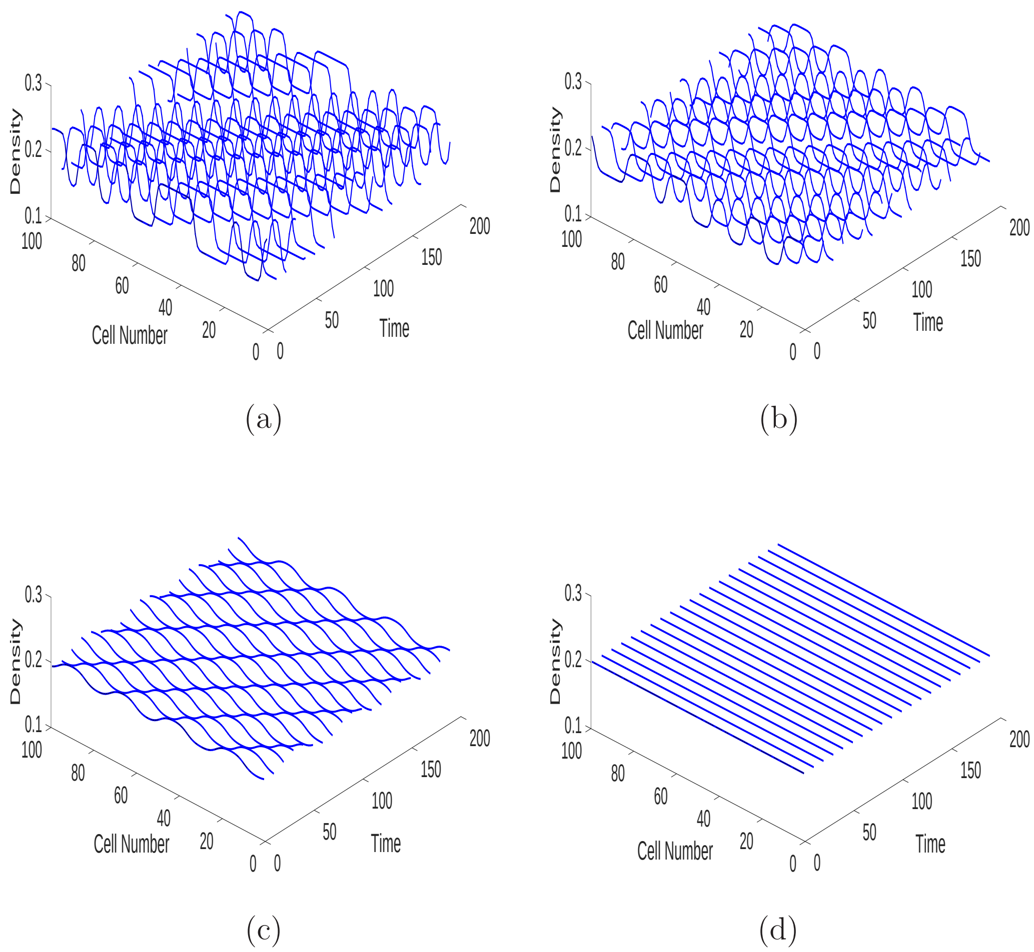

Figure 4.3: Space-time evolutions of density waves when $\lambda = 0.2, p_1 = 2.5, q = 0.5, a = 3.2$ for (a) $c = 0.1$, (b) $c = 0.2$, (c) $c = 0.3$ and (d) $c = 0.4$ respectively.

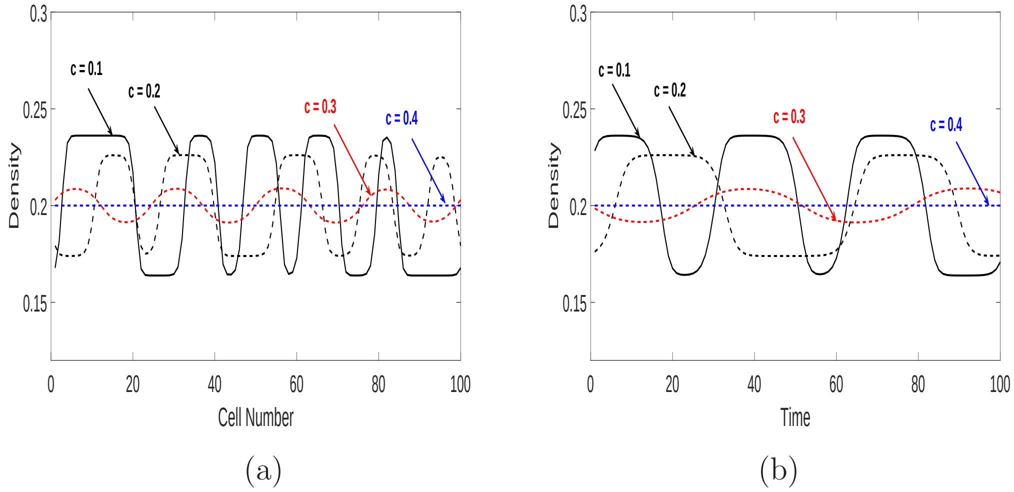

Figure 4.4: Density profiles corresponding to different values of fraction parameter c obtained at (a) fixed time $t = 8 \times 10^4$ sec. and lattice sites varies (b) for fixed lattice site $j = 50$ and time varies from $t = 9.99 \times 10^4 - 10^5$ sec. when $\lambda = 0.2, p_1 = 2.5, q = 0.5$.

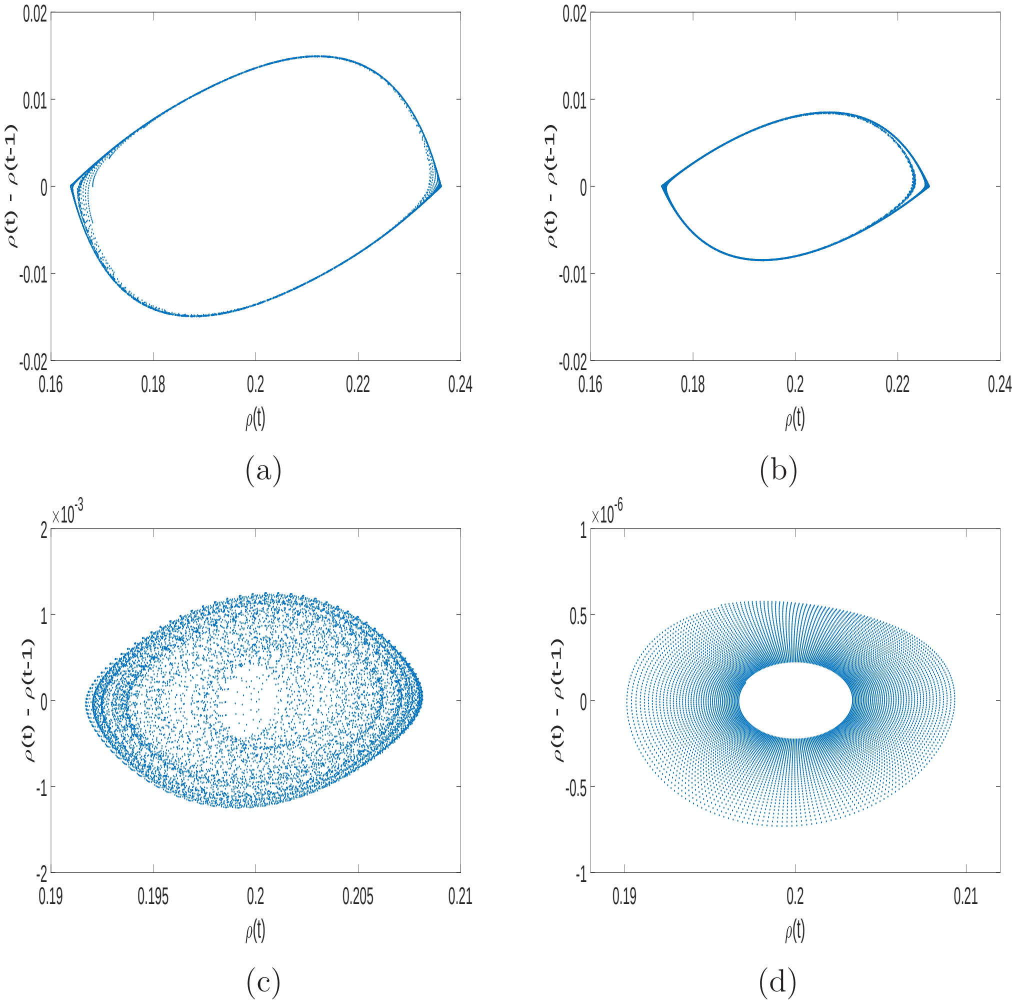

Figure 4.5: Plots of density versus density difference when $\lambda = 0.2, p_1 = 2.5, q = 0.5, a = 3.2$ for (a) $c = 0.1$, (b) $c = 0.2$, (c) $c = 0.3$ and (d) $c = 0.4$ respectively.

To ensure the periodic nature of traffic flow, the phase plots of $\rho(t) - \rho(t-1)$ against $\rho(t)$ is drawn in Fig. 4.5 for $t = 10^4 - 2 \times 10^4$ sec., with respect to the panel of Fig. 4.3. The patterns in Fig. 4.5 represents the closed loop in the phase plane formed by the set of dispersed points. For all values of c, the limit cycle (closed-loop pattern) exhibits the periodic nature of traffic. The right, as well as the left end points in the loop, represent the jammed state of traffic and the free flow traffic respectively; which is also computed via nonlinear stability analysis. When the traffic flow comes into the stable state for increasing values of c the loop start diminishing in size and convert into a single point at $c = 0.4$.

Above results are shown for smaller value of λ. We will further explore the effect of larger value of λ on the traffic dynamics. A noteworthy finding is that the simulation works for $\lambda < 0.5$ which is in contrast to the theoretical results. Linear stability analysis did not provide any condition on λ. Further analysis is required to obtain the bounds on λ. Since the parameter λ, representing the impact of optimal current difference, is assumed to be small ($\lambda = 0.2$), therefore we can conclude that the heterogeneous model and the analysis is correct.

From the results shown above, it is logical to conclude that in heterogeneous traffic, the fraction of vehicles having high or low-sensitivity plays a remarkable role on the stabilization/destabilization of mixed traffic on one lane road.

4.4 Summary of results

4.4.1 Outcomes:

- Lattice hydrodynamic model for heterogeneous traffic on one lane road has been presented by considering optimal current difference effect.
- Two types of vehicles analogous to small and large vehicles with different sensitivities are considered.
- Proportionality parameter corresponds to small and large vehicles is introduced that controls the fraction of vehicles.
- The nature of mixed traffic is studied analytically by using linear and nonlinear analysis.
- Phase diagram in (ρ, a) space is obtained by neutral stability and coexisting curves through which the influence of high-sensitivity vehicles on stability of flow has been examined.

- Effect of fraction parameter on critical phase transitions is shown through five distinct regions in (ρ, c) space.
- High-sensitivity vehicles stimulate the stability in flow while low-sensitivity vehicles negatively impact stability of flow that leads to traffic congestion.

4.4.2 Future scope:

- Proposed model can be further extended to analyze the critical phenomenon lies in actual traffic situations, for example: lane changing, passing and environmental factors etc.
- Additionally, the proposed theoretical and numerical predictions of the model need to be affirmed by investigations based on experiments.

Chapter 5

The effect of passing on traffic flow with delayed feedback control

Prevailing traffic conditions demand an effective transportation system which leads to efficient movement of vehicles even under an inhomogeneous state of flow. Due to increased automobiles, urbanization and population growth, traffic congestion has been increasing through out the world. Increasing jams minimized the capability of transportation infrastructure and leads to increasing travel time, environmental pollution, safety hazards, fuel consumption etc. Thus, advancements in the field of electronics and communications provide efficient methods to develop transportation management strategies. In practice, it is often desirable to avoid chaos in order to improve or change system performance. Given a chaotic attractor, one approach might be to make some major and possibly costly changes in the system that completely change its dynamics to achieve the desired behavior.

The reason behind the choice of control theory is to avoid traffic congestion whatever the cause may be and to diminish it quickly whenever it happens. In terms of control theory, a disturbance is a sign which negatively influence the system output. In terms of vehicular traffic, examples of external disturbance are accidents or bottlenecks etc.

Feedback control refers to an operation that leads to minimize the variation between input and output of the system in the presence of interruptions. In traffic flow theory, one of the most utilized strategy to regulate the unstable and chaotic behavior of traffic, is the decentralized delayed feedback control. Ott et al. [159] have suggested a method (OGY method) which stabilizes chaotic motions onto a desired unstable periodic orbit within a chaotic attractor. They suggested two methods out of which in first method combined feedback with a periodic force of a special form is used and in second method no external force is required. Further, Pyragas [160] gave a continuous method of chaos control using time delayed controlling forces. Pyragas method was then investigated from experimental and theoretical points of view by Just et al. [161] and analytical stability analysis was performed. It was shown that the success of the control scheme is governed by the revolution around an unstable periodic orbit. In addition, Konishi et al. [162, 163] proposed coupled map car

The content of this chapter has been published in Physica A: Statistical Mechanics and its Applications, 510: 446-455,(2018).

following model describing the behavior of a group of vehicles running in a single lane. The condition under which the traffic jams will never occur was derived. Zhao and Gao [164], by utilizing the definition presented by Konishi et al. [162], raised some problem through example. A feedback signal was introduced into the optimal velocity model, which only works when the state is inhomogeneous. Zhao and Gao [165] introduced coupled map car following model by following the method developed by Konishi in order to control the congestion aroused by bottlenecks. Jin and Hu [166] proposed an optimal velocity model using the displacement and velocity differences without taking driver's delay into account. Further, the effect of nonlinear behavior, fuel consumption and emission on traffic flow are recently explored in [167–169].

Lattice hydrodynamic model [1] as discussed in previous Chapters, got much attention of researchers [81–84, 86, 87, 89, 92, 100, 101, 103, 123, 124, 152, 170–173]. In recent past, Ge et al. [94] developed lattice model utilizing the control method and results show that feedback control significantly suppress the traffic jams. In addition to the proposed model, many extended versions were presented, such as, delayed feedback control [95], control method by considering rate of change of density difference [174] at time $t-1$, variation rate of optimal velocity [175], flow rate difference effect [176], feedback control for optimal flux for forward looking sites [177], delayed feedback control based on historic density difference effect [98], double flux difference [97].

But upto our knowledge feedback control has not been applied yet by considering the effect of passing. Thus, a modified model is presented to investigate the influence of passing on traffic dynamics. First is the introductory part, then section 5.1 is devoted to the new model, in section 5.2 theoretical analyses are done, section 5.3 gives the simulation results and 5.4 refers to the concluding remarks.

5.1 Extended lattice model

With the aim to minimize the jamming states and to obtain the stability conditions under homogeneous traffic flow at macroscopic level Nagatani [1] introduced lattice hydrodynamic model (discussed in Chapter 1). The continuity and evolution equations in terms of flow are:
Continuity eq.:

$$\partial_t(\rho_{j+1}) + \rho_0(q_{j+1} - q_j) = 0, \tag{5.1.1}$$

Evolution eq.:

$$\partial_t(q_j) = a[\rho_0 V(\rho_{j+1}) - q_j]. \tag{5.1.2}$$

At macroscopic level, mKdV equation is derived using nonlinear analysis in the basic lattice model which describes the jamming transitions and density waves in an unstable region. In the unstable region, the chaotic behavior produced under the dynamic process of traffic was captured by adding the effect of passing in the evolution equation (1.6.6) by Nagatani [83]. Due to the impact of passing, the continuity equation (1.6.5) remain the same but the evolution equation is modified as follows:

$$\partial_t(q_j) = a[\rho_0 V(\rho_{j+1}) - q_j] + a\gamma_1[\rho_0 V(\rho_{j+1}) - \rho_0 V(\rho_{j+2})], \tag{5.1.3}$$

where the parameter γ_1 is parameter for passing.

Recently, Ge et al. [94] proposed a control method in which the evolution equation was modified to incorporate the control parameter proportional to the flux difference at j and $j+1^{th}$ site. Further, Redhu et al. [95] modified the evolution equation by considering the flux difference of two different states, current and delayed one:

$$\partial_t(q_j) = a[\rho_0 V(\rho_{j+1}) - q_j] + a\zeta[q_{j+1}(t) - q_{j+1}(t-\tau)]. \tag{5.1.4}$$

The purpose behind designing the control signal in lattice model is to avail the dynamic estimation information using intelligent transportation system. As discussed in ref. [83], traffic flow becomes chaotic, when passing is there. Therefore, we modified the evolution equation (5.1.4) by incorporating the effect of passing while the continuity equation remains the same:

$$\begin{aligned}\partial_t(q_j) = \quad & a[\rho_0 V(\rho_{j+1}) - q_j] + a\gamma_1[\rho_0 V(\rho_{j+2}) - \rho_0 V(\rho_{j+2})] + a\zeta \\ & \qquad\qquad\qquad\qquad [q_{j+1}(t) - q_{j+1}(t-\tau)],\end{aligned} \tag{5.1.5}$$

where ζ is the control parameter. Basic lattice model [1] can be recovered for $\zeta = 0$ and $\gamma_1 = 0$. The density equation of the model is given by:

$$\begin{aligned}\rho_j(t+2\tau) - \rho_j(t+\tau) + \tau{\rho_0}^2[V(\rho_{j+1}) - V(\rho_j)] - \tau{\rho_0}^2\gamma_1[V(\rho_{j+2}) - 2V(\rho_{j+1}) + V(\rho_j)] \\ - \zeta[\rho_{j+1}(t+\tau) - 2\rho_{j+1}(t) + \rho_{j+1}(t-\tau)] = 0.\end{aligned} \tag{5.1.6}$$

5.2 Qualitative properties of the proposed model

5.2.1 Stability analysis using control signal

To discuss the effect of delayed feedback control when passing is there, linear stability analysis has been done using control theory. We consider the steady-state solution as the following form:

$$[\rho_n, q_n] = [\rho^*, q^*]. \tag{5.2.1}$$

Using the above steady-state solution, we get the linearized system of equations (5.1.1) and (5.1.5):

$$\partial_t {\rho_{j+1}}^0 + \rho_0({q_{j+1}}^0 - {q_j}^0) = 0, \tag{5.2.2}$$

$$\begin{aligned}\partial_t({q_j}^0) = \quad & a[\rho_0 f_{j+1}(\rho^*){\rho_{j+1}}^0 - {q_j}^0] + a\gamma_1[\rho_0 f_{j+1}(\rho^*){\rho_{j+1}}^0 - \rho_0 f_{j+2}(\rho^*) \\ & {\rho_{j+2}}^0] + a\zeta[{q_{j+1}}^0(t) - {q_{j+1}}^0(t-\tau)],\end{aligned} \tag{5.2.3}$$

where ${\rho_j}^0 = \rho_j - \rho^*$, ${q_j}^0 = q_j - q^*$ and $f_j(\rho^*) = \frac{\partial V(\rho_j)}{\partial(\rho_j)}|_{\rho_j=\rho^*}$. The desired density is denoted by ρ^* and the comprehensive flow of vehicles is q^*. Taking the laplace transformation of equations (5.2.2) and (5.2.3) based on frequency domain analysis, we get:

$$sP_{j+1}(s) - \rho_{j+1}(0) + \rho_0[Q_{j+1}(s) - Q_j(s)] = 0, \tag{5.2.4}$$

$$\begin{aligned}sQ_j(s) - q_j(0) = \quad & a[\rho_0 f_{j+1}(\rho^*)P_{j+1}(s) - Q_j(s)] + a\gamma_1\rho_0[f_{j+1}(\rho^*)P_{j+1}(s) \\ & - f_{j+2}(\rho^*)P_{j+2}(s)] + a\zeta[Q_{j+1}(s) - e^{-\tau s}Q_{j+1}(s)],\end{aligned} \tag{5.2.5}$$

where $L({\rho_j}^0) = P_j(s), L({q_j}^0) = Q_j(s)$, L is the laplace transformation and the complex number frequency denoted by s. The flux equation can be obtained by using value of P_{j+1} from (5.2.4) in (5.2.5) as follows:

$$\begin{aligned}Q_j(s) = & \frac{-(1+\gamma_1)a{\rho_0}^2 f_{j+1}(\rho^*) - a\gamma_1{\rho_0}^2 f_{j+2}(\rho^*) + sa\zeta(1-e^{-\tau s})}{d(s)}Q_{j+1}(s) \\ & + \frac{a\gamma_1\rho_0^2 f_{j+2}(\rho^*)}{d(s)}Q_{j+2}(s) + \frac{(1+\gamma_1)a\rho_0 f_{j+1}(\rho^*)}{d(s)}\rho_{j+1}(0) \\ & - \frac{a\gamma_1\rho_0 f_{j+2}(\rho^*)}{d(s)}\rho_{j+2}(0) + \frac{s}{d(s)}q_j(0),\end{aligned} \tag{5.2.6}$$

where the characteristic polynomial is denoted by:

$$d(s) = s^2 + as - (1+\gamma_1)a{\rho_0}^2 f_{j+1}(\rho^*), \tag{5.2.7}$$

and the transfer functions are obtained as:

$$G_1(s) = \frac{-(1+\gamma_1)a{\rho_0}^2 f_{j+1}(\rho^*) - a\gamma_1{\rho_0}^2 f_{j+2}(\rho^*) + sa\zeta(1-e^{-\tau s})}{d(s)}, \tag{5.2.8}$$

$$G_2(s) = \frac{a\gamma_1\rho_0^2 f_{j+2}(\rho^*)}{d(s)}. \tag{5.2.9}$$

Based on control theory Konishi et al. [163] derived a simple definition describing the occurrence of traffic jams.

Definition 1. Traffic jam will not occur if:

(i) $d(s)$ is stable;
(ii) If H_∞-norm of transfer function $G(s)$ is equal or less than one, i.e.,

$$\|G(s)\|_\infty = \sup_{\omega\varepsilon[0,\infty)} |G(j\omega)| \leq 1.$$

Now, in order to fulfill the first condition of the above definition, Hurwitz stability criteria is used which states that if all the coefficients in characteristic polynomial $d(s)$ are of same sign then it will be stable. The coefficients of $d(s)$ are $1, a, -(1+\gamma_1)a{\rho_0}^2 f_{j+1}(\rho^*)$ and all are positive. Since the sensitivity parameter a is positive always, ${\rho_0}^2 f_{j+1}$ is negative because of the property of optimal velocity function (1.6.7) (given in Chapter 1) which makes the third coefficient positive as well. So, all coefficients are of same sign. Our purpose behind modeling traffic using control theory is to minimize traffic congestion. Which is possible only when the control signal is suitably designed. Therefore, second condition (in above definition) of system stability can be fulfilled if:

$$\|G(s)\|_\infty = \sup_{\omega\varepsilon[0,\infty)} \mid G(j\omega) \mid \leq 1, \tag{5.2.10}$$

$$|G(j\omega)| = \sqrt{G(j\omega).G(-j\omega)} \leq 1. \tag{5.2.11}$$

Thus the absolute value of transfer function $G_1(s)$ is given by:

$$G_1(j\omega) = \sqrt{\frac{\begin{array}{r} 2a^2\omega^2\zeta^2(1-\cos(\tau\omega)) + 2(1+\gamma_1)a^2\omega\zeta\rho_0^2 f_{j+1}(\rho^*)\sin(\tau\omega) \\ + (1+\gamma_1)^2 a^2\rho_0^4 f_{j+1}^2 + a^2{\gamma_1}^2\rho_0^4 f_{j+2}^2 + 2(1+\gamma_1)\gamma_1 a^2\rho_0^4 \\ f_{j+1}(\rho^*) f_{j+2}(\rho^*) + 2a^2\gamma_1\rho_0^2\omega\zeta\sin(\tau\omega) f_{j+2}(\rho^*) \end{array}}{\omega^4 + (1+\gamma_1)^2 a^2\rho_0^4 f_{j+1}^2(\rho^*) + 2\omega^2(1+\gamma_1)a\rho_0^2 f_{j+1}(\rho^*) + a^2\omega^2}}, \tag{5.2.12}$$

and $G_2(s)$ is given with absolute value as:

$$G_2(j\omega) = \sqrt{\frac{a^2{\gamma_1}^2\rho_0^4 {f_{j+2}}^2(\rho^*)}{\omega^4 + (1+\gamma_1)^2 a^2\rho_0^4 f_{j+1}^2(\rho^*) + 2\omega^2(1+\gamma_1)a\rho_0^2 f_{j+1}(\rho^*) + a^2\omega^2}}. \tag{5.2.13}$$

Now it is not easy to get H_∞ norm of transfer function analytically. Therefore, the value of ζ should be obtained in such a way that $\|G(s)\|_\infty \leq 1$ for all $\omega\varepsilon[0,\infty)$. Which holds true if the following inequalities are satisfied for transfer functions:

$$\begin{aligned} &\omega^4 + a\omega^2[a + 2(1+\gamma_1){\rho_0}^2 f_{j+1}(\rho^*)] - 2a^2\omega^2\zeta^2(1-\cos(\tau\omega)) - 2(1+\gamma_1) \\ &a^2\zeta{\rho_0}^2 f_{j+1}(\rho^*)\sin(\tau\omega)\omega - 2a^2\gamma_1{\rho_0}^2\zeta\sin(\tau\omega) f_{j+2}(\rho^*)\omega - a^2{\gamma_1}^2{\rho_0}^4 {f^2}_{j+2} \\ &\qquad -2(1+\gamma_1)\gamma_1 a^2{\rho_0}^4 f_{j+1}(\rho^*) f_{j+2}(\rho^*) \geq 0, \end{aligned} \tag{5.2.14}$$

and

$$\begin{aligned}\omega^4 + a\omega^2[a + 2(1+\gamma_1){\rho_0}^2 f_{j+1}(\rho^*)] + (1+\gamma_1)^2 a^2 {\rho_0}^4 {f^2}_{j+1}(\rho^*) - a^2{\gamma_1}^2{\rho_0}^4 \\ {f^2}_{j+2}(\rho^*) \geq 0.\end{aligned} \tag{5.2.15}$$

To remove the difficulty in obtaining the above condition analytically, we have adopted the following procedure: (1) Bode plot for both transfer functions has been drawn; (2) Confirm that the peak gain of bode plot is not more than 1 so that the inequalities (5.2.14) and (5.2.15) are satisfied. Fig. 5.1(a)-(b) shows the bode plots for relatively small passing,

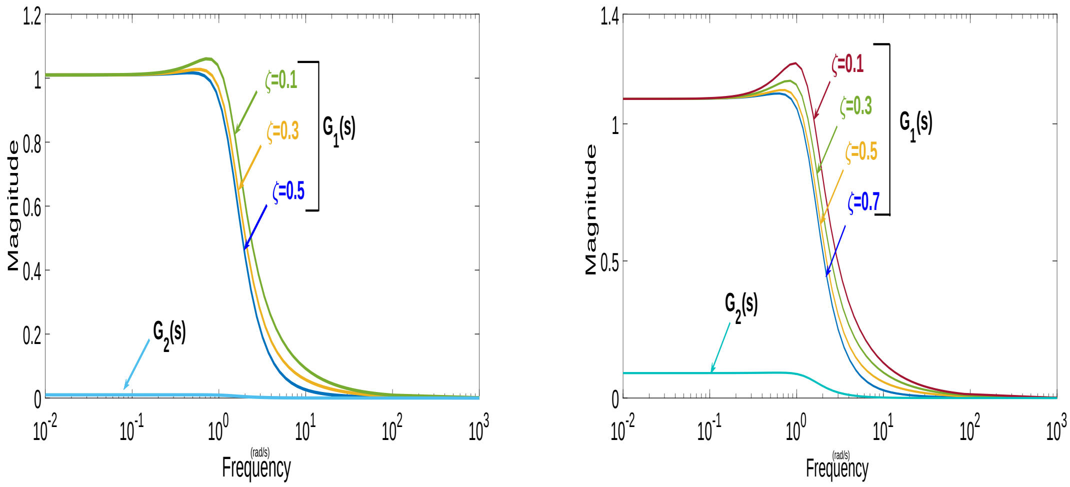

(a) (b)

Figure 5.1: Bode plot for $\zeta = 0.1, 0.3, 0.5$ when (a) $\gamma_1 = 0.01$ and (b) $\gamma_1 = 0.1$

i.e., $\gamma_1 = 0.01$ and higher passing, i.e., $\gamma = 0.1$, respectively. Clearly, for smaller range of frequency, the amplitude of gain function remains constant and decreases sharply and becomes zero for relatively larger range of frequency. Further, it can be observed from the figures that the gain function decreases its amplitude with increasing values of ζ and fulfill broadly the condition $\|G(s)\|_\infty \leq 1$ (Fig 5.1(a)).

Although the definition regarding the disappearance of traffic jams given by Konishi et al. [163] is widely used in traffic flow theory but little effort has been made by Zhao and Gao [164] to redefine the above concept. As the definition is redefined for car following models based on the type of disturbance, helpful or harmful it can be. He pointed out that if $\|G(s)\|_\infty \leq 1$ and the polynomial $d(s)$ is stable, then it is sure that traffic jams will not exist but if $\|G(s)\|_\infty > 1$ and $d(s)$ is stable then it is not sure whether traffic jam occurs or not. The instability condition for the proposed model obtained from the linear analysis (following a similar procedure as in [1]) is given as under:

$$\tau > \frac{(1-2\gamma_1)}{(-3+2\zeta){\rho_0}^2 V'(\rho_0)}. \tag{5.2.16}$$

5.2.2 Nonlinear stability analysis

To explain the density waves in jammed traffic, mKdV equation is required. Thus, to obtain the nonlinear equation, we consider the slow variables X and T around (ρ_c, a_c) as:

$$X = \epsilon(j + bt), \quad T = \epsilon^3(t). \tag{5.2.17}$$

The density at j^{th} site can be defined as:

$$\rho_j = \rho_c + \epsilon R(X, T), \tag{5.2.18}$$

the constant term b needs to be determined. Expand the density equation (5.1.6) with the help of Taylor series expansion upto fifth-order of ϵ by using slow variables X and T given in (5.2.17). Thus a nonlinear equation in the following form is obtained:

$$\begin{aligned} \epsilon^2 k_1 \partial_X R + \epsilon^3 k_2 \partial_X^2 R + \epsilon^4(\partial_T R + k_3 \partial_X^3 R + k_4 \partial_X R^3) + \epsilon^5(k_5 \partial_T \partial_X R \\ + k_6 \partial_X^4 R + k_7 \partial_X^2 R^3) = 0. \end{aligned} \tag{5.2.19}$$

The coefficients $k_i (i = 1, 2, 3, ...7)$ in the nonlinear equation (5.2.19) are given in Table 5.1 and the first and third-order derivatives of V are obtained by $V' = \frac{dV(\rho)}{d\rho}|_{\rho=\rho_c}$ and $V''' = \frac{dV^3(\rho)}{d\rho^3}|_{\rho=\rho_c}$. The value of τ can be defined near the critical point as follows:

$$\tau = \tau_c \epsilon^2 + \tau_c. \tag{5.2.20}$$

After substituting the value of τ from (5.2.20) and $b = -{\rho_c}^2 V'$ in equation (5.2.19) and removing the terms of ϵ with second and third-orders, following nonlinear equation is obtained:

$$\epsilon^4(\partial_T R - g_1 \partial_X^3 R + g_2 \partial_X R^3) + \epsilon^5(g_3 \partial_X^2 R + g_4 \partial_X^4 R + g_5 \partial_X^2 R^3) = 0, \tag{5.2.21}$$

the coefficients $g_i (i = 1, 2, ...5)$ in (5.2.21) are given in Table 5.2. Following transformations can be adopted in order to transform (5.2.21) to standard mKdV equation:

$$T' = g_1 T, \quad R = \sqrt{\frac{g_1}{g_2}} R', \tag{5.2.22}$$

and the transformed form of (5.2.21) can be written as:

$$\partial_{T'} R' - \partial_X^3 R' + \partial_X R'^3 + \epsilon M[R'] = 0, \tag{5.2.23}$$

where $M[R'] = \frac{1}{g_1}[g_3 \partial_X^2 R' + g_4 \partial_X^4 R' + \frac{g_1 g_5}{g_2} \partial_X^2 R'^3]$. By ignoring the term $O(\epsilon)$ from (5.2.23), the solution of standard mKdV equation is obtained:

$$R_0^{'}(X,T^{'}) = \sqrt{L_1}\,\tanh\Big(\sqrt{\frac{L_1}{2}}(X - L_1T^{'})\Big). \tag{5.2.24}$$

The coefficients k_i of the model	
k_1	$b + {\rho_c}^2V'$
k_2	$\frac{3b^2\tau}{2} + (\frac{1-2\gamma_1}{2})\rho_c^2V' - \zeta b^2\tau$
k_3	$\frac{7}{6}b^3\tau^2 + (\frac{1-6\gamma_1}{6})\rho_c^2V'$
k_4	$\frac{\rho_c^2V'''}{6}$
k_5	$3b\tau - 2\zeta b\tau$
k_6	$\frac{5b^4\tau^3}{8} + (\frac{1}{24} - \frac{7\gamma_1}{12}){\rho_c}^2V' - \frac{\zeta}{24}(2b^4\tau^3 + 12b^2\tau)$
k_7	${\rho_c}^2V'''(\frac{1-2\gamma_1}{12})$

Table 5.1: The coefficients k_i of the model

The propagation velocity, to represent the kink antikink type of density waves, is denoted by L_1 and can be obtained by solving the condition:

$$(R_0^{'}, M[R_0^{'}]) \equiv \int_{-\infty}^{\infty} dX R_0^{'} M[R_0^{'}] = 0, \tag{5.2.25}$$

with $M[R_0^{'}] = M[R^{'}]$. From (5.2.25), we got the appropriate value of L_1 as:

$$L_1 = \frac{5g_2g_3}{2g_2g_4 - 3g_1g_5}. \tag{5.2.26}$$

Hence, the solution representing the kink antikink density waves is obtained as follows:

$$\rho_j = \rho_c + \epsilon\sqrt{\frac{g_1L_1}{g_2}}\tanh\Big(\sqrt{\frac{L_1}{2}}(X - L_1g_1T)\Big), \tag{5.2.27}$$

where $\epsilon^2 = \left(\frac{a_c}{a} - 1\right)$ and the amplitude D of the solution is given by $D = \sqrt{\frac{g_1}{g_2}\epsilon^2L_1}$. The above kink solution (5.2.27) exists if the following inequality holds:

$$-14{\gamma_1}^2 - (12\zeta^2 - 36\zeta + 13)\gamma_1 + (2\zeta^2 - 6\zeta + 1) > 0, \tag{5.2.28}$$

which is true under the following condition:

$$0 \leq \gamma_1 < f(\zeta),$$

where

$$f(\zeta) = \frac{1}{28}(-13 + 36\zeta - 12\zeta^2 \pm (-3 + 2\zeta)\sqrt{(25 - 108\zeta + 36\zeta^2)}). \tag{5.2.29}$$

The coefficients g_i of the model	
g_1	$-\frac{7b^3{\tau_c}^2}{6} - (\frac{1-6\gamma_1}{6}){\rho_c}^2V'$
g_2	$\frac{\rho_c^2V'''}{6}$
g_3	$\frac{3b^2\tau_c}{2} - \zeta b^2\tau_c$
g_4	$\frac{5b^4{\tau_c}^3}{8} + (\frac{1}{24} - \frac{7\gamma_1}{12}){\rho_c}^2V' - \frac{\zeta}{24}(2b^4{\tau_c}^3 + 6b^2\tau_c) + (3 - 2\zeta)b\tau_c g_1$
g_5	$\rho_c^2V'''(\frac{1-2\gamma_1}{12}) - (3-2\zeta)b\tau_c g_2$

Table 5.2: The coefficients g_i of the model

If $\gamma_1 \geq f(\zeta)$ then mKdV equation (5.2.23) cannot be derived through nonlinear analysis. On the other hand the kink solution (5.2.27) described by $\rho_j = \rho_c \pm D$, represents the coexisting phase which is the combination of both congested flow and freely moving phase respectively when $\gamma_1 < f(\zeta)$.

Fig. 5.2(a) represents the phase plane in (ρ, a) space for $\gamma_1 = 0.01$ while the values of control parameter ζ varies. It is clear from the Fig. 5.2(a) that the neutral stability curves (black solid curves) along with coexisting curves (blue dotted curves) lower down with increasing values of ζ. It happens because when passing occurs then the control parameter helps in reducing the congestion. The neutral stability curves obtained from linear and coexisting curves obtained from nonlinear analysis, divide the entire plot into three distinct regions:

stable, unstable and metastable region. Fig. 5.2(b) represents the phase plot for $\gamma_1 = 0.1$. As the value of control parameter ζ is increasing the stable region is getting wider which shows that jamming situations can be avoided with effective control even at the higher rate of passing.

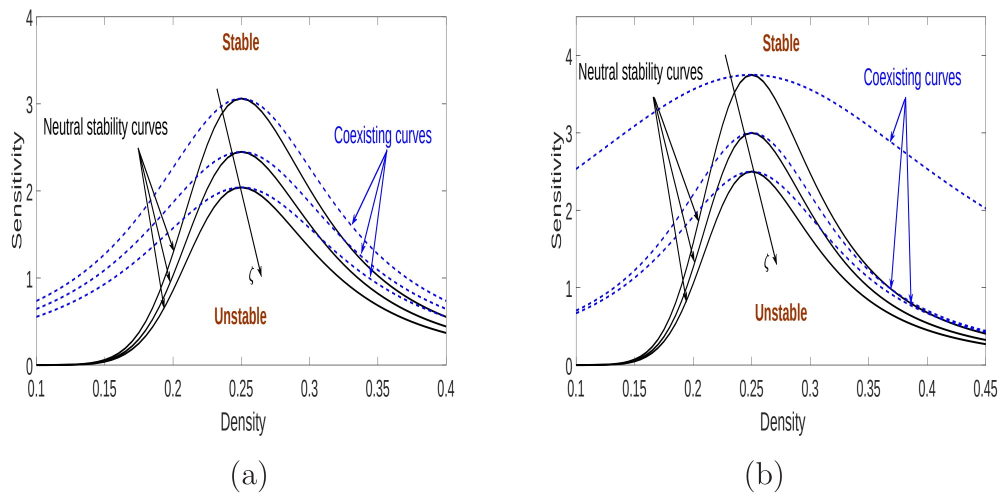

Figure 5.2: Phase plot in (ρ, a) space for $\zeta = 0, 0.3, 0.5$ (a) for $\gamma_1 = 0.01$ (b) for $\gamma_1 = 0.1$.

5.3 Discussion of results

For investigating the capability of the proposed model in alleviating traffic jams and to validate theoretical results, simulations are carried out by using periodic boundary conditions. For this, the whole space is divided into 140 lattice sites. Density at initial stage is adopted as $\rho_0 = \rho_c = 0.25$, maximal velocity $v_{\max} = 2$ and sensitivity parameter takes the values $a = 2.1, 2.7$ for $\gamma_1 = 0.01, 0.1$ respectively. In order to describe the traffic phenomena at different sites, the density at sites $50 - 55$ and $56 - 60$ is chosen as 0.5 and 0.2 respectively.

5.3.1 Early time effect of feedback control

Fig. 5.3 shows the density profiles at different sites when control parameter varies at time $t = 1 : 200$ sec. for $\gamma_1 = 0.01$. It can be observed from Fig. 5.3(a)-5.3(c) that the perturbation at initial stage comes out in terms of kink density waves in unstable region. The amplitude of density waves is higher without control, i.e, for $\zeta = 0$ and the oscillation is around critical density $\rho_c = 0.25$ but as the feedback control is applied the amplitude of density waves decreases and the free flow region gets wider. Similar results found in Fig.

5.4 when passing rate is $\gamma_1 = 0.1$. There exist more oscillations around critical density at a higher rate of passing but feedback control helps in overcoming the unstable states.

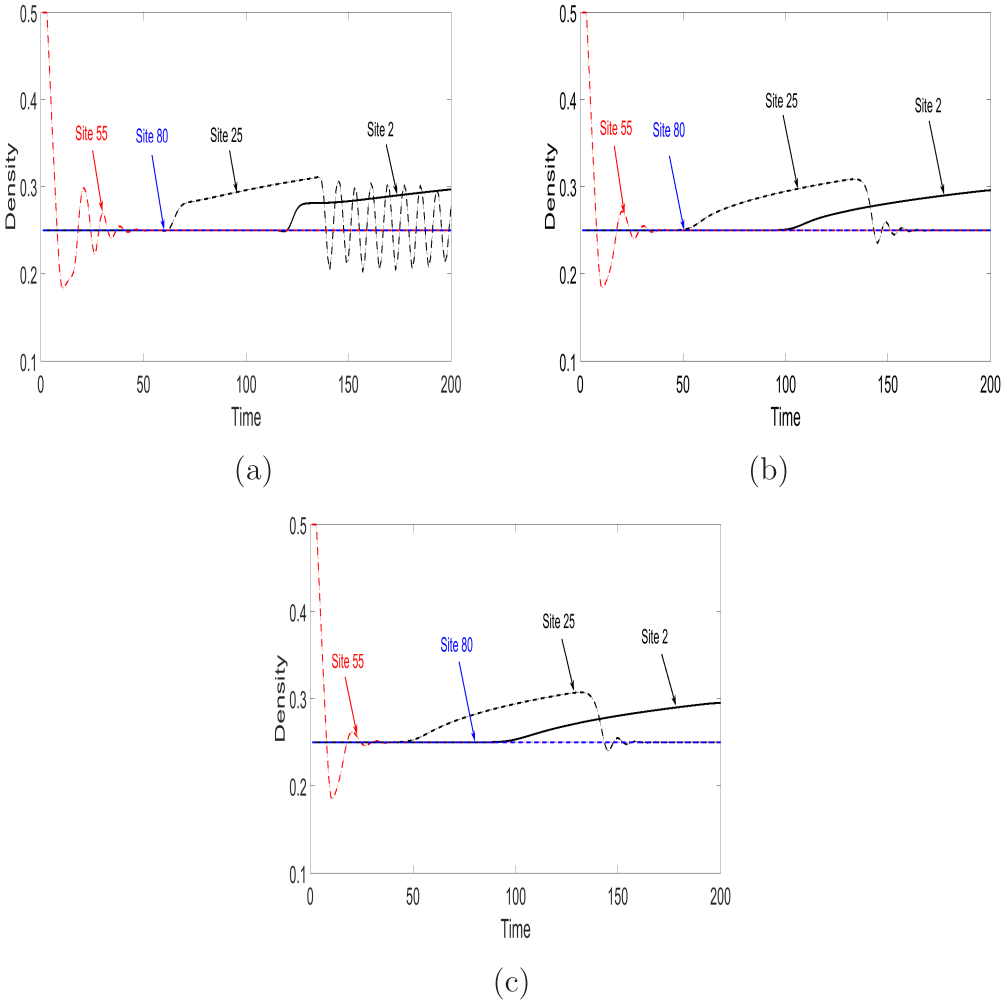

Figure 5.3: Density profiles for $\zeta = 0, 0.3, 0.5$ at time $t = 1 - 200$ sec. when $\gamma_1 = 0.01$.

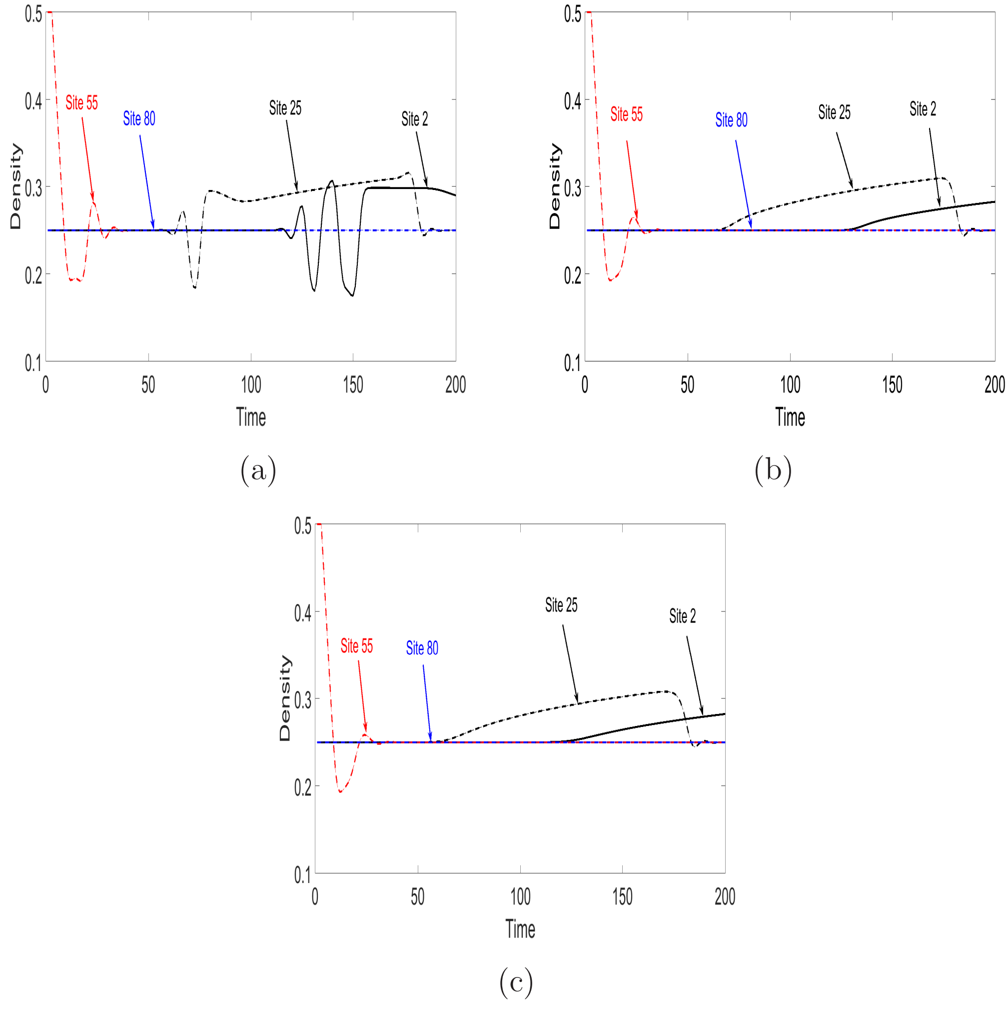

Figure 5.4: Density profiles for $\zeta = 0, 0.3, 0.5$ at time $t = 1 - 200$ sec. when $\gamma_1 = 0.1$.

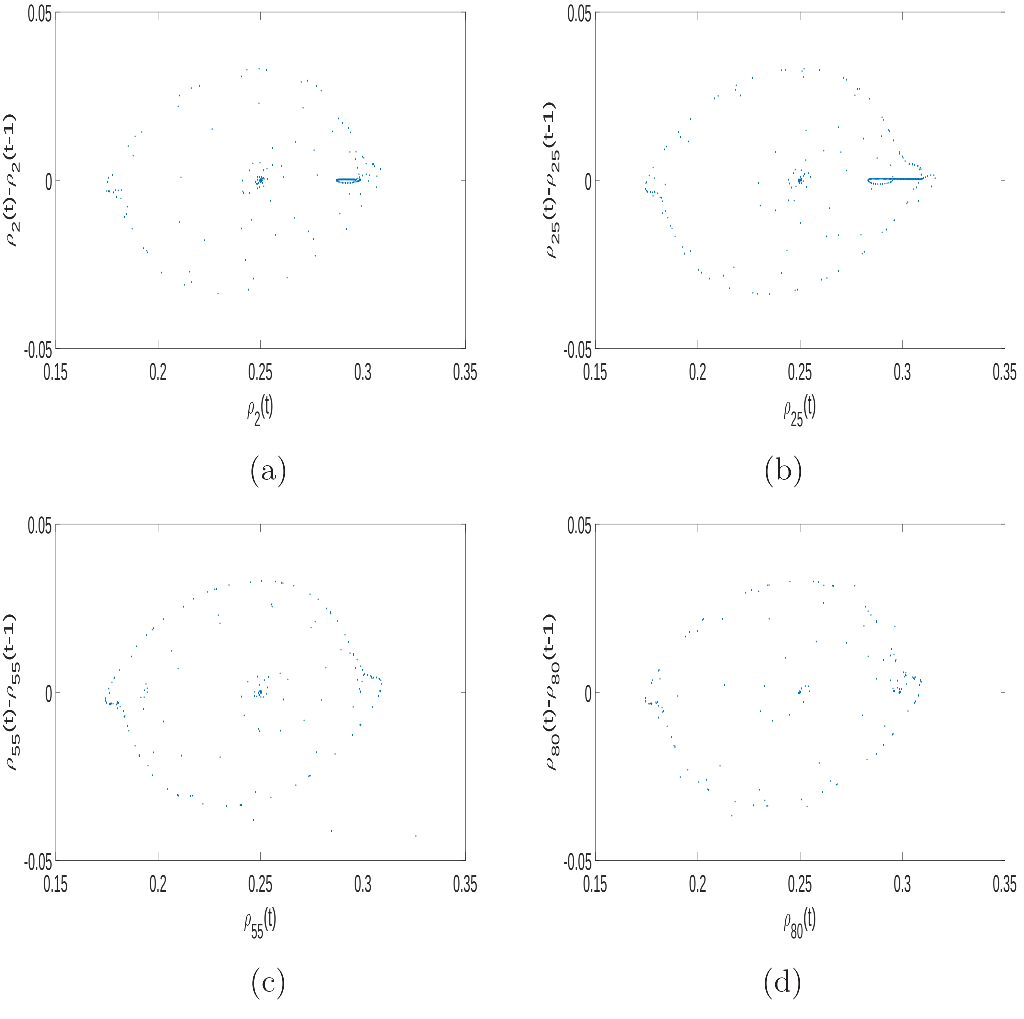

Figure 5.5: Plots of density difference $\rho_j(t) - \rho_j(t-1)$ against $\rho_j(t)$ when $\gamma_1 = 0.1$ at time $t = 1 - 500$ sec. for $\zeta = 0$ at different sites.

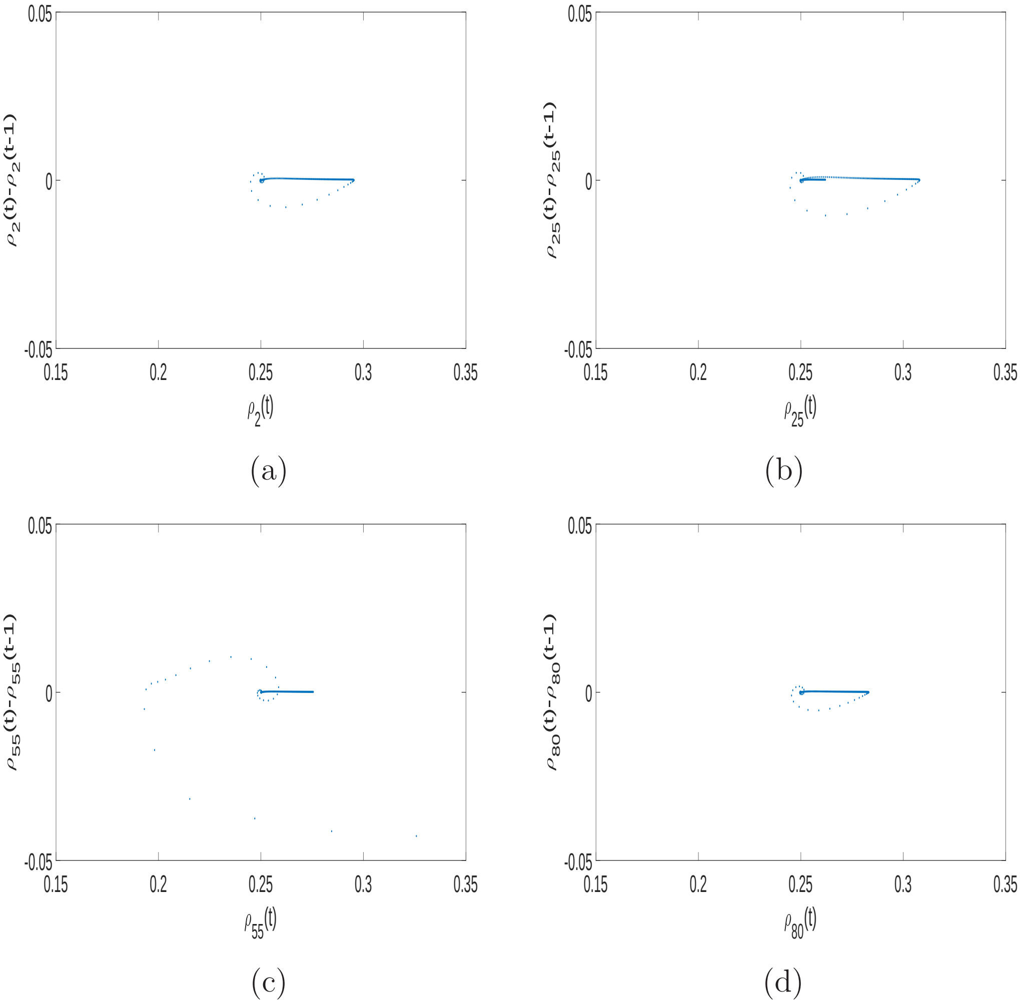

Figure 5.6: Plots of density difference $\rho_j(t) - \rho_j(t-1)$ against $\rho_j(t)$ when $\gamma_1 = 0.1$ at time $t = 1 - 500$ sec. for $\zeta = 0.5$ at different sites.

Fig. 5.5 and 5.6 represent the plots of density difference against density at different site for $\gamma_1 = 0.1$ when $\zeta = 0, 0.5$ respectively. It can be depicted from the figures that the set of dispersed points represents the jamming states in the absence of control. The size of loop in Fig. 5.5(a)-5.5(d) is bigger than in Fig. 5.6(a)-5.6(d) when control takes the value $\zeta = 0.5$. Thus, it can be concluded that the control signal helps in suppressing traffic congestion.

5.3.2 Long time effect of feedback control

Fig. 5.7 represents the spatiotemporal evolutions of density waves for $\gamma_1 = 0.01$ at time $t = 20100 - 20300$ sec. for different values of control parameter ζ. It can be observed from the figures that the perturbation at initial level results to kink density waves in an unstable region. For lower values of ζ, density waves show higher amplitude; but as the value of control becomes higher the amplitude of density waves die out completely and the flow becomes stable. Fig. 5.8 can be explained in a similar manner as for $\gamma_1 = 0.1$, jamming situation arises but effective control can overcome the situation. The density profiles corresponding to panel of Fig. 5.7 are shown in Fig. 5.9 at time $t = 20100 - 20300$ sec. for $\gamma_1 = 0.01$ when control parameter ζ varies. Traffic jams are represented by kink density waves in an unstable region as shown in Fig. 5.9(a)-5.9(c). Density waves come out with higher amplitude when no control is there but as soon as the control parameter is rising the amplitude die out completely and free flow region turns wider. Similarly, in Fig. 5.10(a)-5.10(c), there exist sharp peak in pattern of density waves that is due to higher rate of passing $\gamma_1 = 0.1$ but it can be minimized due to effective control.

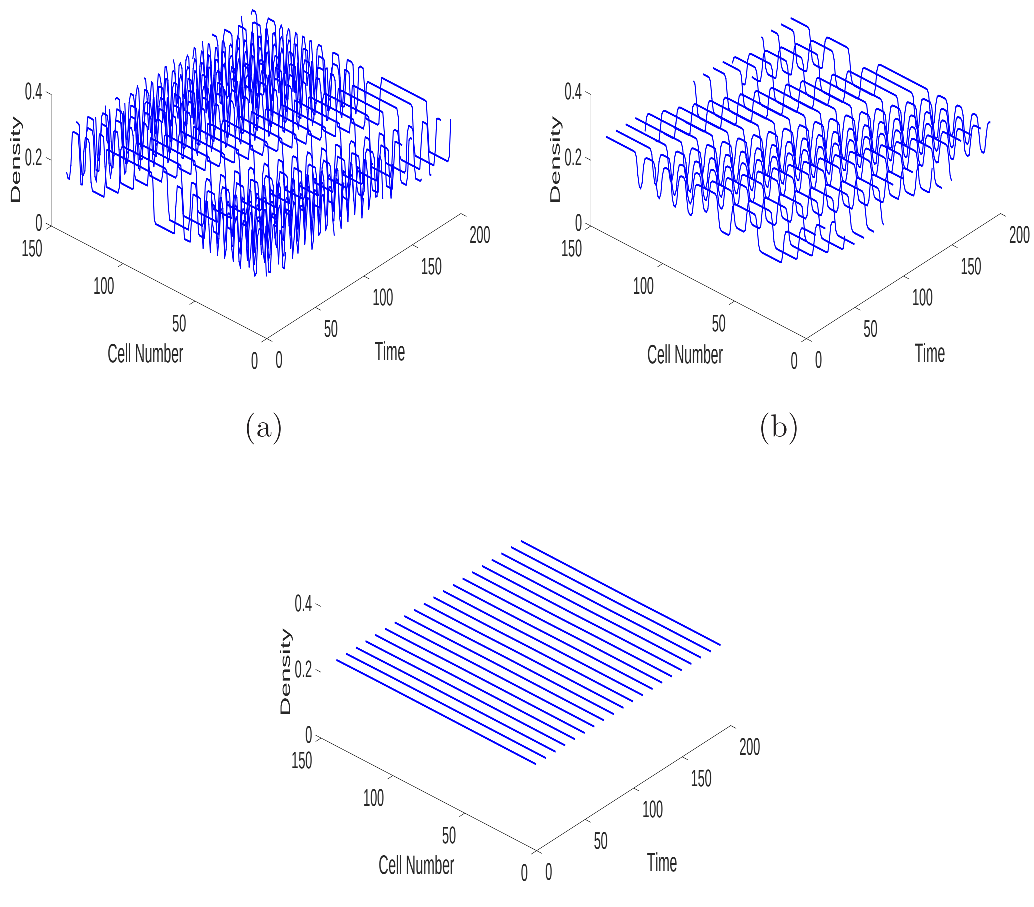

Figure 5.7: Spatiotemporal evolutions of density waves for $\zeta = 0, 0.3, 0.5$ at time $t = 20100 - 20300$ sec. when $\gamma_1 = 0.01$.

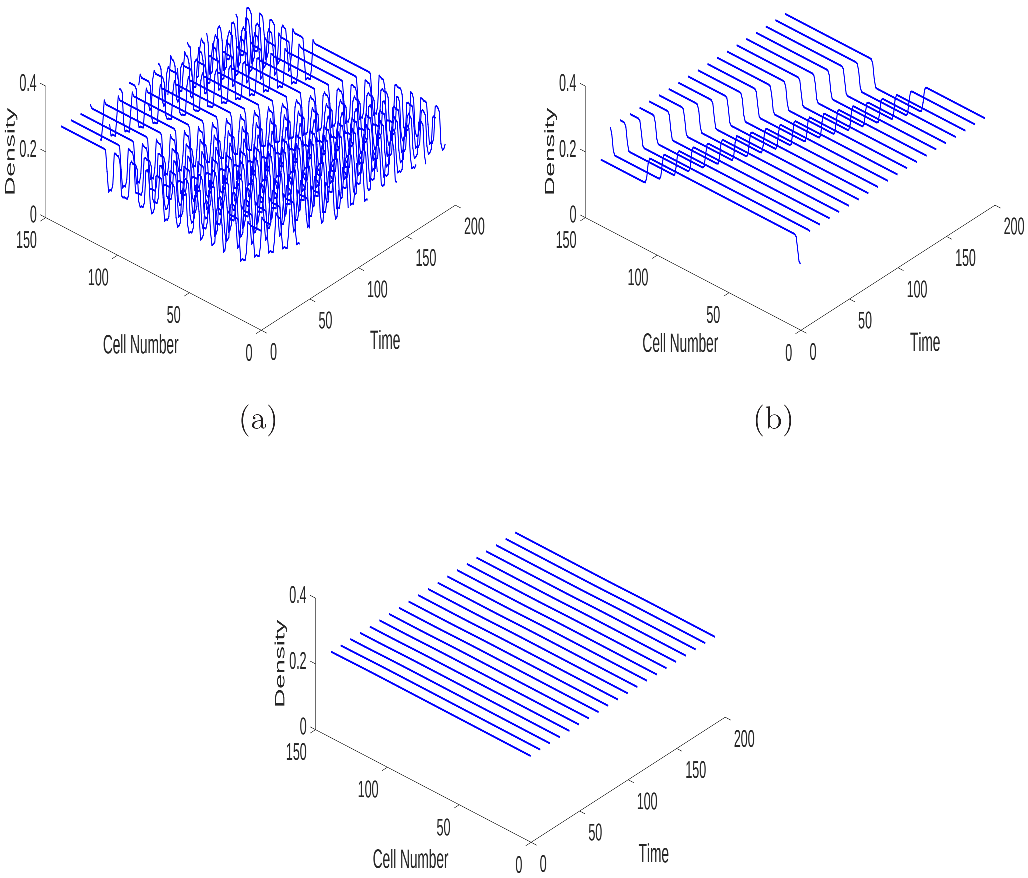

(a) (b) (c)

Figure 5.8: Spatiotemporal evolutions of density waves for $\zeta = 0, 0.3, 0.5$ at time $t = 20100 - 20300$ sec. when $\gamma_1 = 0.1$.

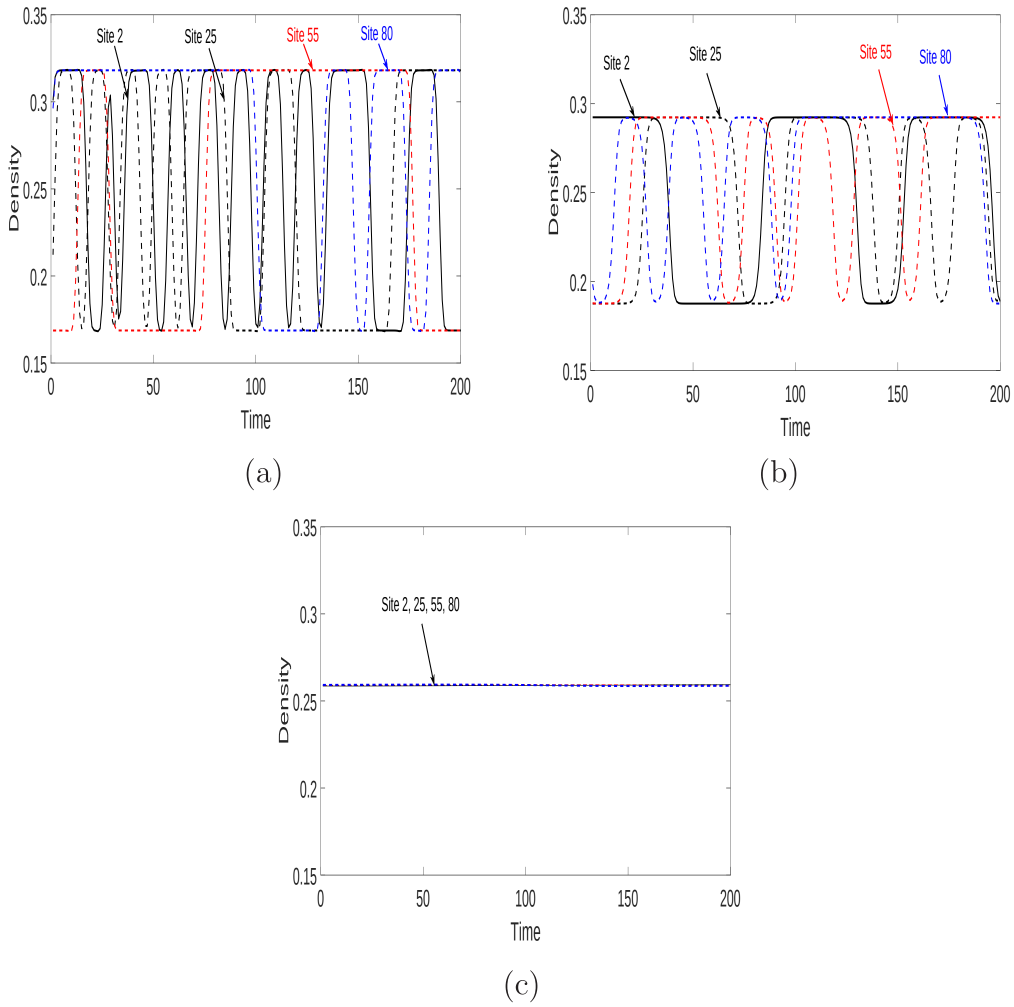

Figure 5.9: Density profiles for $\zeta = 0, 0.3, 0.5$ at time $t = 20100 - 20300$ sec. when $\gamma_1 = 0.01$.

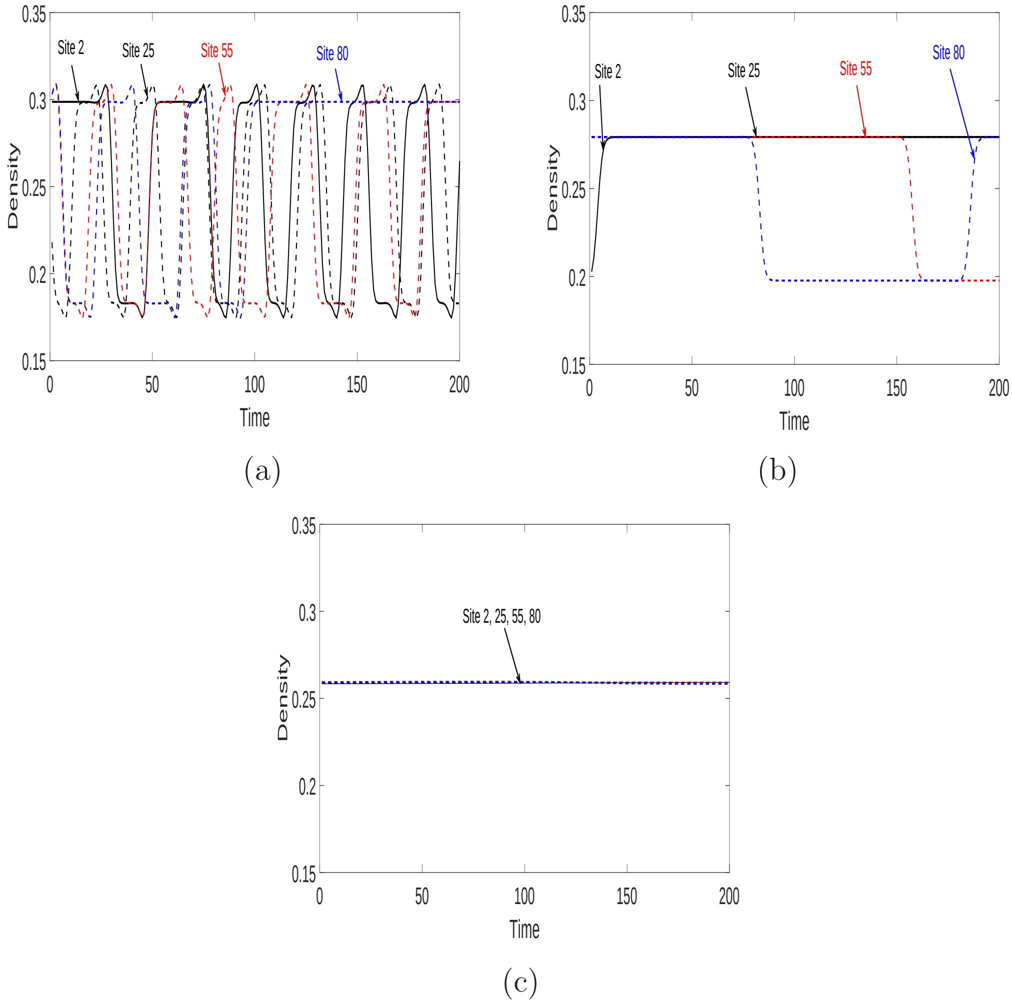

Figure 5.10: Density profiles for $\zeta = 0, 0.3, 0.5$ at time $t = 20100 - 20300$ sec. when $\gamma_1 = 0.1$.

5.4 Conclusion and future scope

- One dimensional lattice model is extended using delayed feedback control with passing.
- The stability conditions for the model are derived using control theory.
- Nonlinear analysis is performed to attain mKdV equation. In addition, the condition under which the mKdV equation cannot be derived is obtained, which corresponds to the higher rate of passing.
- Simulations are conducted and results indicate that higher rate of passing makes the system more unstable but control parameter helps in controlling jams.

- The proposed model can be extended by incorporating important phenomena such as anticipation effect [81, 90–92], interruption probability [101–103] etc. for curved road.
- The effects of passing using feedback control have been shown in the proposed model. But because of the complexity of the model chaotic region cannot be obtained in γ_1-sensitivity space. Therefore, further analysis is required to obtain the range of passing constant and control parameter that can indicate the boundary between kink and chaotic region if it exists.

Chapter 6

The observation of bidirectional traffic flow on two dimensional network

Whole world is facing different types of problems because of increasing vehicular traffic such as environmental pollution, excessive noise, increasing accidents etc. Therefore, it is important to represent traffic dynamics using mathematical models in order to find better traffic flow patterns in city traffic.

Additionally, the theory of traffic is developed based on the vehicular flow on single or multilanes and their interactions with other vehicles, pedestrians and traffic signals present on road networks. But the process of freely moving vehicles sometimes get affected or interrupted due to several factors, i.e., road geometry, design speed, proportion of heavy vehicles, number of lanes and intersections present along the road that stimulate traffic congestion. Out of them the effect of road geometry on traffic dynamics (Ex. curved road and curved road with slope) are presented in Chapters 2 and 3 which can be minimized with the help of intelligent driver's traits. The effect of percentage of heavy and small vehicles (heterogeneous traffic) is explained in Chapter 4 and found that the optimal current difference effect help in overcoming congestion. But the interesting question is what type of jamming situations are there at road intersections and how to overcome them? Thus, having the target to minimize congestion and to help in designing the transportation infrastructure; researchers try to estimate the future traffic situations with the help of empirical models. The jamming transitions between homogeneous and congested traffic flow have been found in the one dimensional [1, 25, 114, 117–121] traffic models.

Besides the one dimensional models, BML [178] have proposed two dimensional cellular automata model on a square lattice ($N \times N$ system) using periodic boundary conditions. The intersection between east and north-bound street is represented by each lattice cell. The spatial extension between the two intersections is totally ignored. The cell can be in two states, empty or occupied, by the vehicle moving towards east or north directions. The vehicles moving in east and north directions update their positions respectively, at odd and even time steps in order to allow movement in two different directions. The vehicle will move ahead only if the cell in front of it is empty otherwise it will not move forward. It has been

The content of this chapter is communicated in SCI journal.

found that phase transitions from a freely moving phase to a perfectly jammed phase occurs with increasing car density. Further, extensions were made for the traffic problems with two level crossing [179] and direction changing [180].

Although above discussed models describe the complex and non-equilibrium phenomena in an effective manner but are not able to completely correlate theory with the actually observed traffic flows. Thus, the series of realistic models further got addition by the development of two dimensional lattice model proposed by Nagatani [124]. Subsequently, the lattice model was further extended for triangular lattice [139] as well. In addition, extensions were made by incorporating the effect of optimal current difference effect and passing [89, 140] on a square lattice and optimal current difference effect on triangular lattice [88].

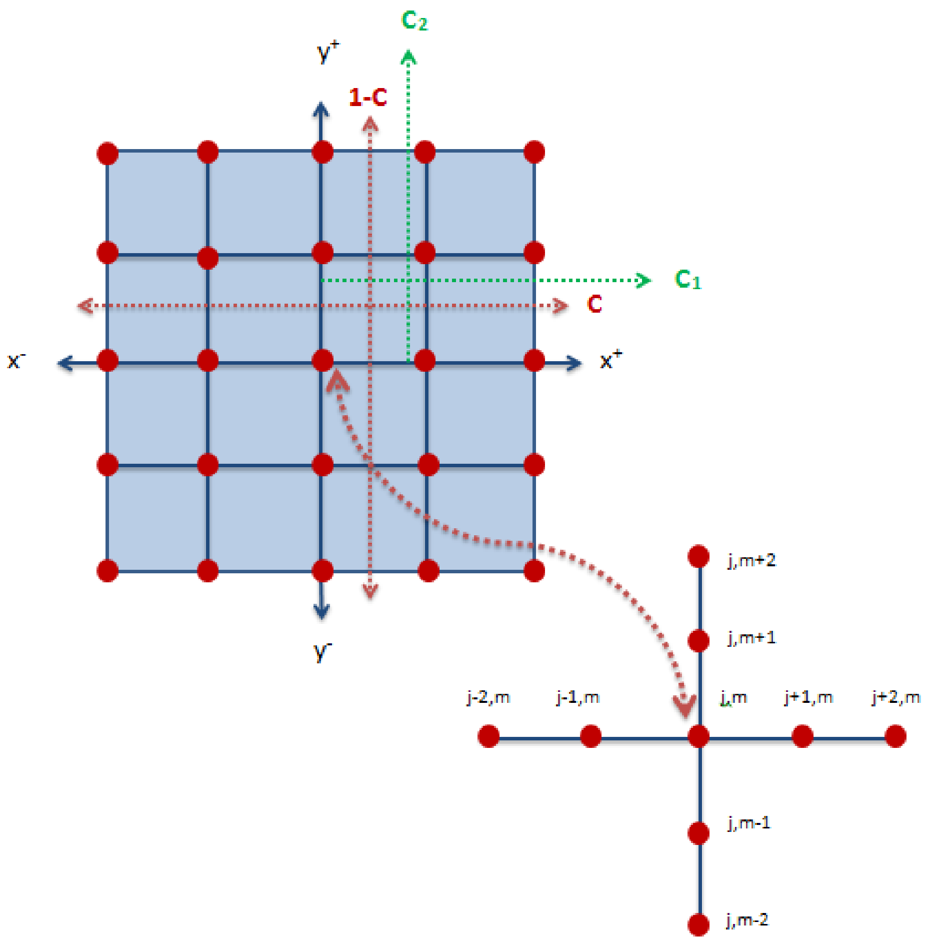

Figure 6.1: An illustration of bidirectional flow in lattice model.

In real traffic situations, vehicles not only move in one direction but can move towards any possible direction. So, according to the direction to which the vehicles are moving, vehicular flow varies. For example, the road networks in urban areas consist of different routes that are connected to different regions or parts of the city: market, govt. offices, parks, and residential areas. Thus, the flow of traffic in its wider sense varies according to the regions to which the lanes are connected. In the whole process, moving from one place to another; drivers play an important role, as drivers always adjust the speed of their vehicle according to the observed traffic situations for attaining the maximal velocity and to avoid traffic jams. Although, the above discussed models effectively describe the properties of complex mechanism and are closely associated with real traffic problems. But none of them describe the properties of bidirectional traffic flow, so by keeping this idea, the Chapter is presented for bidirectional traffic flow on a square lattice. As the flow of traffic at current site depends on the difference of optimal currents of ahead sites, thus the effect of optimal current difference has also been incorporated to the bidirectional flow model.

The organization of Chapter is given by the following sections: the model for bidirectional flow on a square lattice is given in section 6.1. Then by means of linear and nonlinear analysis in section 6.2 and 6.3, it has been shown that the proposed model is efficient in capturing the phenomena of bidirectional traffic flow. The validity of theoretical results is confirmed through numerical simulation in section 6.4. Then section 6.5 is devoted to the summary of results.

6.1 Two dimensional lattice hydrodynamic model

The basic idea behind two dimensional lattice model [124] is that two types of vehicles: east-bound(north-bound); moves in the positive x-direction(y-direction) and can interfere each other only at the crossing point. In addition to it one more assumption is that while moving in respective directions no vehicle can turn back and change its type, i.e., in each category, the number of vehicles will remain conserved. The speed and density of east-bound(north-bound) vehicles is denoted by $u_1(x,y,t)[u_2(x,y,t)]$ and $\rho_x(x,y,t)[\rho_y(x,y,t)]$ respectively. Thus the continuity equations relating the local density to the local average speed of each type of vehicles are given as follows:
Continuity eq.:

$$\partial_t \rho_x(x,y,t) + \partial_x(\rho_x(x,y,t)u_1(x,y,t)) = 0, \tag{6.1.1}$$

$$\partial_t \rho_y(x,y,t) + \partial_y(\rho_y(x,y,t)u_2(x,y,t)) = 0. \tag{6.1.2}$$

As the traffic current is adjusted by the optimal current with some delay time τ that allows the traffic current to attain the optimum level thus, the evolution equations expressing the traffic current are given below:

Evolution eq.:

$$\rho_x(x,y,t+\tau)u_1(x,y,t+\tau) = C\rho_0 V(\rho(x+x_0,y,t)), \tag{6.1.3}$$
$$\rho_y(x,y,t+\tau)u_2(x,y,t+\tau) = (1-C)\rho_0 V(\rho(x,y+y_0,t)), \tag{6.1.4}$$

the parameter C denotes the fraction of east-bound cars. Total average density is ρ_0 and $\rho(x,y,t) = \rho_x(x,y,t) + \rho_y(x,y,t)$ denotes the local density. x_0 and y_0 denotes respectively the average headway of vehicles moving in east and north directions, respectively. $V(\cdot)$ takes the following form [124]:

$$V(\rho_{j,m}(t)) = \frac{V_{\max}}{2}\Big[\tanh\Big(\frac{2}{\rho_0} - \frac{\rho_{j,m}(t)}{\rho_0{}^2} - \frac{1}{\rho_c}\Big) + \tanh\Big(\frac{1}{\rho_c}\Big)\Big]. \tag{6.1.5}$$

Further, the above model was extended by Gupta and Redhu [89] considering the effect of optimal current difference; as the traffic current in x-direction is not only adjusted by the optimal current at position $(x+x_0,y)$ with delay time $t-\tau$ but also by the optimal current difference at $(x+2x_0,y)$ and $(x+x_0,y)$ at time $t-\tau$. Thus by incorporating the effect of optimal current difference following equations were derived:

$$\begin{aligned}\rho_x(x,y,t+\tau)u_1(x,y,t+\tau) &= C\rho_0 V(\rho(x+x_0,y,t)) + \lambda C\rho_0\\ &\quad [V(\rho(x+2x_0,y,t)) - V(\rho(x+x_0,y,t))], \qquad (6.1.6)\\ \rho_y(x,y,t+\tau)u_2(x,y,t+\tau) &= (1-C)\rho_0 V(\rho(x,y+y_0,t)) + \lambda(1-C)\rho_0\\ &\quad [V(\rho(x,y+2y_0,t)) - V(\rho(x,y+y_0,t))], \qquad (6.1.7)\end{aligned}$$

where λ denotes the reaction coefficient corresponding to optimal current difference.

6.1.1 Lattice model for bidirectional flow

Although the above models present the traffic phenomena in a more realistic way but in actual traffic conditions there exist no restrictions corresponding to the direction to which vehicle is going. As the vehicle can move in any direction according to the suitable choice of driver. So, we consider a system size of $N \times N$ lattice sites in four different directions (see Fig. 6.1), with the aim to present the traffic situations in a more accurate way. The assumptions of the model are that the east-bound cars move only towards $x^{+\mathrm{ve}}$-direction, west-bound towards $x^{-\mathrm{ve}}$-direction, north-bound towards $y^{+\mathrm{ve}}$-direction and south-bound towards $y^{-\mathrm{ve}}$-direction. The fraction of vehicles moving in positive (east-bound) and negative (west-bound) x-directions among all vehicles is C, proportion of east-bound cars among east-bound and west-bound cars is C_1. Proportion of north-bound cars in north-bound and south-bound cars is C_2. Thus by adopting this idea into lattice model, following continuity equations are formed:

$$\partial_t\rho_{x^+}(x,y,t)+\partial_x(\rho_{x^+}(x,y,t)u_1(x,y,t))=0, \tag{6.1.8}$$

$$\partial_t\rho_{x^-}(x,y,t)+\partial_x(\rho_{x^-}(x,y,t)u_2(x,y,t))=0, \tag{6.1.9}$$

$$\partial_t\rho_{y^+}(x,y,t)+\partial_y(\rho_{y^+}(x,y,t)u_3(x,y,t))=0, \tag{6.1.10}$$

$$\partial_t\rho_{y^-}(x,y,t)+\partial_y(\rho_{y^-}(x,y,t)u_4(x,y,t))=0, \tag{6.1.11}$$

where $\rho_{x^+}(x,y,t)$, $\rho_{x^-}(x,y,t)$, $\rho_{y^+}(x,y,t)$ and $\rho_{y^-}(x,y,t)$ denotes the density of east, west, north and south-bound vehicles and $u_1(x,y,t)$, $u_2(x,y,t)$, $u_3(x,y,t)$, $u_4(x,y,t)$ denotes respectively the velocity of these vehicles. The motion of vehicles moving in east, west, north and south directions is explained by the evolution equations:

$$\begin{aligned}\rho_{x^+}(x,y,t+\tau)u_1(x,y,t+\tau)&=CC_1\rho_0V(\rho(x+x_0,y,t))\\&\quad+\lambda CC_1\rho_0[V(\rho(x+2x_0,y,t))-V(\rho(x+x_0,y,t))],\end{aligned} \tag{6.1.12}$$

$$\begin{aligned}\rho_{x^-}(x,y,t+\tau)u_2(x,y,t+\tau)&=C(1-C_1)\rho_0V(\rho(x-x_0,y,t))\\&\quad+\lambda C(1-C_1)\rho_0[V(\rho(x-2x_0,y,t))-V(\rho(x-x_0,y,t))],\end{aligned} \tag{6.1.13}$$

$$\begin{aligned}\rho_{y^+}(x,y,t+\tau)u_3(x,y,t+\tau)&=(1-C)C_2\rho_0V(\rho(x,y+y_0,t))\\&\quad+\lambda(1-C)C_2\rho_0[V(\rho(x,y+2y_0,t))-V(\rho(x,y+y_0,t))],\end{aligned} \tag{6.1.14}$$

$$\begin{aligned}\rho_{y^-}(x,y,t+\tau)u_4(x,y,t+\tau)&=(1-C)(1-C_2)\rho_0V(\rho(x,y-y_0,t))\\&\quad+\lambda(1-C)(1-C_2)\rho_0[V(\rho(x,y-2y_0,t))-V(\rho(x,y-y_0,t))],\end{aligned} \tag{6.1.15}$$

where the flux of vehicles in each direction is denoted respectively: $\rho_{x^+}(x,y,t+\tau)u_1(x,y,t+\tau)$, $\rho_{x^-}(x,y,t+\tau)u_2(x,y,t+\tau)$, $\rho_{y^+}(x,y,t+\tau)u_3(x,y,t+\tau)$ and $\rho_{y^-}(x,y,t+\tau)u_4(x,y,t+\tau)$. The average densities in x^+, x^- and y^+, y^- directions can be expressed respectively as $\rho_{0x^+}=C_1\rho_{0x}=CC_1\rho_0$, $\rho_{0x^-}=(1-C_1)\rho_{0x}=(1-C_1)C\rho_0$, $\rho_{0y^+}=C_2\rho_{0y}=C_2(1-C)\rho_0$, $\rho_{0y^-}=(1-C_2)\rho_{0y}=(1-C_2)(1-C)\rho_0$. The combined density of the bidirectional flow on square lattice can be expressed by the addition of densities in each direction, i.e., $\rho(x,y,t)=\rho_{x^+}(x,y,t)+\rho_{x^-}(x,y,t)+\rho_{y^+}(x,y,t)+\rho_{y^-}(x,y,t)$. We choose $\frac{1}{CC_1\rho_0}$, $\frac{1}{C(1-C_1)\rho_0}$, $\frac{1}{(1-C)C_2\rho_0}$, $\frac{1}{(1-C)(1-C_2)\rho_0}$ for average headway in east, west, north and south directions, respectively. By combining the difference form of equations (6.1.8), (6.1.9), (6.1.10) and (6.1.11) with (6.1.12), (6.1.13), (6.1.14) and (6.1.15), the density equation for the bidirectional flow is:

$$\begin{aligned}
&\rho_{j,m}(t+2\tau) - \rho_{j,m}(t+\tau) + \tau(CC_1)^2{\rho_0}^2[V(\rho_{j+1,m}(t)) - V(\rho_{j,m}(t))] \\
&+ \tau(C(1-C_1))^2{\rho_0}^2[V(\rho_{j-1,m}(t)) - V(\rho_{j,m}(t))] + \tau(C_2(1-C))^2{\rho_0}^2 \\
&[V(\rho_{j,m+1}(t)) - V(\rho_{j,m}(t))] + \tau((1-C)(1-C_2))^2{\rho_0}^2[V(\rho_{j,m-1}(t)) \\
&- V(\rho_{j,m}(t))] + \lambda\tau(CC_1)^2{\rho_0}^2[V(\rho_{j+2,m}(t)) - 2V(\rho_{j+1,m}(t)) \\
&+ V(\rho_{j,m}(t))] + \lambda\tau(C(1-C_1))^2{\rho_0}^2[V(\rho_{j-2,m}(t)) - 2V(\rho_{j-1,m}(t)) \\
&+ V(\rho_{j,m}(t))] + \lambda\tau((1-C)C_2)^2{\rho_0}^2[V(\rho_{j,m+2}(t)) - 2V(\rho_{j,m+1}(t)) \\
&+ V(\rho_{j,m}(t))] + \lambda\tau((1-C)(1-C_2))^2{\rho_0}^2[V(\rho_{j,m-2}(t)) - 2V(\rho_{j,m-1}(t)) \\
&+ V(\rho_{j,m}(t))] = 0.
\end{aligned} \tag{6.1.16}$$

Proposed model recovers the two dimensional model [89] for $C_1 = C_2 = 1$. In addition, without taking effect of optimal current difference, i.e., ($\lambda = 0$) it recovers Nagatani's model [124] for two dimensional system.

6.2 Linear stability analysis

In order to obtain the stability conditions of the proposed model, we apply the linear stability analysis to density equation (6.1.16). Initially, we consider the stability of homogeneous flow, i.e., the flow is moving with constant density ρ_0 and constant velocity $V(\rho_0)$. Therefore, the steady-state solution of homogeneous bidirectional flow is considered as:

$$\rho_{j,m}(t) = \rho_0, \tag{6.2.1}$$

$$u_{1j,m}(t) = u_{2j,m}(t) = u_{3j,m}(t) = u_{4j,m}(t) = V(\rho_0). \tag{6.2.2}$$

In order to check whether the disturbances given to uniform flow amplify with time or not; we added small perturbation to the steady-state flow in terms of $y_{j,m}(t)$. If the fluctuations amplify then flow is unstable otherwise stable. The density profile is given by:

$$\rho_{j,m}(t) = \rho_0 + y_{j,m}(t), \tag{6.2.3}$$

by using the perturbed density (6.2.3) in (6.1.16) and linearizing it we obtain:

$$\begin{aligned}
&y_{j,m}(t+2\tau) - y_{j,m}(t+\tau) + \tau(CC_1)^2{\rho_0}^2V'(\rho_0)[y_{j+1,m}(t) \\
&- y_{j,m}(t)] + \tau(C(1-C_1))^2{\rho_0}^2V'(\rho_0)[y_{j-1,m}(t) - y_{j,m}(t)] \\
&+ \tau(C_2(1-C))^2{\rho_0}^2V'(\rho_0)[y_{j,m+1}(t) - y_{j,m}(t)]+ \\
&\tau((1-C)(1-C_2))^2{\rho_0}^2V'(\rho_0)[y_{j,m-1}(t) - y_{j,m}(t)] + \lambda\tau(CC_1)^2 \\
&{\rho_0}^2V'(\rho_0)[y_{j+2,m}(t) - 2y_{j+1,m}(t) + y_{j,m}(t)] + \lambda\tau(C(1-C_1))^2 \\
&{\rho_0}^2V'(\rho_0)[y_{j-2,m}(t) - 2y_{j-1,m}(t) + y_{j,m}(t)] + \lambda\tau((1-C)C_2)^2 \\
&{\rho_0}^2V'(\rho_0)[y_{j,m+2}(t) - 2y_{j,m+1}(t) + y_{j,m}(t)] + \lambda\tau \\
&((1-C)(1-C_2))^2{\rho_0}^2V'(\rho_0)[y_{j,m-2}(t) - 2y_{j,m-1}(t) + y_{j,m}(t)] = 0.
\end{aligned} \tag{6.2.4}$$

Then by expanding $y_{j,m}(t) = e^{ik(j+m)+zt}$ where k is wave number, into equation (6.2.4) following equation is obtained:

$$\begin{aligned}
&e^{2z\tau} - e^{z\tau} + \tau(CC_1)^2{\rho_0}^2V'(\rho_0)[e^{ik}-1] + \tau(C(1-C_1))^2{\rho_0}^2V'(\rho_0)[e^{-ik}-1] \\
&+ \tau(C_2(1-C))^2{\rho_0}^2V'(\rho_0)[e^{ik}-1] + \tau((1-C)(1-C_2))^2{\rho_0}^2V'(\rho_0) \\
&[e^{-ik}-1] + \lambda\tau(CC_1)^2{\rho_0}^2V'(\rho_0)[e^{2ik} - 2e^{ik} + 1] + \lambda\tau(C(1-C_1))^2 \\
&{\rho_0}^2V'(\rho_0)[e^{-2ik} - 2e^{-ik} + 1] + \lambda\tau((1-C)C_2)^2{\rho_0}^2V'(\rho_0) \\
&[e^{2ik} - 2e^{ik} + 1] + \lambda\tau((1-C)(1-C_2))^2{\rho_0}^2V'(\rho_0)[e^{-2ik} - 2e^{-ik} + 1] = 0,
\end{aligned} \tag{6.2.5}$$

by solving (6.2.5) using $z = z_1(ik) + z_2(ik)^2 + ...$ for z; we obtain the coefficients z_1 and z_2 as follows:

$$\begin{aligned}
z_1 =& -[(CC_1)^2 - (C(1-C_1))^2 + (C_2(1-C))^2 - ((1-C_2)(1-C))^2] \qquad (6.2.6)\\
&{\rho_0}^2V'(\rho_0), \\
z_2 =& -\frac{3}{2}{z_1}^2\tau - (\frac{1}{2}+\lambda)[(CC_1)^2 + (C(1-C_1))^2 + (C_2(1-C))^2 \qquad (6.2.7)\\
&+ ((1-C_2)(1-C))^2]{\rho_0}^2V'(\rho_0).
\end{aligned}$$

From the above values it can be concluded that the uniform flow will be unstable for $z_2 < 0$ for long-wavelength modes; on the other side the flow will be stable if $z_2 > 0$. Therefore, the instability condition is obtained as:

$$\tau = -\tfrac{1+2\lambda}{3{z_1}^2}f_1{\rho_0}^2V'(\rho_0), \tag{6.2.8}$$

$$\tau = -\tfrac{1+2\lambda}{3{f_2}^2{\rho_0}^2V'(\rho_0)}f_1, \tag{6.2.9}$$

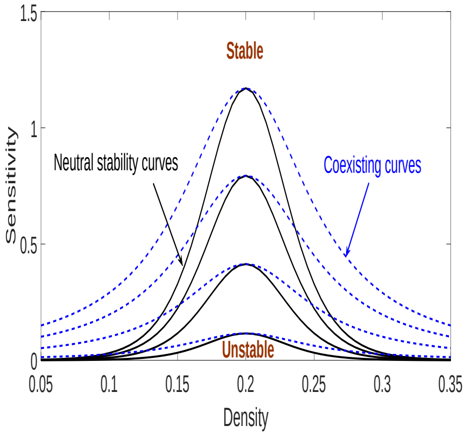

(a)

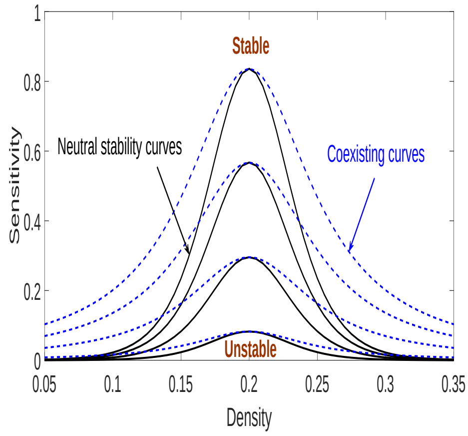

(b)

Figure 6.2: Phase diagram in parameter space (ρ, a) for $C_1 = C_2 = 0.1$, $C_1 = C_2 = 0.2$, $C_1 = C_2 = 0.3$, $C_1 = C_2 = 0.4$ when $\rho_0 = \rho_c = 0.2$ (a) $\lambda = 0$ (b) $\lambda = 0.2$.

where $f_1 = (CC_1)^2 + (C(1-C_1))^2 + (C_2(1-C))^2 + ((1-C_2)(1-C))^2$ and $f_2 = (CC_1)^2 - (C(1-C_1))^2 + (C_2(1-C))^2 - ((1-C_2)(1-C))^2$. The homogeneous flow will be unstable under the following condition:

$$\tau > -\frac{1+2\lambda}{3{f_2}^2{\rho_0}^2V'(\rho_0)}f_1. \qquad (6.2.10)$$

6.2.1 Phase plots for equal fraction parameters $(C_1 = C_2)$

Fig. 6.2(a) display the stability curves (black solid curves obtained by linear analysis and blue dotted curves through nonlinear analysis) in (ρ, a) plane for equal values of fractions C_1 and C_2 when $\lambda = 0$. The entire space is divided into three distinct regions: stable region out of coexisting curves, metastable region between neutral stability and coexisting curves and unstable region within neutral stability curves. It is clear from the figure that the apex of each curve decreases with increasing values of fractions upto $C_1 = C_2 = 0.4$. Which shows that when the percentage of vehicles is equal in positive x and y-directions and is less than 0.5 the stable region will get wider and flow start becoming uniform over the whole space.

Fig. 6.2(b) shows the phase plane by taking into account the effect of optimal current difference for equal fractions C_1 and C_2. Both the stability curves (neutral and coexisting) lower down with increasing fractions but the stable region in Fig. 6.2(b) is wider than in Fig. 6.2(a). The results can be verified in relation to actual traffic situations as for $C_1 = C_2 = 0.4$, the fraction of vehicular traffic in each direction is almost equal which leads to the stability in flow. But equal pair of fractions less than 0.4 indicates that out of four directions, negative one are congested and the positive one are freely flowing. So, one can conclude that in case of equal pair of fractions, the optimal current difference helps in stabilizing the bidirectional flow more quickly.

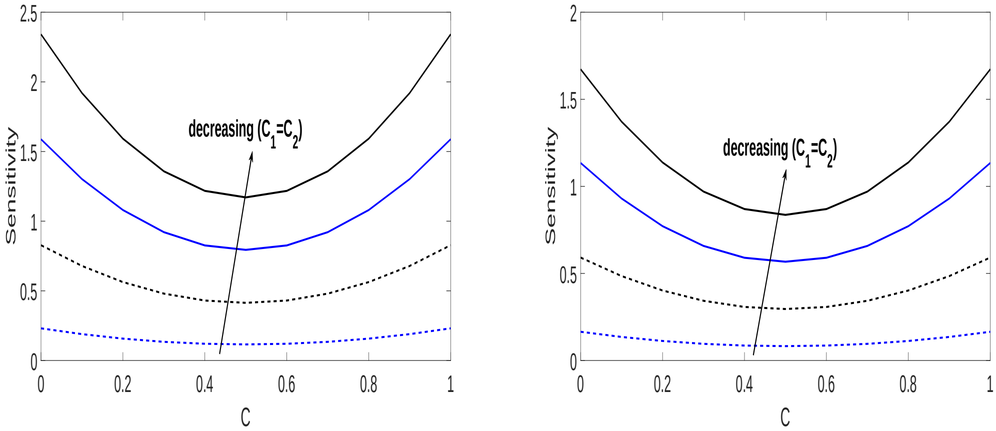

(a) (b)

Figure 6.3: Plots of critical points versus critical sensitivity for $C_1 = C_2 = 0.1$, $C_1 = C_2 = 0.2$, $C_1 = C_2 = 0.3$, $C_1 = C_2 = 0.4$ when $\rho_0 = \rho_c = 0.2$ (a) $\lambda = 0$ (b) $\lambda = 0.2$.

Fig. 6.3(a)-6.3(b) shows the plots of C versus critical sensitivity when $\lambda = 0$ and $\lambda = 0.2$ respectively. Both the figures can be described in a same way as the curves in phase plane start becoming straight with increasing values of equal fractions. Corresponding to the lowest value of equal fractions, i.e., $C_1 = C_2 = 0.1$ (black solid curve), there is a larger bend in the curve indicating the convergence of traffic towards opposite directions which leads to traffic jams due to an uneven division of cars. For the highest value of equal fractional pair, i.e., $C_1 = C_2 = 0.4$ (blue dotted curve) the bend completely vanishes and the curve appears as a straight line which indicates the stability in bidirectional flow. One more observation is that each curve is symmetric about $C = 0.5$. When the fraction C takes the value higher than 0.5, sensitivity start increasing, the reason behind it is that similar to real traffic situations, when the total percentage of vehicles towards east-bound and west-bound directions is 50 the flow will be uniform in both directions but if it is less or more than 0.5 then the flow of vehicles will be concentrated towards any one of the directions.

6.2.2 Phase plots for unequal fraction parameters ($C_1 \neq C_2$)

Fig. 6.4 gives the stability curves (black solid and blue dotted curves) in (ρ, a) plane for unequal fractions C_1 and C_2 when $\lambda = 0.2$. Fig. 6.4(a) corresponds to fixed fraction $C_1 = 0.1$ and Fig. 6.4(b) corresponds to fixed fraction parameter $C_2 = 0.1$. It can be noticed in the figures that the peak of each curve decreases with an increasing value of C_2 (Fig. 6.4(a)) and C_1 (Fig. 6.4(b)) when $\lambda = 0.2$.

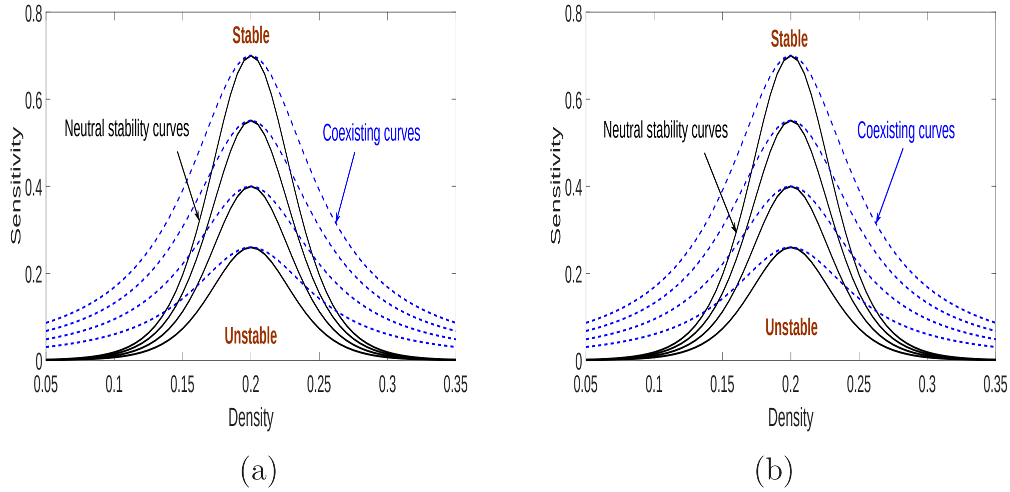

Figure 6.4: Phase plot in the (ρ, a) plane when $\lambda = 0.2$ and $\rho_0 = \rho_c = 0.2$ (a) when C_1 is fixed (b) when C_2 is fixed.

It can be explained by the fact that when the fraction of east-bound cars remain fixed as 0.1, i.e., 10 percent vehicles are moving in positive x direction, then for different fractions of north-bound cars, i.e., $C_2 = 0.2, 0.3, 0.4, 0.5$, the flow will be more stable when the fraction of vehicles is becoming approximately half. The results are verifiable, as in real traffic situations when the distribution of vehicles starts becoming uniform in different directions the jamming states of traffic vanishes.

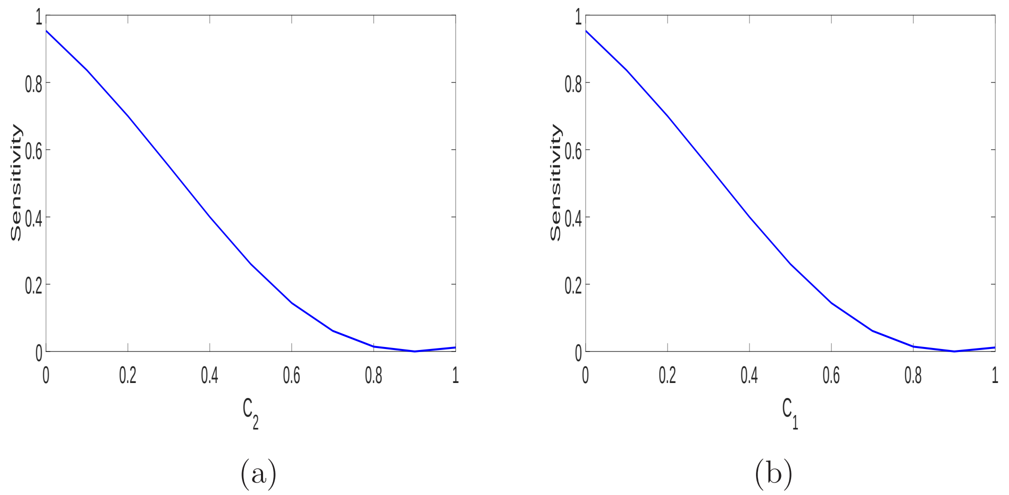

Figure 6.5: Plots of critical points versus critical sensitivity when $\lambda = 0.2$ and $\rho_0 = \rho_c = 0.2$ (a) when C_1 is fixed (b) when C_2 is fixed.

Fig. 6.5(a)-6.5(b) shows the plots of critical points C_2 and C_1 versus sensitivity when $\lambda = 0.2$, respectively. Both the fraction parameters behave in a similar way when one of them remain fixed. The blue solid curves in both figures are decreasing corresponding to increasing values of north-bound and east-bound cars. Which can be explained by the fact that when the fraction (C_1 or C_2) is fixed as 0.1, i.e., only 10 percent vehicles out of total fraction are moving in east or north directions then the flow towards negative x and y directions will be more which causes congestion. The jams can be under control if the fraction of vehicles is approximately half.

6.3 Nonlinear analysis

Vehicular density above a critical level turns into traffic jams which appear in term of density waves propagating in backward direction. Therefore, to capture the varying nature of traffic around critical point (ρ_c, a_c) reductive perturbation method is used. Slow scales are introduced for space and time variables and the slow variables X and T are defined as:

$$X = \epsilon(j + m + bt), \qquad T = \epsilon^3(t) \qquad (0 < \epsilon \leq 1), \tag{6.3.1}$$

the constant term b in (6.3.1) needs to be obtained. Density around (ρ_c, a_c) is defined as:

$$\rho_{j,m}(t) = \rho_c + \epsilon R(X, T). \tag{6.3.2}$$

By using (6.3.2) and expanding (6.1.16) with the help of Taylor series expansion upto fifth-order of ϵ, following nonlinear equation is obtained:

$$\begin{aligned}\epsilon^2 k_1 \partial_X R + \epsilon^3 k_2 \partial_X^2 R + \epsilon^4(\partial_T R + k_3 \partial_X^3 R + k_4 \partial_X R^3) + \epsilon^5(k_5 \partial_T \partial_X R \\ + k_6 \partial_X^4 R + k_7 \partial_X^2 R^3) = 0.\end{aligned} \tag{6.3.3}$$

Table 6.1 gives the values of $k_i's(i = 1, 2, 3, ..., 7)$, where $V' = \left.\frac{dV(\rho)}{d\rho}\right|_{\rho=\rho_c}$ and $V''' = \left.\frac{d^3V(\rho)}{d\rho^3}\right|_{\rho=\rho_c}$. After choosing the value of delay time τ in the neighborhood of (ρ_c, a_c) as:

$$\tau = \tau_c(\epsilon^2 + 1), \tag{6.3.4}$$

and by substituting the constant value $b = -f_2 {\rho_c}^2 V'$, the terms of ϵ having second and third-order completely vanished and we get:

$$\epsilon^4(\partial_T R - g_1 \partial_X^3 R + g_2 \partial_X R^3) + \epsilon^5(g_3 \partial_X^2 R + g_4 \partial_X^4 R + g_5 \partial_X^2 R^3) = 0. \tag{6.3.5}$$

Table 6.2 shows coefficients of $g_i(i = 1, 2, ..., 5)$. Equation (6.3.5) can be transformed to mKdV equation by using following transformation:

$$T' = g_1 T, \quad R = \sqrt{\frac{g_1}{g_2}} R'. \tag{6.3.6}$$

So, resulting equation (6.3.5) is given by:

$$\partial_{T'} R' - \partial_X^3 R' + \partial_X R'^3 + \epsilon M[R'] = 0, \tag{6.3.7}$$

The coefficients k_i of the model	
k_1	$b + f_2 {\rho_c}^2 V'$
k_2	$\frac{3b^2\tau}{2} + (\frac{1}{2} + \lambda) f_1 \rho_c^2 V'$
k_3	$\frac{7}{6} b^3 \tau^2 + (\frac{1}{6} + \lambda) f_2 \rho_c^2 V'$
k_4	$\frac{f_2 \rho_c^2 V'''}{6}$
k_5	$3b\tau$
k_6	$\frac{5b^4\tau^3}{8} + (\frac{1}{24} + \frac{7}{12}\lambda) f_1 {\rho_c}^2 V'$
k_7	$(\frac{1+2\lambda}{12}) f_1 {\rho_c}^2 V'''$

Table 6.1: The coefficients k_i of the model

The coefficients g_i of the model	
g_1	$-\frac{7b^3{\tau_c}^2}{6} - (\frac{1+6\lambda}{6}) f_2 {\rho_c}^2 V'$
g_2	$\frac{f_2 \rho_c^2 V'''}{6}$
g_3	$\frac{3b^2\tau_c}{2}$
g_4	$\frac{15b^4{\tau_c}^3}{24} + (\frac{1+14\lambda}{24}) f_1 {\rho_c}^2 V' + 3b\tau_c g_1$
g_5	$(\frac{1+2\lambda}{12}) f_1 \rho_c^2 V''' - 3b\tau_c g_2$

Table 6.2: The coefficients g_i of the model

where $M[R^{'}] = \frac{1}{g_1}[g_3\partial_X^2 R^{'} + g_4\partial_X^4 R^{'} + \frac{g_1 g_5}{g_2}\partial_X^2 R^{'3}]$. By ignoring correction term $O(\epsilon)$ from (6.3.7), we obtain the solution:

$$R_0^{'}(X, T^{'}) = \sqrt{L_1}\,\tanh\Big(\sqrt{\frac{L_1}{2}}(X - L_1 T^{'})\Big). \tag{6.3.8}$$

Here, to represent the kink antikink density waves, the propagation velocity is denoted by L_1 and is obtained by solving the condition given below:

$$(R_0^{'}, M[R_0^{'}]) \equiv \int_{-\infty}^{\infty} dX R_0^{'} M[R_0^{'}] = 0, \tag{6.3.9}$$

with $M[R_0^{'}] = M[R^{'}]$. From (6.3.9), the suitable choice of L_1 is obtained as:

$$L_1 = \frac{5 g_2 g_3}{2 g_2 g_4 - 3 g_1 g_5}. \tag{6.3.10}$$

Hence, the solution representing the kink antikink wave is given as under:

$$\rho_{j,m}(t) = \rho_c + \epsilon\sqrt{\frac{g_1 L_1}{g_2}}\tanh\Big(\sqrt{\frac{L_1}{2}}(X - L_1 g_1 T)\Big), \tag{6.3.11}$$

where $\epsilon^2 = \Big(\frac{a_c}{a} - 1\Big)$.

6.4 Numerical simulation

To investigate the capability of the modified model in describing the jamming transitions for a square lattice with respect to optimal current difference effect and to validate the theoretical investigations, simulation is performed for a system size of 140×140 lattices using periodic boundary conditions and initial conditions are chosen as:

$$\rho_{(j,m)}(0) = \rho_{(j,m)}(1) = \begin{cases} \rho_0; & (j,m) \neq (\frac{N}{2}, \frac{N}{2}), (\frac{N}{2} - 1, \frac{N}{2} - 1) \\ \rho_0 - \sigma; & (j,m) = (\frac{N}{2}, \frac{N}{2}) \\ \rho_0 + \sigma; & (j,m) = (\frac{N}{2} - 1, \frac{N}{2} - 1), \end{cases} \tag{6.4.1}$$

where initial density is set uniformly over the whole space as $\rho_0 = 0.2$ and the local disturbance at initial stage is given in terms of $\sigma = 0.1$ at the center of a square lattice. In order to describe the jamming transitions for two dimensional bidirectional flow, we take two different cases for fraction parameters C_1 and C_2 which corresponds to positive x and positive y directions respectively.

6.4.1 When fraction parameters are equal ($C_1 = C_2$)

6.4.1.1 Without optimal current difference effect ($\lambda = 0$)

Under the case of equal fractions, we further explore the behavior characteristics of bidirectional flow without the effect of optimal current difference, i.e., $\lambda = 0$. Firstly the choice of fraction parameters C_1 and C_2 is made on the bases of equal values and the sensitivity parameter is taken as $a = 0.5$. Fig. 6.6(a)-6.6(c) shows the traffic patterns for equal pair of values of fraction parameters C_1 and C_2 at time $t = 2 \times 10^3$. The jammed region is shown by blue color which shows the density higher than ρ_0. The pattern in Fig. 6.6(a) shows that when the fraction of vehicles moving towards positive x and y-directions is 0.1 the whole flow exhibit diagonal pattern that indicates that more vehicles are moving towards opposite directions. As the value of equal fraction of vehicles moving towards east and north directions is rising, the distribution of vehicles is becoming uniform over the whole space which can be seen by blue shaded region in Fig. 6.6(b)-6.6(c). It can be explained by the fact that when the percentage of vehicles in each direction is approximately 50, the flow is uniform and when the percentage is greater than that in any direction the flow is concentrated towards that direction only.

Fig. 6.7 shows the density profile for equal values of fractions C_1 and C_2 at time $t = 15 \times 10^3$ for single horizontal road at $y = 40$. It can be depicted from Fig. 6.7(a) that for $C_1 = C_2 = 0.1$, kink antikink density wave with higher amplitude is there which exhibit the jamming transitions between the freely moving phase and the congested phase. But as the value of the fractional pair is rising, the density wave is coming with a lower amplitude in Fig. 6.7(c) exhibiting the periodic behavior. It can be explained by the fact that when the flow towards east-bound and north-bound directions is only 10 percent, jamming situations will not occur in respective directions but in opposite directions. But the flow will be uniform over the whole space when the fractions are nearly 0.5.

Fig. 6.8 shows the plots of density versus density difference at $t = 15 \times 10^3 - 2 \times 10^4$ for different equal pairs of fractions with respect to the panel of Fig. 6.6. The set of dispersed points are represented by the the closed loop in the figure. It can be observed from Fig. 6.8(a)-6.8(c) that the loop start shrinking in its size corresponding to increasing values of fractional pair. The increasing values indicate that the vehicular traffic is going to distribute uniformly in each direction that leads to the reduction of traffic jams.

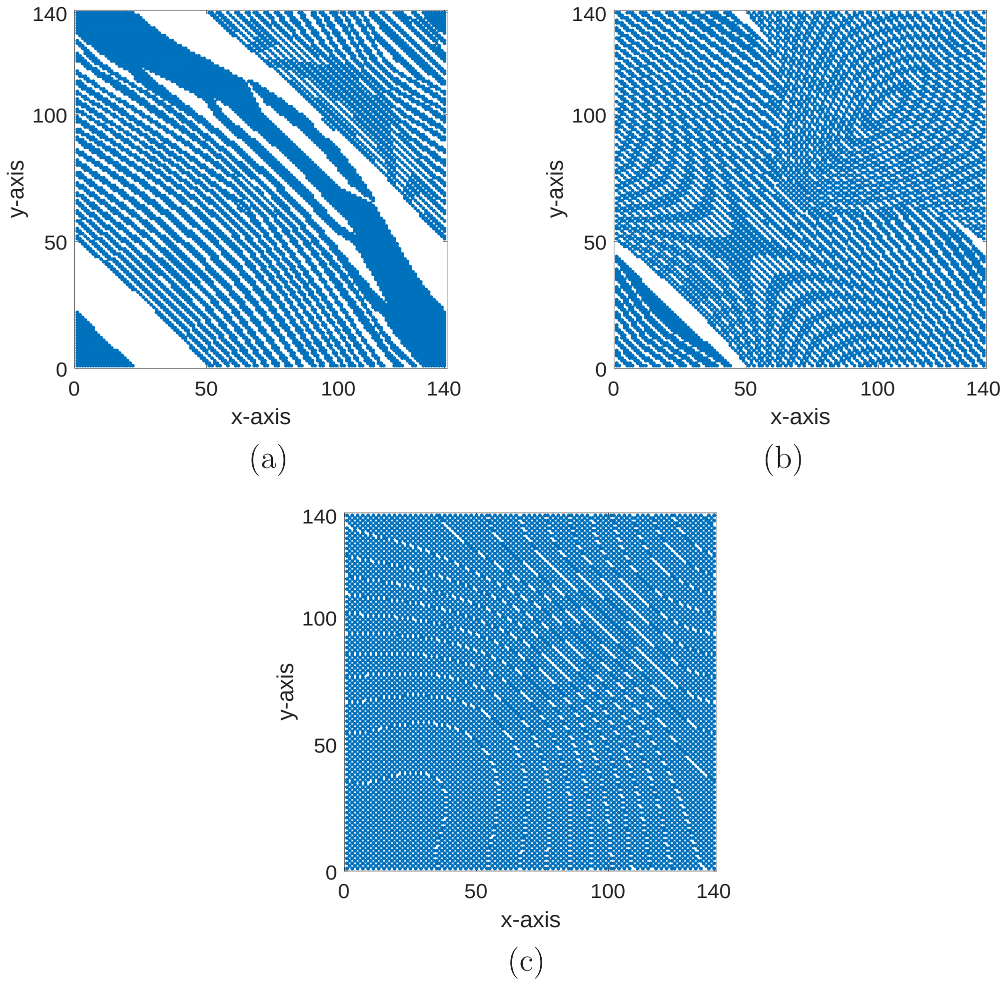

Figure 6.6: Traffic patterns at $t = 2 \times 10^3, a = 0.5, \lambda = 0$ for equal values of C_1 and C_2 (a) $C_1 = C_2 = 0.1$ (b) $C_1 = C_2 = 0.2$ (c) $C_1 = C_2 = 0.4$.

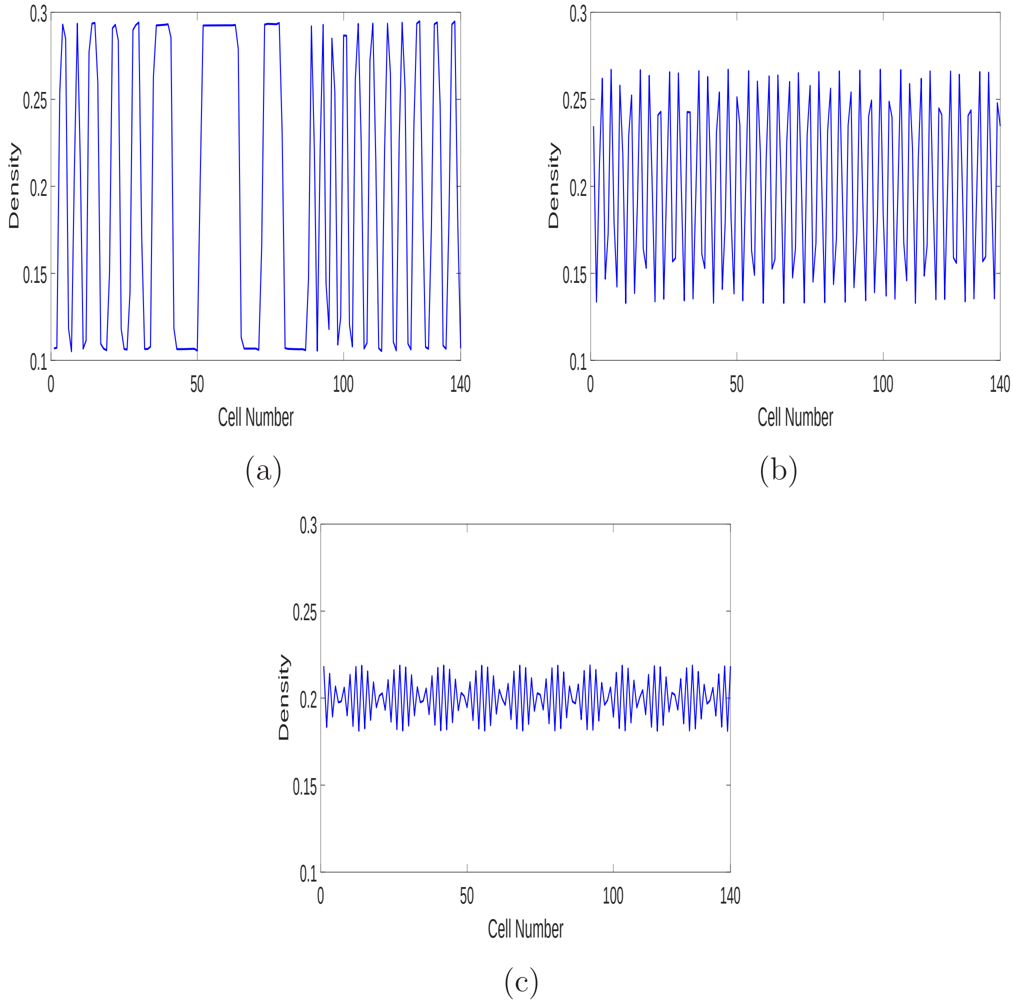

Figure 6.7: Density wave profile at $t = 15 \times 10^3, a = 0.5, \lambda = 0$ for equal values of C_1 and C_2 (a) $C_1 = C_2 = 0.1$ (b) $C_1 = C_2 = 0.2$ (c) $C_1 = C_2 = 0.4$.

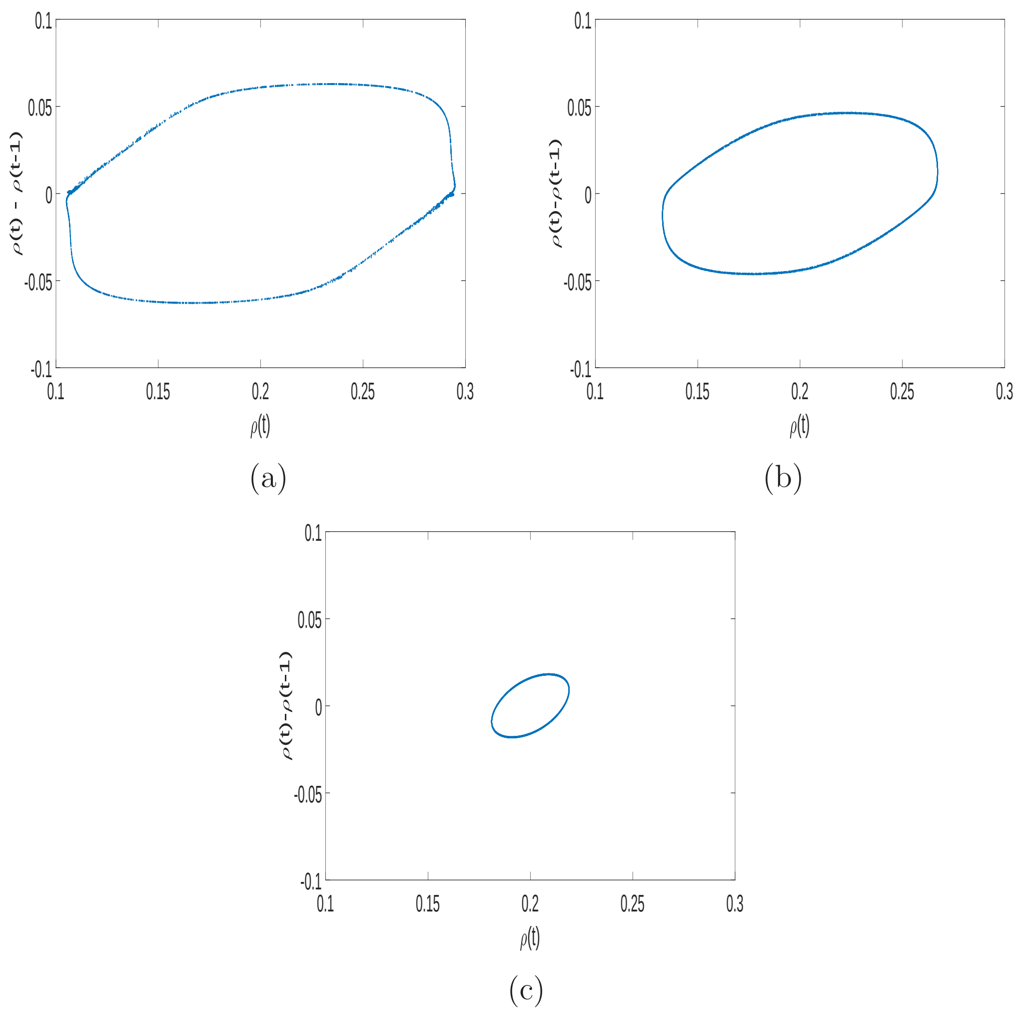

Figure 6.8: Phase plots of density versus density difference at $t = 15\times10^3 - 2\times10^4, a = 0.5, \lambda = 0$ for equal values of C_1 and C_2 (a) $C_1 = C_2 = 0.1$ (b) $C_1 = C_2 = 0.2$ (c) $C_1 = C_2 = 0.4$.

6.4.1.2 With the effect of optimal current difference ($\lambda = 0.2$)

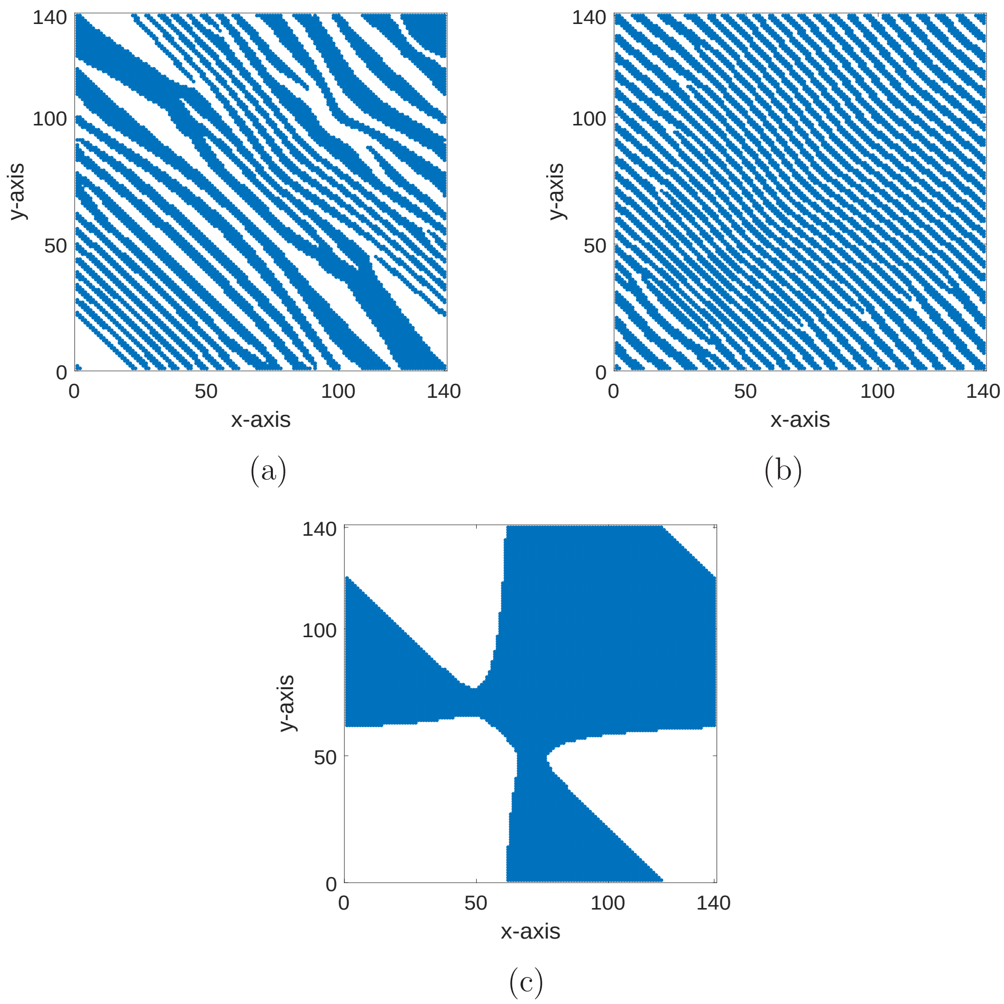

Figure 6.9: Traffic patterns at $t = 2 \times 10^3, a = 0.5, \lambda = 0.2$ for equal values of C_1 and C_2 (a) $C_1 = C_2 = 0.1$ (b) $C_1 = C_2 = 0.2$ (c) $C_1 = C_2 = 0.4$.

Now we consider the situation of bidirectional flow on the square lattice by taking the effect of optimal current difference $\lambda = 0.2$ and compare the results with the previous case, i.e., $\lambda = 0$. Fig. 6.9 shows the traffic patterns at $t = 2\times10^3$ for equal values of fraction parameters C_1 and C_2 when $\lambda = 0.2$. The results show that for lower values of pair of fractions traffic comes out in a diagonal pattern but as soon as the fractional pair increases the whole flow start distributing uniformly over the whole. Therefore the white region, that represents the free flowing region, gets wider. But in the previous case as in Fig. 6.6, when optimal current difference is zero, the whole space is shaded by blue color, i.e., the density of vehicles is more.

Fig. 6.10 and Fig. 6.11 shows the density wave profile and scatter plots for equal fractions. Which can be justified in a similar manner that the higher values of equal pair makes the flow stable as the amplitude of density wave in Fig. 6.10(c) die out and the loop in Fig. 6.11(c) converges to single point. But when $\lambda = 0$ as explained in Fig. 6.7 the density wave comes out with higher amplitude and in Fig. 6.8 the size of loop is greater.

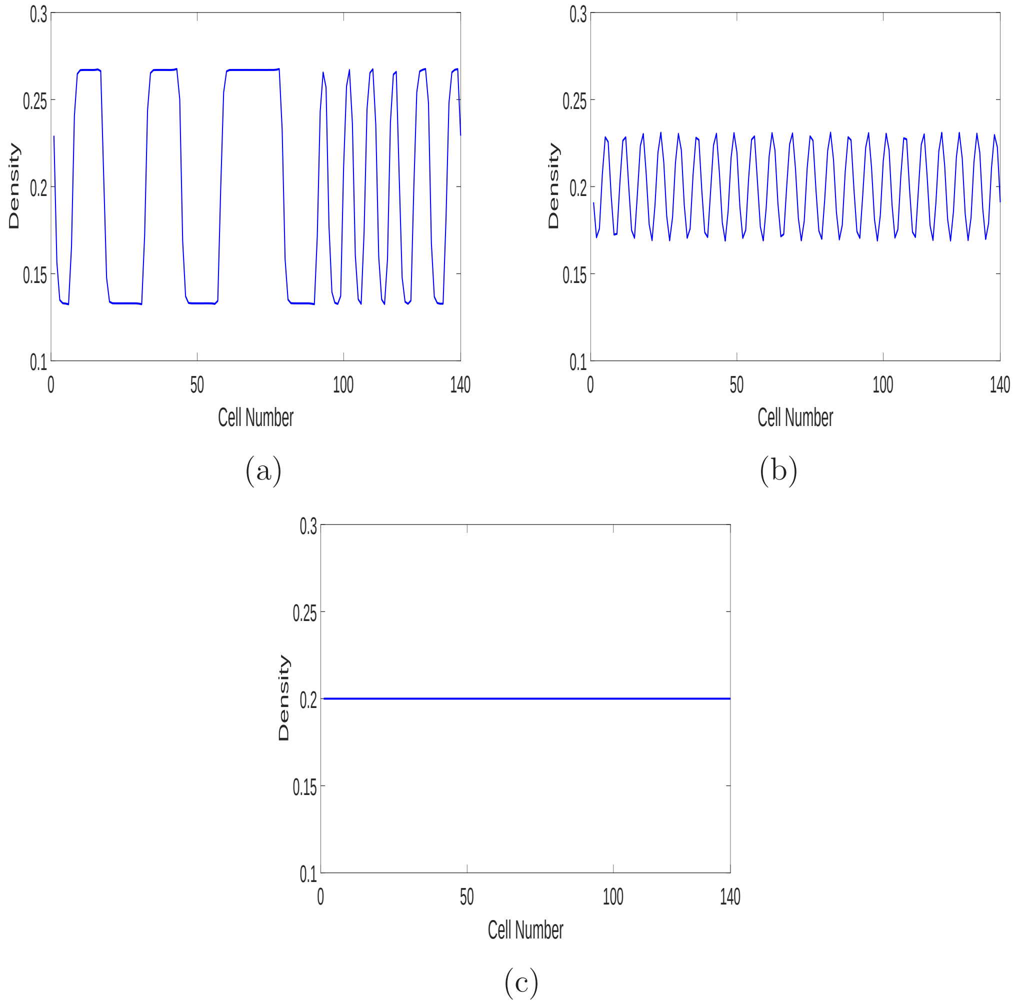

Figure 6.10: Density wave profile at $t = 15 \times 10^3, a = 0.5, \lambda = 0.2$ for equal values of C_1 and C_2 (a) $C_1 = C_2 = 0.1$ (b) $C_1 = C_2 = 0.2$ (c) $C_1 = C_2 = 0.4$.

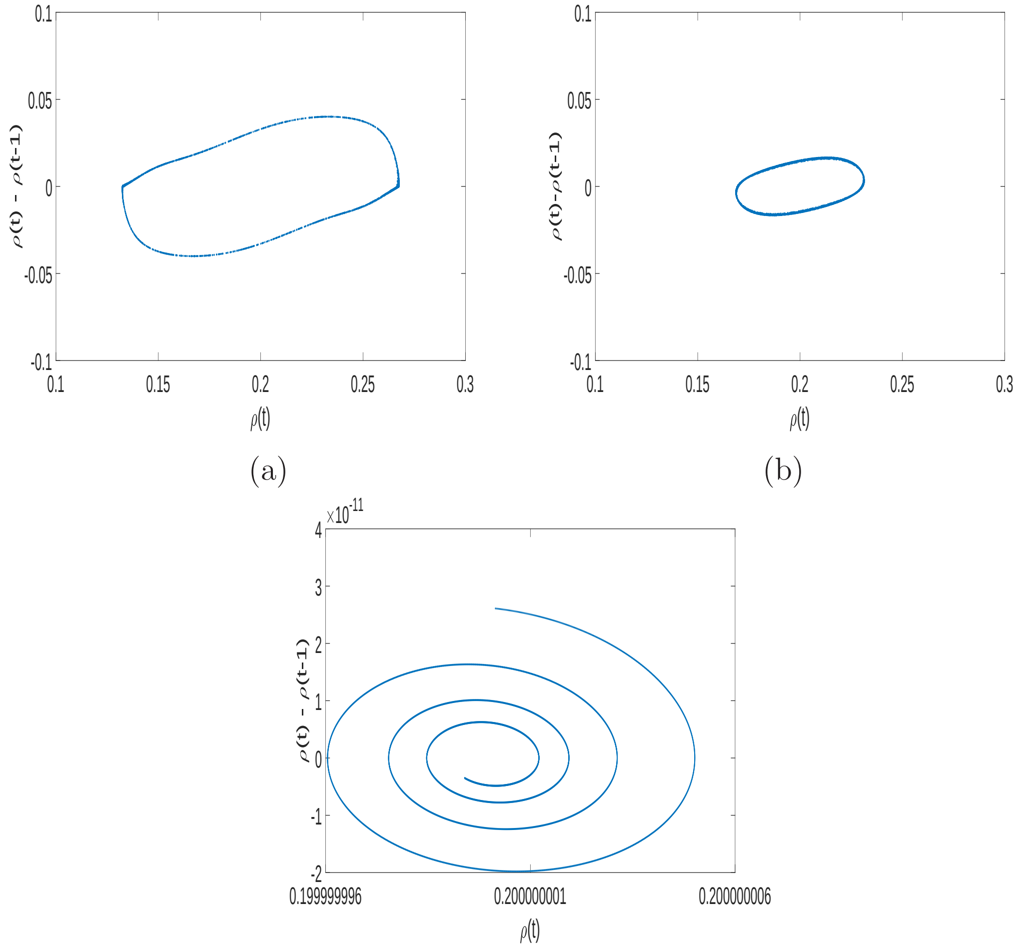

(a) (b)

(c)

Figure 6.11: Phase plots of density versus density difference at $t = 15\times10^3 - 2\times10^4, a = 0.5, \lambda = 0.2$ for equal values of C_1 and C_2 (a) $C_1 = C_2 = 0.1$ (b) $C_1 = C_2 = 0.2$ (c) $C_1 = C_2 = 0.4$.

6.4.2 When fraction parameters are unequal ($C_1 \neq C_2$) for ($\lambda = 0.2$)

6.4.2.1 Fixed fraction parameter C_1:

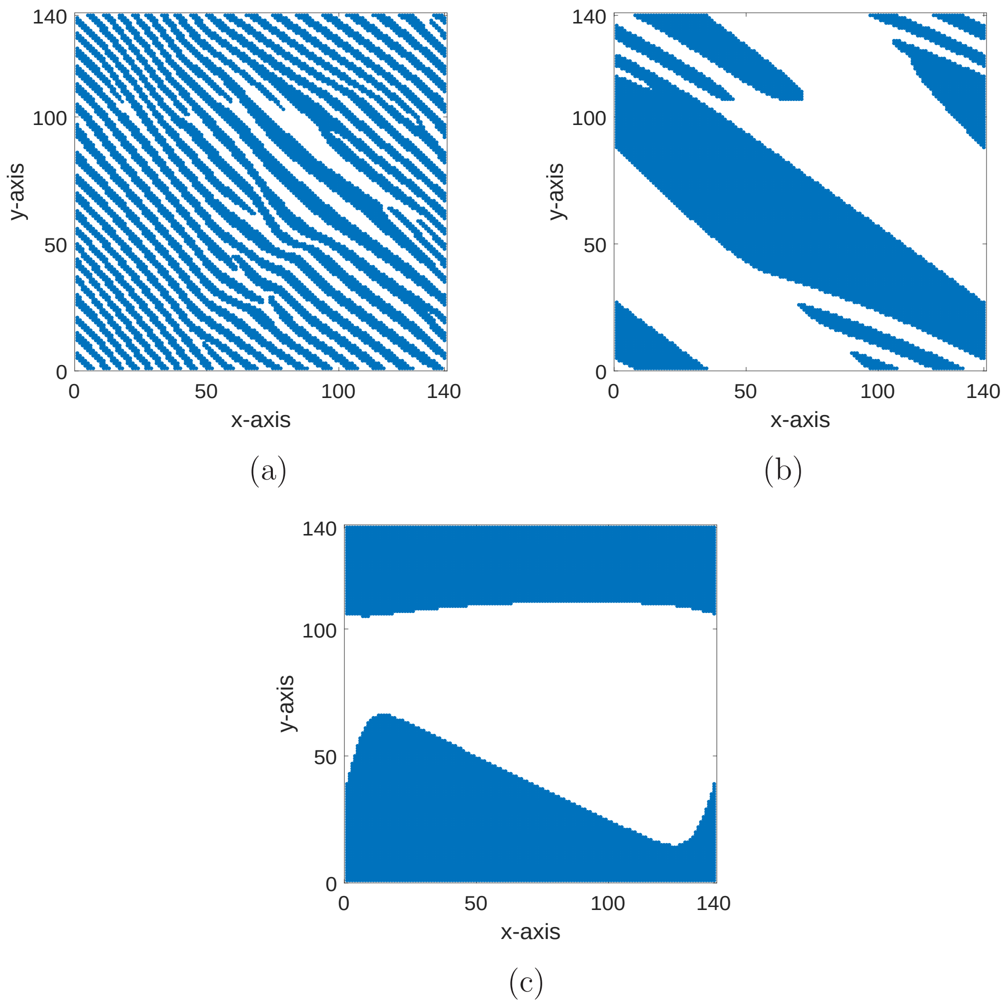

Figure 6.12: Traffic patterns at $t = 2 \times 10^3, a = 0.6, \lambda = 0.2$ for fixed $C_1 = 0.1$ (a) $C_2 = 0.2$ (b) $C_2 = 0.3$ (c) $C_2 = 0.5$.

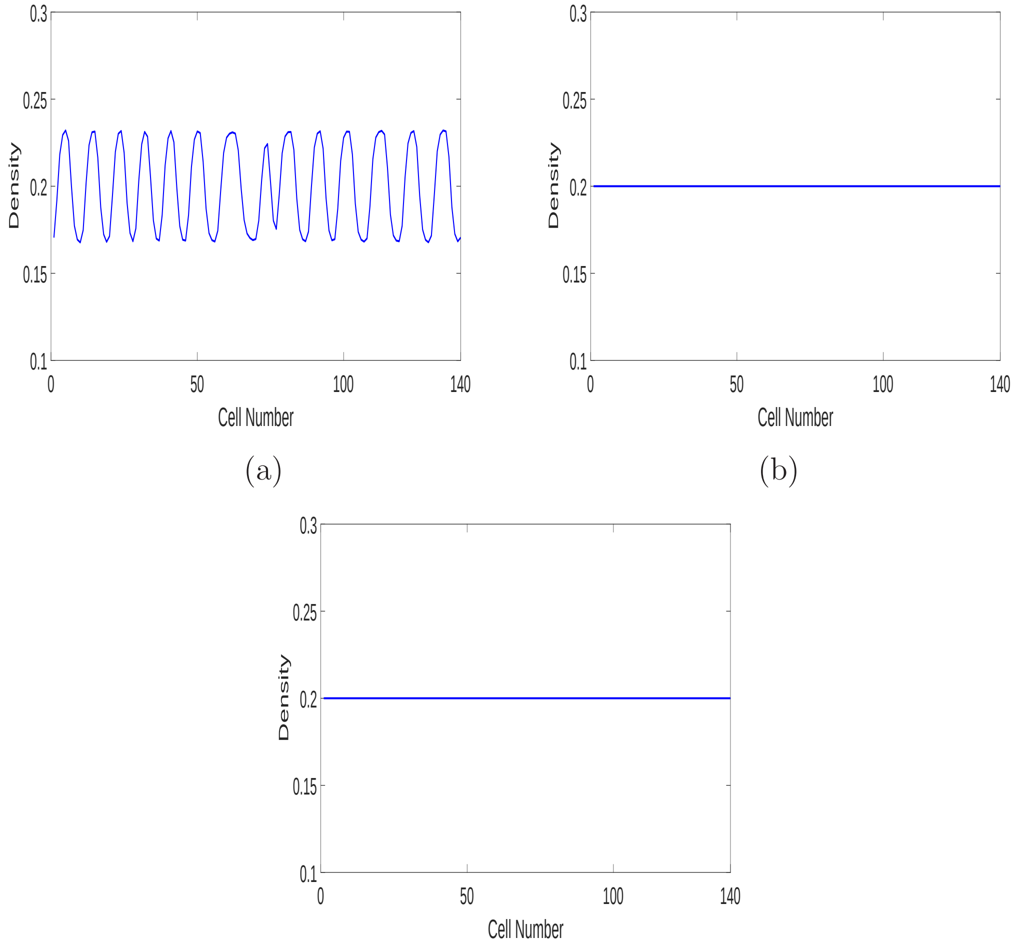

(a) (b) (c)

Figure 6.13: Density wave profile at $t = 15 \times 10^3$, $a = 0.6$, $\lambda = 0.2$ for fixed $C_1 = 0.1$ (a) $C_2 = 0.2$ (b) $C_2 = 0.3$ (c) $C_2 = 0.5$.

In order to fully describe the flow of vehicles moving in positive x and y as well as negative x and y-directions, we made the choice for unequal fractions with the optimal current difference effect. When the fraction parameter C_1 is fixed then the traffic pattern in Fig. 6.12(a) shows diagonal pattern and in Fig. 6.12(b)-6.12(c) the dense region shown with blue color start decreasing. The density is diminishing and the flow is uniform for higher values of C_2 corresponding to fixed C_1. In Fig. 6.12(c) the dense region is shown by blue color along x-axis which is consistent to the real traffic situations. The density waves and the loop patterns also shows similar results in Fig. 6.13 and Fig. 6.14, the amplitude of density wave (Fig. 6.13(b)) completely vanished at early stage for $C_2 = 0.3$ and the loop in Fig. 6.14(c) start converging to a single point corresponding to increasing values of C_2 which refers to the stability of flow.

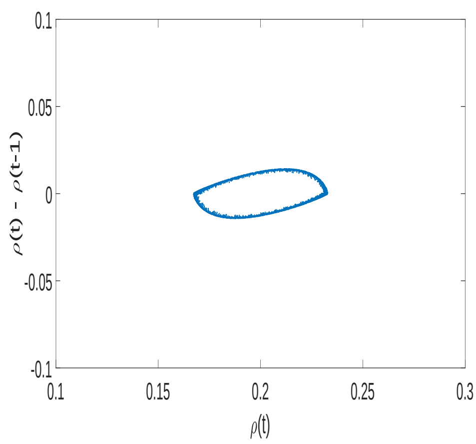

(a)

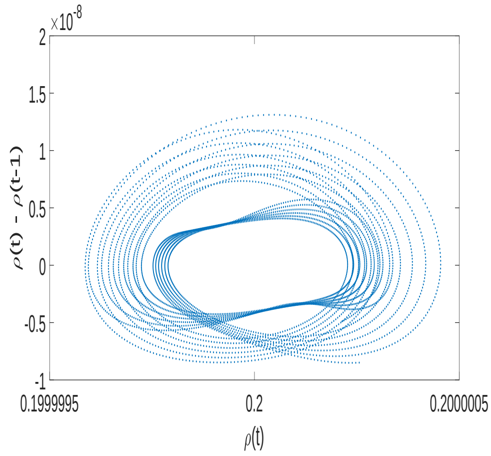

(b)

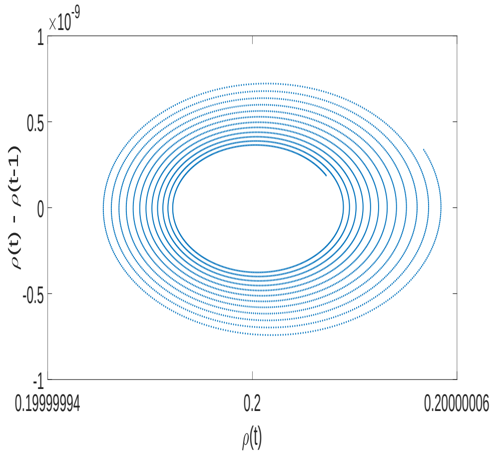

(c)

Figure 6.14: Phase plots of density versus density difference at $t = 15\times10^3 - 2\times10^4, a = 0.6, \lambda = 0.2$ for fixed $C_1 = 0.1$ (a) $C_2 = 0.2$ (b) $C_2 = 0.3$ (c) $C_2 = 0.5$.

6.4.2.2 Fixed fraction parameter C_2:

Similar results hold for fixed C_2 as given in Fig. 6.15 but the difference is that the dense region appears along y-axis in Fig. 6.15(c) which was along x-axis in Fig. 6.12. The density waves in Fig. 6.16(a) comes out in kink pattern which turns into straight line in Fig. 6.16(b)-6.16(c). The loop in Fig. 6.17(a)-6.17(c) shrink in size and converges to single point for increasing values of C_1.

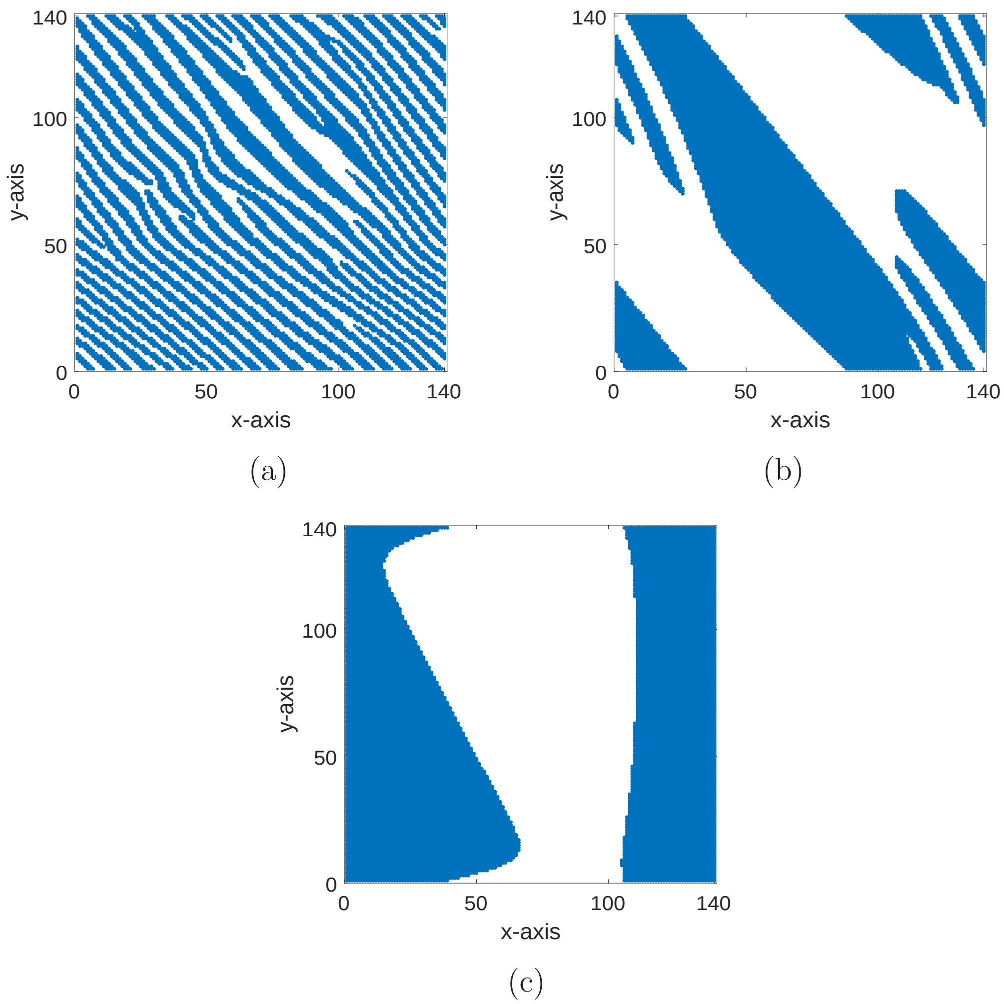

Figure 6.15: Traffic patterns at $t = 2 \times 10^3, a = 0.6, \lambda = 0.2$ for fixed $C_2 = 0.1$ (a) $C_1 = 0.2$ (b) $C_1 = 0.3$ (c) $C_1 = 0.5$.

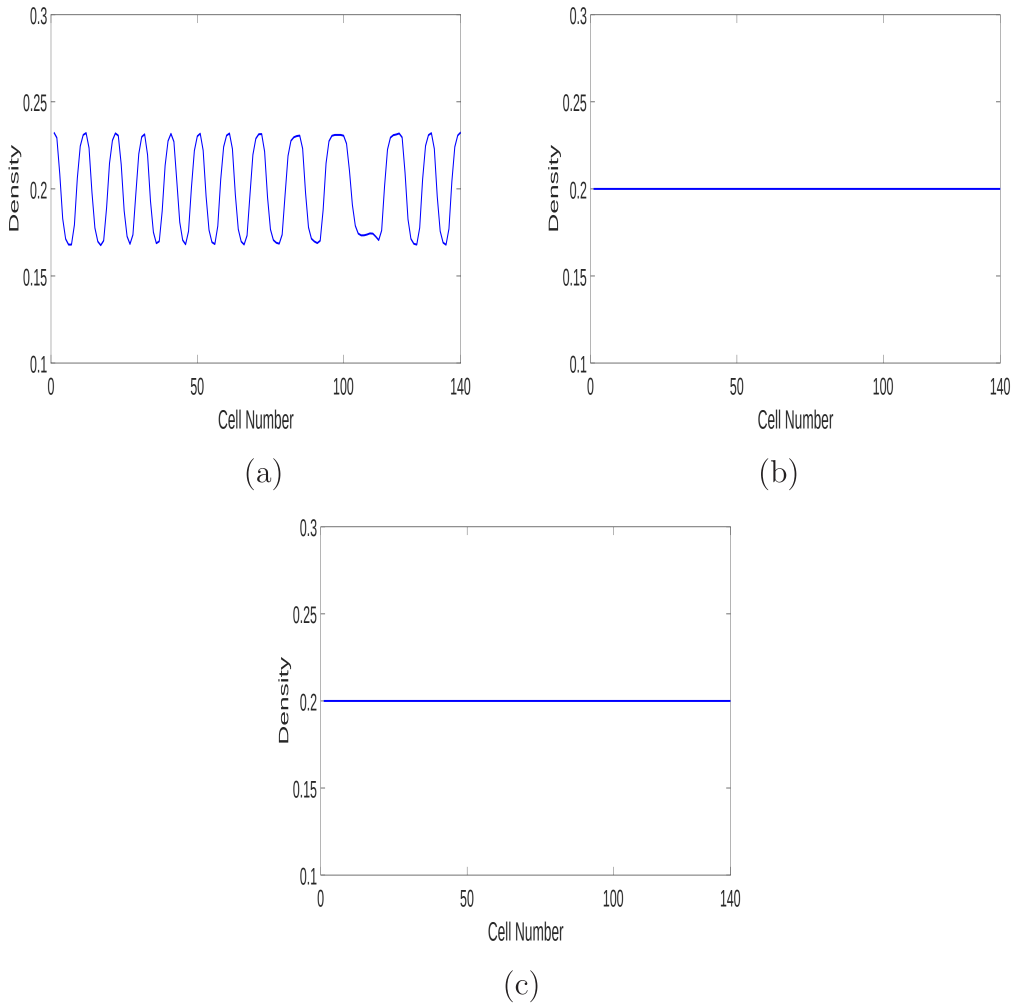

Figure 6.16: Density wave profile at $t = 15\times10^3, a = 0.6, \lambda = 0.2$ for fixed $C_2 = 0.1$ (a) $C_1 = 0.2$ (b) $C_1 = 0.3$ (c) $C_1 = 0.5$.

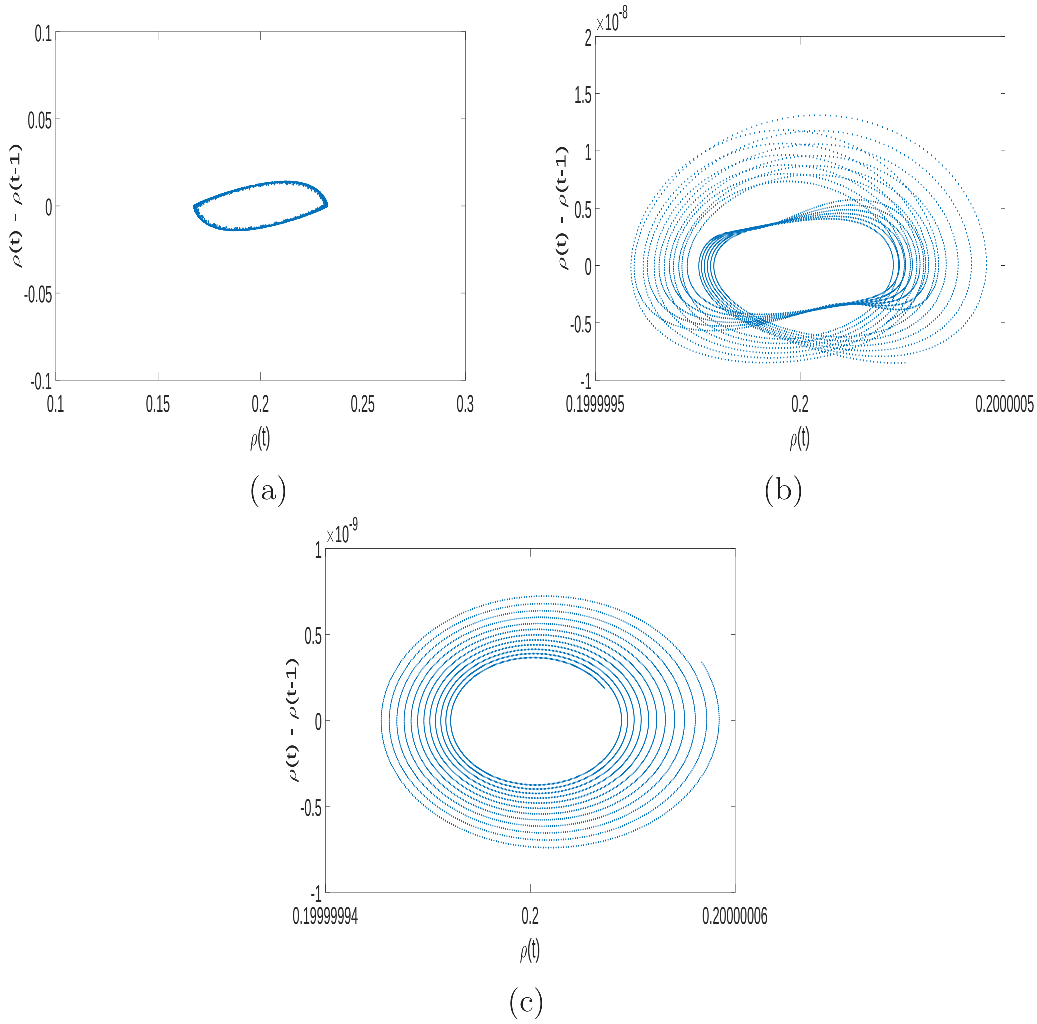

Figure 6.17: Phase plots of density versus density difference at $t = 15\times10^3 - 2\times10^4, a = 0.6, \lambda = 0.2$ for fixed $C_2 = 0.1$ (a) $C_1 = 0.2$ (b) $C_1 = 0.3$ (c) $C_1 = 0.5$.

6.5 Conclusion

- A modified lattice model is presented for bidirectional flow on a square lattice by keeping the effect of optimal current difference.

- Four different direction of vehicle movement on a two dimensional lattice are considered and it is assumed that out of the total fraction (C) of cars, half are moving in x and another half in y-directions (positive as well as negative). Then, to explore different configurations of traffic moving in four different directions, two different cases corresponding to the fraction parameters C_1 and C_2 for fixed $C = 0.5$ are chosen, one is equal case and the other is explained for unequal case because the traffic exhibits distinct configurations when moving in four different directions.

- By using linear stability analysis neutral stability curves are obtained in (ρ, a) phase plane. Results are shown that below the critical point, phase transitions occur among free flow phase, coexisting phase and jammed phase . Because the critical sensitivity decreases corresponding to increasing fractional pair in both cases, therefore no phase transition occurs above the critical point.
- To explore the properties of traffic around (ρ_c, a_c) when the density is higher, mKdV equation is derived and the jams are represented in terms of kink density waves.
- The effect of optimal current is analyzed under two states and found that the flow is more smooth when $\lambda = 0.2$. The density of vehicles is uniform over the whole space when the vehicles moving in each direction are equal in percentage.
- Simulation results are found in good agreement with theoretical results.

Chapter 7

Summary and future scope

The present thesis contributes to the analysis and development of traffic flow models using lattice hydrodynamic approach. We now summarize all the proposed models that are presented in the thesis along with the possible future scope based on the significance of lattice approach.

7.1 Summary

Lattice models are basically a combination of both microscopic and macroscopic models and are simple to explain the properties of large scale systems and networks. Mathematically, the models consist of the system of continuity equation and evolution equation involving global variables like density, flow, and velocity. One of the major benefits of this approach is its computational efficiency as compared to other approaches. The non trivial jamming transitions and separation of traffic flow phases can be effectively analyzed through theoretical investigation of these models. In addition, the evolution of traffic jams can be represented in terms of density waves. The density waves like shock waves, kink density waves and solitary density waves can be obtained by the solution of burger's, KdV, mKdV equations in stable, metastable and unstable regions, respectively. Moreover, the lattice models are very helpful in estimation, prediction and control of traffic flow on a road networks.

Motivated by the advantages of lattice hydrodynamic models in describing and analyzing the traffic characteristics in a realistic manner, present study is conducted. The first Chapter provides a basic background of traffic flow theory. Different modeling approaches describing important features of traffic flow are discussed with brief details. In addition, the limitations or the complexities of the existing approaches are also mentioned. The major and the most important contribution of the development of traffic flow theory is the representation of traffic jams in terms of density waves. Therefore, experimental studies conducted in recent past are also discussed. In the similar fashion, lattice models came into existence which incorporates the properties of both microscopic and macroscopic models. Moreover, lattice model is able to overcome the limitations of existing models because it can completely analyze the micro details of traffic using global variables. Further, the recent developments in traffic flow theory using lattice approach are discussed.

After having an idea about the basic background and developments of the lattice hydrodynamic approach, it was found that the importance of the effect of geometric designs of the road needs to be incorporated in the lattice model. Because all the existing models have described the properties of single lane road, two lane road or single lane road with slope or curve without discussing the importance of driver's behavior on different type of roads. Therefore, Chapter 2 and 3 are devoted to the analyses of geometric design effects on traffic flow along with driver's characteristics. In Chapter 2 the effect of driver's behavior and curved road are analyzed. Based on different driver's characteristics namely aggressive, normal and timid; different drivers observe inter-vehicular spacing differently. Aggressive (timid) drivers overestimate (underestimate) downstream density as compared to normal drivers. Moreover, the drivers experience difficulties while driving on roads having some curves or slopes and driving on such roads require skillful driving aptitude. Therefore, real features of road geometry including driver's behavior are presented. The results are shown that increase in aggressive drivers and radian of curved road enhances the stability in traffic flow. The simulations are conducted and the results are compared and found with theoretical findings. The results indicate that for small radian of curved road, when the traffic is in unstable state, aggressive drivers can help in reducing traffic congestion.

Following the similar idea of road geometry and driver's characteristics, the properties of traffic flow are analyzed in Chapter 3. In Chapter 2 the curved road without slope is considered but in actual road networks the curved road may not have same level everywhere, it may consist road indents called slope. Driving on a road having curved shape as well as slope is much more complicated. But skillful drivers can perceive and judge the traffic situations quickly and then try to control their vehicle accordingly. The results are shown that the slope have a negative impact on stabilization of traffic flow but skillful drivers can overcome it easily. Thus, the results presented in this chapter are an attempt to make a qualitative improvement over the past studies.

Traffic flow is a mechanical process in which three major aspects which affects the movement of vehicles are: drivers, road infrastructure and different kind of vehicles. Following the same tradition of modeling traffic flow using lattice hydrodynamic approach, third and most important aspect, i.e., vehicular heterogeneity is considered in Chapter 4. It deals with the influence of vehicular heterogeneity on the dynamics of traffic flow. All the existing lattice models discussed in previous Chapters consider the traffic to be homogeneous; thus in the new model, two different classes of vehicles are considered. One type of vehicles are considered to be small and the other one is large. Small vehicles are assumed to have high sensitivity as compared to the large ones. The effects of the fraction of high sensitivity vehicles on critical phase transitions are investigated in the phase-plane for density versus fraction parameter. It is concluded that the critical line divides the whole space into five distinct regions. Among them (I) and (V) regions are found to be stable; (II) and (IV) are sensitive to the fraction of small and large vehicles and (III) region represents the totally unstable state of traffic. Simulations are also performed to justify the theoretical predictions.

The most common phenomena that occur in traffic flow dynamics is passing/overtaking that has been incorporated in Chapter 5 using control theory. The efficiency of the control signal in overcoming the congestion is shown at lower and higher rate of passing. Simulations are carried out for testing the influence of feedback control on steady-state and transient behavior of lattice model at lower and higher rate of passing. All the existing models in the literature claims the one way homogeneous traffic but the movement of vehicles on road is not restricted towards one direction only. Therefore in Chapter 6, lattice model is extended for two-dimensional network of square lattice where the flow is bidirectional. As the existing models for two dimensional system assume the flow towards north and east directions only. But in actual traffic situations, traffic can move in any possible direction based on the choice of driver. Therefore, south and west directions are also considered along with north and east directions of flow with respect to the optimal current difference effect. Results show that the flow can be stable when the fraction of vehicles moving in each direction is approximately same otherwise unequal fraction of vehicles can create traffic congestion.

The validity of the models presented in the thesis is checked for the particular choice of parameters that can recover the results of existing models in the literature. Moreover, results of the proposed models are compared with existing models. It has been found that the models presented in this thesis are an improvement over the past studies and we hope that our work would help in gaining deeper insight into traffic flow dynamics.

7.2 Future scope

In the final section, we list some future research directions based on the study performed in this thesis.

- The newly developed models (Chapter 2 and 3) are an improvement over past studies based on lattice approach by considering road geometry (curved road and curved road with slope), yet some other phenomena related to road geometry can be examined, e.g., bottlenecks, merging and bifurcating junctions. In addition, the effect of road conditions can also be incorporated in lattice model.

- Tollgates play a major role in traffic flow dynamics and there exist two types of tollgates: electronic and manual. Among them, electronic tollgates are of great importance than manual tollgates. Therefore, the effect of both types can be investigated by utilizing the lattice model.

- While moving on the road, drivers can control their vehicle's speed on the basis of the taillight of the front vehicle. Therefore, the taillight of the front vehicle plays an important role and can be examined by utilizing lattice approach. Some existing studies can be helpful for modeling the suggested phenomena.

- Nowadays, the automobile industry is focusing in the advancement of autonomous vehicles. Autonomous vehicles are helpful in the reduction of accident rates that could happen due to driver's distraction. So choosing the idea of autonomous vehicles and with the help of emerging technology, qualitative improvements can take place in lattice model.
- Last but not the least, experimental studies can also be performed to validate the results of existing models.

References

[1] T Nagatani. Modified KdV equation for jamming transition in the continuum models of traffic. *Physica A: Statistical Mechanics and its Applications*, 261(3-4):599–607, 1998.

[2] VL Knoop. Introduction to traffic flow theory: An introduction with exercises. 2017.

[3] M Treiber and A Kesting. Traffic flow dynamics: data, models and simulation. *Physics Today*, 67(3):54, 2014.

[4] B Piccoli. Traffic flow on networks: conservation laws models. 2006.

[5] PG LeFloch. *Hyperbolic Systems of Conservation Laws: The Theory of Classical and Nonclassical Shock Waves*. Springer Science & Business Media, 2002.

[6] D Ni. *Traffic flow theory: Characteristics, Experimental Methods, and Numerical Techniques*. Butterworth-Heinemann, 2015.

[7] M Rose. Modeling of freeway traffic. 2004.

[8] R Herman and K Gardels. Vehicular traffic flow. *Scientific American*, 209(6):35–43, 1963.

[9] DC Gazis. Mathematical theory of automobile traffic. *Science*, 157(3786):273–281, 1967.

[10] RW Rothery. Transportation research board (trb) special report 165. *Traffic Flow Theory*, 1998.

[11] D Chowdhury, L Santen, and A Schadschneider. Statistical physics of vehicular traffic and some related systems. *Physics Reports*, 329(4-6):199–329, 2000.

[12] RE Chandler, R Herman, and EW Montroll. Traffic dynamics: studies in car following. *Operations Research*, 6(2):165–184, 1958.

[13] R Herman. Car-following and steady state flow. In *Theory of Traffic Flow Symposium Proceedings*, 1-13, 1959.

[14] R Herman and RB Potts. Single lane traffic theory and experiment. 1959.

[15] DC Gazis, R Herman, and RB Potts. Car-following theory of steady-state traffic flow. *Operations Research*, 7(4):499–505, 1959.

[16] DC Gazis, R Herman, and RW Rothery. Nonlinear follow-the-leader models of traffic flow. *Operations Research*, 9(4):545–567, 1961.

[17] LA Pipes. An operational analysis of traffic dynamics. *Journal of Applied Physics*, 24(3):274–281, 1953.

[18] LA Pipes. Car following models and the fundamental diagram of road traffic. *Transportation Research/UK/*, 1966.

[19] TW Forbes. Human factor considerations in traffic flow theory. *Highway Research Record*, (15), 1963.

[20] E Kometani. Dynamic behavior of traffic with a nonlinear spacing-speed relationship. *Theory of Traffic Flow (Proc. of Sym. on TTF (GM))*, 105-119, 1959.

[21] GF Newell. A simplified car-following theory: a lower order model. *Transportation Research Part B: Methodological*, 36(3):195–205, 2002.

[22] M Bando, K Hasebe, A Nakayama, A Shibata, and Y Sugiyama. Dynamical model of traffic congestion and numerical simulation. *Physical Review E*, 51(2):1035–1042, 1995.

[23] M Bando, K Hasebe, K Nakanishi, A Nakayama, A Shibata, and Y Sugiyama. Phenomenological study of dynamical model of traffic flow. *Journal de Physique I*, 5(11):1389–1399, 1995.

[24] D Helbing and B Tilch. Generalized force model of traffic dynamics. *Physical Review E*, 58(1):133–138, 1998.

[25] R Jiang, Q Wu, and Z Zhu. Full velocity difference model for a car-following theory. *Physical Review E*, 64(1):017101, 2001.

[26] TQ Tang, HJ Huang, and ZY Gao. Stability of the car-following model on two lanes. *Physical Review E*, 72(6):066124, 2005.

[27] HM Zhang and T Kim. A car-following theory for multiphase vehicular traffic flow. *Transportation Research Part B: Methodological*, 39(5):385–399, 2005.

[28] X Zhao and Z Gao. A new car-following model: full velocity and acceleration difference model. *The European Physical Journal B-Condensed Matter and Complex Systems*, 47(1):145–150, 2005.

[29] HX Ge, HB Zhu, and SQ Dai. Effect of looking backward on traffic flow in a cooperative driving car following model. *The European Physical Journal B-Condensed Matter and Complex Systems*, 54(4):503–507, 2006.

[30] ZP Li and YC Liu. A velocity-difference-separation model for car-following theory. *Chinese Physics*, 15(7):1570–1576, 2006.

[31] GH Peng, XH Cai, CQ Liu, BF Cao, and MX Tuo. Optimal velocity difference model for a car-following theory. *Physics Letters A*, 375(45):3973–3977, 2011.

[32] LJ Zheng, C Tian, DH Sun, and WN Liu. A new car-following model with consideration of anticipation driving behavior. *Nonlinear Dynamics*, 70(2):1205–1211, 2012.

[33] A Kesting, M Treiber, and D Helbing. Mobil: General lane-changing model for car-following models. *Transportation Research Record*, 1999(1):86–94, 2007.

[34] Y Li, L Zhang, H Zheng, X He, S Peeta, T Zheng, and Y Li. Nonlane-discipline-based car-following model for electric vehicles in transportation-cyber-physical systems. *IEEE Transactions on Intelligent Transportation Systems*, 19(1):38–47, 2018.

[35] Z Jin, Z Li, R Cheng, and H Ge. Nonlinear density wave investigation for an extended car-following model considering driver's memory and jerk. *Modern Physics Letters B*, 32(01):1750366, 2018.

[36] P Tan, DH Sun, D Chen, M Zhao, and T Chen. Stability analysis of car-following model on straight and curved roads considering the preceding vehicle's velocity feedback control. *Modern Physics Letters B*, 32(21):1850238, 2018.

[37] YZ Zheng, R Cheng, and HX Ge. Multiple information feedback control scheme for an improved car-following model. *Asian Journal of Control*, 19(1):215–223, 2017.

[38] G Zhang, DH Sun, M Zhao, XY Liao, WN Liu, and T Zhou. An extended car-following model accounting for cooperation driving system with velocity uncertainty. *Physica A: Statistical Mechanics and its Applications*, 505:1008–1017, 2018.

[39] M Saifuzzaman and Z Zheng. Incorporating human-factors in car-following models: a review of recent developments and research needs. *Transportation Research Part C: Emerging Technologies*, 48:379–403, 2014.

[40] H Lazar, K Rhoulami, and D Rahmani. A review analysis of optimal velocity models. *Periodica Polytechnica Transportation Engineering*, 44(2):123–131, 2016.

[41] MJ Lighthill and GB Whitham. On kinematic waves II. a theory of traffic flow on long crowded roads. *Proceedings of the Royal Society of London. Series A. Mathematical and Physical Sciences*, 229(1178):317–345, 1955.

[42] PI Richards. Shock waves on the highway. *Operations Research*, 4(1):42–51, 1956.

[43] HJ Payne. Model of freeway traffic and control. *Mathematical Model of Public System*, 51-61, 1971.

[44] WF Phillips. A kinetic model for traffic flow with continuum implications. *Transportation Planning and Technology*, 5(3):131–138, 1979.

[45] R Kuhne. Freeway speed distribution and acceleration noise: calculations from a stochastic continuum theory and comparision with measurements. *Transportation and Traffic Theory*, 12:119–137, 1987.

[46] R Kuhne and P Michalopoulos. Continuum flow models. *Traffic Flow Theory: A State of the Art Report Revised Monograph on Traffic Flow Theory*, 1997.

[47] BS Kerner and P Konhäuser. Cluster effect in initially homogeneous traffic flow. *Physical Review E*, 48(4):R2335–R2338, 1993.

[48] CF Daganzo. Requiem for second-order fluid approximations of traffic flow. *Transportation Research Part B: Methodological*, 29(4):277–286, 1995.

[49] A Aw and M Rascle. Resurrection of "second order" models of traffic flow. *SIAM Journal On Applied Mathematics*, 60(3):916–938, 2000.

[50] HM Zhang. A non-equilibrium traffic model devoid of gas-like behavior. *Transportation Research Part B: Methodological*, 36(3):275–290, 2002.

[51] V Tyagi, S Darbha, and KR Rajagopal. A review of the mathematical models for traffic flow. *International Journal of Advances in Engineering Sciences and Applied Mathematics*, 1(1):53–68, 2009.

[52] H Huang, TQ Tang, and Z Gao. Continuum modeling for two-lane traffic flow. *Acta Mechanica Sinica*, 22(2):131–137, 2006.

[53] DH Sun and GH Peng. A viscous continuum traffic flow model with consideration of the coupling effect for two-lane freeways. *Chinese Physics B*, 18(9):3724–3735, 2009.

[54] R Mohan and G Ramadurai. Heterogeneous traffic flow modelling using second-order macroscopic continuum model. *Physics Letters A*, 381(3):115–123, 2017.

[55] C Tian and DH Sun. Continuum modeling for two-lane traffic flow with consideration of the traffic interruption probability. *Chinese Physics B*, 19(12):120501, 2010.

[56] R Cheng, F Liu, and H Ge. A new continuum model based on full velocity difference model considering traffic jerk effect. *Nonlinear Dynamics*, 89(1):639–649, 2017.

[57] C Zhai and W Wu. Analysis of drivers' characteristics on continuum model with traffic jerk effect. *Physics Letters A*, 382(47):3381–3392, 2018.

[58] R Cheng, H Ge, and J Wang. An improved continuum model for traffic flow considering driver's memory during a period of time and numerical tests. *Physics Letters A*, 381(34):2792–2800, 2017.

[59] R Cheng, H Ge, and J Wang. An extended continuum model accounting for the driver's timid and aggressive attributions. *Physics Letters A*, 381(15):1302–1312, 2017.

[60] R Cheng, H Ge, and J Wang. KdV–burgers equation in a new continuum model based on full velocity difference model considering anticipation effect. *Physica A: Statistical Mechanics and its Applications*, 481:52–59, 2017.

[61] R Cheng, H Ge, and J Wang. An extended macro traffic flow model accounting for multiple optimal velocity functions with different probabilities. *Physics Letters A*, 381(32):2608–2620, 2017.

[62] DL Fan, YC Zhang, Y Shi, Y Xue, and FP Wei. An extended continuum traffic model with the consideration of the optimal velocity difference. *Physica A: Statistical Mechanics and its Applications*, 508:402–413, 2018.

[63] Y Li, H Yang, B Yang, T Zheng, and C Zhang. An extended continuum model incorporating the electronic throttle dynamics for traffic flow. *Nonlinear Dynamics*, 93:1923–1931, 2018.

[64] I Prigogine and R Herman. *Kinetic theory of vehicular traffic*. American Elsevier Publishing Company, 1971.

[65] BD Greenshields, W Channing, HH Miller, and JR Bibbins. A study of traffic capacity. In *Highway research board proceedings*. National Research Council (USA), Highway Research Board,1935, 935.

[66] H Greenberg. An analysis of traffic flow. *Operations Research*, 7(1):79–85, 1959.

[67] RT Underwood. Speed, volume, and density relationship: Quality and theory of traffic flow, yale bureau of highway traffic. *New Haven, Connecticut*, 1961:141–188, 2008.

[68] MZF Li. A generic characterization of equilibrium speed-flow curves. *Transportation Science*, 42(2):220–235, 2008.

[69] JM Del Castillo, P Pintado, and FG Benitez. The reaction time of drivers and the stability of traffic flow. *Transportation Research Part B: Methodological*, 28(1):35–60, 1994.

[70] BS Kerner. Phase transitions in traffic flow. In *'Traffic and Granular Flow' 99*. Springer, 253–283, 2000.

[71] J Treiterer. Ohio state technical report no. *PB*, 246:094, 1975.

[72] Y Sugiyama, M Fukui, M Kikuchi, K Hasebe, A Nakayama, K Nishinari, S Tadaki, and S Yukawa. Traffic jams without bottlenecks experimental evidence for the physical mechanism of the formation of a jam. *New Journal of Physics*, 10(3):033001, 2008.

[73] A Nakayama, M Fukui, M Kikuchi, K Hasebe, K Nishinari, Y Sugiyama, S Tadaki, and S Yukawa. Metastability in the formation of an experimental traffic jam. *New Journal of Physics*, 11(8):083025, 2009.

[74] M Muramatsu and T Nagatani. Soliton and kink jams in traffic flow with open boundaries. *Physical Review E*, 60(1):180–187, 1999.

[75] DA Kurtze and DC Hong. Traffic jams, granular flow, and soliton selection. *Physical Review E*, 52(1):218–221, 1995.

[76] TS Komatsu and S Sasa. Kink soliton characterizing traffic congestion. *Physical Review E*, 52(5):5574–5582, 1995.

[77] HJ Payne. Freflo: A macroscopic simulation model of freeway traffic. *Transportation Research Record*, (722):68–77, 1979.

[78] P Redhu. *Analyses of Lattice Hydrodynamic Models in Traffic Flow*. PhD thesis, Indian Institute of Technology Ropar, 2015.

[79] T Nagatani. Jamming transitions and the modified korteweg–de vries equation in a two-lane traffic flow. *Physica A: Statistical Mechanics and its Applications*, 265(1-2):297–310, 1999.

[80] GH Peng, XH Cai, CQ Liu, and MX Tuo. A new lattice model of traffic flow with the anticipation effect of potential lane changing. *Physics Letters A*, 376(4):447–451, 2012.

[81] AK Gupta and P Redhu. Analyses of driver's anticipation effect in sensing relative flux in a new lattice model for two-lane traffic system. *Physica A: Statistical Mechanics and its Applications*, 392(22):5622–5632, 2013.

[82] S Sharma. Lattice hydrodynamic modeling of two-lane traffic flow with timid and aggressive driving behavior. *Physica A: Statistical Mechanics and its Applications*, 421:401–411, 2015.

[83] T Nagatani. Chaotic jam and phase transition in traffic flow with passing. *Physical Review E*, 60(2):1535–1541, 1999.

[84] S Sharma. Modeling and analyses of driver's characteristics in a traffic system with passing. *Nonlinear Dynamics*, 86(3):2093–2104, 2016.

[85] AK Gupta, S Sharma, and P Redhu. Effect of multi-phase optimal velocity function on jamming transition in a lattice hydrodynamic model with passing. *Nonlinear Dynamics*, 80(3):1091–1108, 2015.

[86] GH Peng. A new lattice model of two-lane traffic flow with the consideration of optimal current difference. *Communications in Nonlinear Science and Numerical Simulation*, 18(3):559–566, 2013.

[87] S Sharma. Effect of driver's anticipation in a new two-lane lattice model with the consideration of optimal current difference. *Nonlinear Dynamics*, 81(1-2):991–1003, 2015.

[88] P Redhu and AK Gupta. Phase transition in a two-dimensional triangular flow with consideration of optimal current difference effect. *Nonlinear Dynamics*, 78(2):957–968, 2014.

[89] AK Gupta and P Redhu. Jamming transition of a two-dimensional traffic dynamics with consideration of optimal current difference. *Physics Letters A*, 377(34-36):2027–2033, 2013.

[90] GH Peng. A new lattice model of the traffic flow with the consideration of the driver anticipation effect in a two-lane system. *Nonlinear Dynamics*, 73(1-2):1035–1043, 2013.

[91] YR Kang and DH Sun. Lattice hydrodynamic traffic flow model with explicit drivers' physical delay. *Nonlinear Dynamics*, 71(3):531–537, 2013.

[92] AK Gupta and P Redhu. Analyses of the driver's anticipation effect in a new lattice hydrodynamic traffic flow model with passing. *Nonlinear Dynamics*, 76(2):1001–1011, 2014.

[93] GH Peng, F Nie, B Cao, and C Liu. A driver's memory lattice model of traffic flow and its numerical simulation. *Nonlinear Dynamics*, 67(3):1811–1815, 2012.

[94] H Ge, Y Cui, KQ Zhu, and R Cheng. The control method for the lattice hydrodynamic model. *Communications in Nonlinear Science and Numerical Simulation*, 22(1-3):903–908, 2015.

[95] P Redhu and AK Gupta. Delayed-feedback control in a lattice hydrodynamic model. *Communications in Nonlinear Science and Numerical Simulation*, 27(1-3):263–270, 2015.

[96] S Qin, Z He, and R Cheng. An extended lattice hydrodynamic model based on control theory considering the memory effect of flux difference. *Physica A: Statistical Mechanics and its Applications*, 509:809–816, 2018.

[97] S Qin, H Ge, and R Cheng. A new control method based on the lattice hydrodynamic model considering the double flux difference. *Chinese Physics B*, 27(5):050503, 2018.

[98] GH Peng, S Yang, and H Zhao. A delayed-feedback control method for the lattice hydrodynamic model caused by the historic density difference effect. *Physica A: Statistical Mechanics and its Applications*, 509:855–860, 2018.

[99] H Ge and R Cheng. The "backward looking" effect in the lattice hydrodynamic model. *Physica A: Statistical Mechanics and its Applications*, 387(28):6952–6958, 2008.

[100] P Redhu and AK Gupta. Effect of forward looking sites on a multi-phase lattice hydrodynamic model. *Physica A: Statistical Mechanics and its Applications*, 445:150–160, 2016.

[101] GH Peng, XH Cai, BF Cao, and CQ Liu. A new lattice model of traffic flow with the consideration of the traffic interruption probability. *Physica A: Statistical Mechanics and its Applications*, 391(3):656–663, 2012.

[102] GH Peng, HD He, and WZ Lu. A new lattice model with the consideration of the traffic interruption probability for two-lane traffic flow. *Nonlinear Dynamics*, 81(1-2):417–424, 2015.

[103] P Redhu and AK Gupta. Jamming transitions and the effect of interruption probability in a lattice traffic flow model with passing. *Physica A: Statistical Mechanics And its Applications*, 421:249–260, 2015.

[104] JL Cao and ZK Shi. A novel lattice traffic flow model on a curved road. *International Journal of Modern Physics C*, 26(11):1550121, 2015.

[105] J Zhou and ZK Shi. Lattice hydrodynamic model for traffic flow on curved road. *Nonlinear Dynamics*, 83(3):1217–1236, 2016.

[106] J Zhou, ZK Shi, and CP Wang. Lattice hydrodynamic model for two-lane traffic flow on curved road. *Nonlinear Dynamics*, 85(3):1423–1443, 2016.

[107] YD Jin, J Zhou, ZK Shi, HL Zhang, and CP Wang. Lattice hydrodynamic model for traffic flow on curved road with passing. *Nonlinear Dynamics*, 89(1):107–124, 2017.

[108] R Cheng and Y Wang. An extended lattice hydrodynamic model considering the delayed feedback control on a curved road. *Physica A: Statistical Mechanics and its Applications*, 513:510–517, 2019.

[109] JF Tian, ZZ Yuan, B Jia, and W Tao. Dynamic congested traffic states of density difference lattice hydrodynamic model with on-ramp. *Discrete Dynamics in Nature and Society*, 2013, 2013, Article ID 941238.

[110] YC Zhang, Y Xue, Y Shi, Y Guo, and FP Wei. Congested traffic patterns of two-lane lattice hydrodynamic model with partial reduced lane. *Physica A: Statistical Mechanics and its Applications*, 502:135–147, 2018.

[111] G Zhang, DH Sun, and M Zhao. Phase transition of a new lattice hydrodynamic model with consideration of on-ramp and off-ramp. *Communications in Nonlinear Science and Numerical Simulation*, 54:347–355, 2018.

[112] R Kaur and S Sharma. Analyses of a heterogeneous lattice hydrodynamic model with low and high-sensitivity vehicles. *Physics Letters A*, 382(22):1449–1455, 2018.

[113] H Zhao, G Zhang, W Li, T Gu, and D Zhou. Lattice hydrodynamic modeling of traffic flow with consideration of historical current integration effect. *Physica A: Statistical Mechanics and its Applications*, 503:1204–1211, 2018.

[114] H Ge, SQ Dai, LY Dong, and Yu Xue. Stabilization effect of traffic flow in an extended car-following model based on an intelligent transportation system application. *Physical Review E*, 70(6):066134, 2004.

[115] K Nagel and M Schreckenberg. A cellular automaton model for freeway traffic. *Journal de Physique I*, 2(12):2221–2229, 1992.

[116] BS Kerner, SL Klenov, and DE Wolf. Cellular automata approach to three-phase traffic theory. *Journal of Physics A: Mathematical and General*, 35(47):9971–10013, 2002.

[117] AK Gupta and VK Katiyar. Analyses of shock waves and jams in traffic flow. *Journal of Physics A: Mathematical and General*, 38(19):4069–4083, 2005.

[118] R Jiang, QS Wu, and ZJ Zhu. A new continuum model for traffic flow and numerical tests. *Transportation Research Part B: Methodological*, 36(5):405–419, 2002.

[119] AK Gupta and VK Katiyar. A new anisotropic continuum model for traffic flow. *Physica A: Statistical Mechanics and its Applications*, 368(2):551–559, 2006.

[120] E De Angelis. Nonlinear hydrodynamic models of traffic flow modelling and mathematical problems. *Mathematical and Computer Modelling*, 29(7):83–95, 1999.

[121] I Bonzani. Hydrodynamic models of traffic flow: Drivers' behaviour and nonlinear diffusion. *Mathematical and Computer Modelling*, 31(6-7):1–8, 2000.

[122] GH Peng, XH Cai, BF Cao, and CQ Liu. Non-lane-based lattice hydrodynamic model of traffic flow considering the lateral effects of the lane width. *Physics Letters A*, 375(30-31):2823–2827, 2011.

[123] AK Gupta and P Redhu. Analysis of a modified two-lane lattice model by considering the density difference effect. *Communications in Nonlinear Science and Numerical Simulation*, 19(5):1600–1610, 2014.

[124] T Nagatani. Jamming transition in a two-dimensional traffic flow model. *Physical Review E*, 59(5):4857–4864, 1999.

[125] TQ Tang, C Li, H Huang, and HY Shang. A new fundamental diagram theory with the individual difference of the driver's perception ability. *Nonlinear Dynamics*, 67(3):2255–2265, 2012.

[126] TQ Tang, J He, SC Yang, and HY Shang. A car-following model accounting for the driver's attribution. *Physica A: Statistical Mechanics and its Applications*, 413:583–591, 2014.

[127] TQ Tang, YP Wang, GZ Yu, and HJ Huang. A stochastic lwr model with consideration of the driver's individual property. *Communications in Theoretical Physics*, 58(4):583–589, 2012.

[128] TQ Tang, HJ Huang, and HY Shang. Influences of the driver's bounded rationality on micro driving behavior, fuel consumption and emissions. *Transportation Research Part D: Transport and Environment*, 41:423–432, 2015.

[129] TQ Tang, XF Luo, and K Liu. Impacts of the driver's bounded rationality on the traffic running cost under the car-following model. *Physica A: Statistical Mechanics and its Applications*, 457:316–321, 2016.

[130] WX Zhu and LD Zhang. Friction coefficient and radius of curvature effects upon traffic flow on a curved road. *Physica A: Statistical Mechanics and its Applications*, 391(20):4597–4605, 2012.

[131] TQ Tang, YP Wang, XB Yang, and YH Wu. A new car-following model accounting for varying road condition. *Nonlinear Dynamics*, 70(2):1397–1405, 2012.

[132] TQ Tang, JG Li, HJ Huang, and XB Yang. A car-following model with real-time road conditions and numerical tests. *Measurement*, 48:63–76, 2014.

[133] TQ Tang, L Caccetta, YH Wu, HJ Huang, and XB Yang. A macro model for traffic flow on road networks with varying road conditions. *Journal of Advanced Transportation*, 48(4):304–317, 2014.

[134] BG Ros, VL Knoop, T Takahashi, I Sakata, BV Arem, and SP Hoogendoorn. Optimization of traffic flow at freeway sags by controlling the acceleration of vehicles equipped with in-car systems. *Transportation Research Part C: Emerging Technologies*, 71:1–18, 2016.

[135] T Nagatani. Dividing traffic cluster into parts by signal control. *Physica A: Statistical Mechanics and its Applications*, 491:463–470, 2018.

[136] LC Edie. Car-following and steady-state theory for noncongested traffic. *Operations Research*, 9(1):66–76, 1961.

[137] GF Newell. Nonlinear effects in the dynamics of car following. *Operations Research*, 9(2):209–229, 1961.

[138] T Wang, Z Gao, XM Zhao, JF Tian, and WY Zhang. Flow difference effect in the two-lane lattice hydrodynamic model. *Chinese Physics B*, 21(7):070507, 2012.

[139] T Nagatani. Jamming transition in traffic flow on triangular lattice. *Physica A: Statistical Mechanics and its Applications*, 271(1-2):200–221, 1999.

[140] P Redhu and AK Gupta. The role of passing in a two-dimensional network. *Nonlinear Dynamics*, 86(1):389–399, 2016.

[141] GH Peng. A new lattice model of traffic flow with the consideration of individual difference of anticipation driving behavior. *Communications in Nonlinear Science and Numerical Simulation*, 18(10):2801–2806, 2013.

[142] XL Li, T Song, H Kuang, and SQ Dai. Phase transition on speed limit traffic with slope. *Chinese Physics B*, 17(8):3014–3020, 2008.

[143] HD He, WZ Lu, Y Xue, and LY Dong. Dynamic characteristics and simulation of traffic flow with slope. *Chinese Physics B*, 18(7):2703–2708, 2009.

[144] K Komada, S Masukura, and T Nagatani. Effect of gravitational force upon traffic flow with gradients. *Physica A: Statistical Mechanics and its Applications*, 388(14):2880–2894, 2009.

[145] S Lan, Y Liu, B Liu, P Sheng, T Wang, and X Li. Effect of slopes in highway on traffic flow. *International Journal of Modern Physics C*, 22(04):319–331, 2011.

[146] WX Zhu and RL Yu. Nonlinear analysis of traffic flow on a gradient highway. *Physica A: Statistical Mechanics and its Applications*, 391(4):954–965, 2012.

[147] J Chen, Z Shi, Y Hu, L Yu, and Y Fang. An extended macroscopic model for traffic flow on a highway with slopes. *International Journal of Modern Physics C*, 24(09):1350061, 2013.

[148] WX Zhu and LD Zhang. A novel lattice traffic flow model and its solitary density waves. *International Journal of Modern Physics C*, 23(03):1250025, 2012.

[149] AK Gupta, S Sharma, and P Redhu. Analyses of lattice traffic flow model on a gradient highway. *Communications in Theoretical Physics*, 62(3):393–404, 2014.

[150] XP Meng and LY Yan. Stability analysis in a curved road traffic flow model based on control theory. *Asian Journal of Control*, 19(5):1844–1853, 2017.

[151] R Kaur and S Sharma. Analysis of drivers characteristics on a curved road in a lattice model. *Physica A: Statistical Mechanics and its Applications*, 471:59–67, 2017.

[152] JF Tian, ZZ Yuan, B Jia, MH Li, and GJ Jiang. The stabilization effect of the density difference in the modified lattice hydrodynamic model of traffic flow. *Physica A: Statistical Mechanics and its Applications*, 391(19):4476–4482, 2012.

[153] GCK Wong and SC Wong. A multi-class traffic flow model–an extension of lwr model with heterogeneous drivers. *Transportation Research Part A: Policy and Practice*, 36(9):827–841, 2002.

[154] HM Zhang and W Jin. Kinematic wave traffic flow model for mixed traffic. *Transportation Research Record: Journal of the Transportation Research Board*, (1802):197–204, 2002.

[155] CF Tang, R Jiang, QS Wu, B Wiwatanapataphee, and YH Wu. Mixed traffic flow in anisotropic continuum model. *Transportation Research Record*, 1999(1):13–22, 2007.

[156] TQ Tang, HJ Huang, SG Zhao, and HY Shang. A new dynamic model for heterogeneous traffic flow. *Physics Letters A*, 373(29):2461–2466, 2009.

[157] AD Mason and AW Woods. Car-following model of multispecies systems of road traffic. *Physical Review E*, 55(3):2203–2214, 1997.

[158] Z Li, X Xu, S Xu, and Y Qian. A heterogeneous traffic flow model consisting of two types of vehicles with different sensitivities. *Communications in Nonlinear Science and Numerical Simulation*, 42:132–145, 2017.

[159] E Ott, C Grebogi, and JA Yorke. Controling chaos. *Physical Review Letters*, 64(11):1196–1199, 1990.

[160] K Pyragas. Continuous control of chaos by self-controlling feedback. *Physics Letters A*, 170(6):421–428, 1992.

[161] W Just, T Bernard, M Ostheimer, E Reibold, and H Benner. Mechanism of time-delayed feedback control. *Physical Review Letters*, 78(2):203–206, 1997.

[162] K Konishi, H Kokame, and K Hirata. Coupled map car-following model and its delayed-feedback control. *Physical Review E*, 60(4):4000–4007, 1999.

[163] K Konishi, H Kokame, and K Hirata. Decentralized delayed-feedback control of an optimal velocity traffic model. *The European Physical Journal B-Condensed Matter and Complex Systems*, 15(4):715–722, 2000.

[164] X Zhao and Z Gao. Controlling traffic jams by a feedback signal. *The European Physical Journal B-Condensed Matter and Complex Systems*, 43(4):565–572, 2005.

[165] X Zhao and Z Gao. A control method for congested traffic induced by bottlenecks in the coupled map car-following model. *Physica A: Statistical Mechanics and its Applications*, 366:513–522, 2006.

[166] Y Jin and H Hu. Stabilization of traffic flow in optimal velocity model via delayed-feedback control. *Communications in Nonlinear Science and Numerical Simulation*, 18(4):1027–1034, 2013.

[167] ZH Ou, SQ Dai, P Zhang, and LY Dong. Nonlinear analysis in the aw–rascle anticipation model of traffic flow. *SIAM Journal on Applied Mathematics*, 67(3):605–618, 2007.

[168] TQ Tang, Q Yu, SC Yang, and C Ding. Impacts of the vehicle's fuel consumption and exhaust emissions on the trip cost allowing late arrival under car-following model. *Physica A: Statistical Mechanics and its Applications*, 431:52–62, 2015.

[169] TQ Tang, ZY Yi, and QF Lin. Effects of signal light on the fuel consumption and emissions under car-following model. *Physica A: Statistical Mechanics and its Applications*, 469:200–205, 2017.

[170] JF Tian, B Jia, XG Li, and Z Gao. Flow difference effect in the lattice hydrodynamic model. *Chinese Physics B*, 19(4):040303, 2010.

[171] C Tian, DH Sun, and M Zhang. Nonlinear analysis of lattice model with consideration of optimal current difference. *Communications in Nonlinear Science and Numerical Simulation*, 16(11):4524–4529, 2011.

[172] DH Sun, M Zhang, and T Chuan. Multiple optimal current difference effect in the lattice traffic flow model. *Modern Physics Letters B*, 28(11):1450091, 2014.

[173] M Zhao, DH Sun, and C Tian. Density waves in a lattice hydrodynamic traffic flow model with the anticipation effect. *Chinese Physics B*, 21(4):048901, 2012.

[174] Y Li, L Zhang, T Zheng, and Y Li. Lattice hydrodynamic model based delay feedback control of vehicular traffic flow considering the effects of density change rate difference. *Communications in Nonlinear Science and Numerical Simulation*, 29(1-3):224–232, 2015.

[175] C Zhu, S Zhong, G Li, and S Ma. New control strategy for the lattice hydrodynamic model of traffic flow. *Physica A: Statistical Mechanics and its Applications*, 468:445–453, 2017.

[176] Y Wang, R Cheng, and H Ge. A lattice hydrodynamic model based on delayed feedback control considering the effect of flow rate difference. *Physica A: Statistical Mechanics and its Applications*, 479:478–484, 2017.

[177] Y Wang, H Ge, and R Cheng. An improved lattice hydrodynamic model considering the influence of optimal flux for forward looking sites. *Physics Letters A*, 381(41):3523–3528, 2017.

[178] O Biham, AA Middleton, and D Levine. Self-organization and a dynamical transition in traffic-flow models. *Physical Review A*, 46(10):R6124–R6127, 1992.

[179] T Nagatani. Jamming transition in the traffic-flow model with two-level crossings. *Physical Review E*, 48(5):3290–3294, 1993.

[180] JA Cuesta, FC Martínez, JM Molera, and A Sánchez. Phase transitions in two-dimensional traffic-flow models. *Physical Review E*, 48(6):R4175–R4178, 1993.

[181] K Brauer. The korteweg-de vries equation: history, exact solutions, and graphical representation. *University of Osnabrück/Germany1*, 2000.

Appendix

Calculation for solution of mKdV equation

The mKdV equation is given by:

$$\partial_T R - \partial_X^3 R + 3R^2 \partial_X R = 0, \tag{7.2.1}$$

Let us consider a wave solution of the following form:

$$R(X,T) = Z(X - L_1 T) = Z(\xi), \tag{7.2.2}$$

where $\xi = X - L_1 T$ and L_1 is the propagation speed of the wave. After substituting equation (7.2.2) into (7.2.1) we obtain following ordinary differential equation:

$$-L_1 \frac{dZ}{d\xi} - \frac{d^3 Z}{d\xi^3} + 3Z^2 \frac{dZ}{d\xi} = 0. \tag{7.2.3}$$

By integration with respect to ξ we obtain following equation:

$$-\text{Ł}_1 Z - \frac{d^2 Z}{d\xi^2} + Z^3 = O_1, \tag{7.2.4}$$

where O_1 is the constant of integration. As $\xi \to \pm\infty$, $Z \to 0$, $\frac{dZ}{d\xi} \to 0$, $\frac{d^2 Z}{d\xi^2} \to 0$ which implies $O_1 = 0$ (see [181]) and (7.2.4) can be written as:

$$-\text{Ł}_1 Z - \frac{d^2 Z}{d\xi^2} + Z^3 = 0. \tag{7.2.5}$$

Again by integrating (7.2.5) we obtain:

$$-\text{Ł}_1 \frac{Z^2}{2} - \frac{1}{2}\left(\frac{dZ}{d\xi}\right)^2 + \frac{Z^4}{4} = O_2, \tag{7.2.6}$$

where O_2 is a constant of integration and take the value 0 because of the same reason given above. Thus (7.2.6) can be rewritten as:

$$-\text{Ł}_1 \frac{Z^2}{2} - \frac{1}{2}\left(\frac{dZ}{d\xi}\right)^2 + \frac{Z^4}{4} = 0. \tag{7.2.7}$$

By solving (7.2.7) we obtain:

$$d\xi = \sqrt{2} \frac{dZ}{Z\sqrt{Z^2 - 2L_1}}. \tag{7.2.8}$$

After simplification we get:

$$R(X,T) = \sqrt{2L_1}\tanh\Big(\sqrt{\frac{L_1}{2}}(X - 2L_1T)\Big), \tag{7.2.9}$$

which is the solution of mKdV equation.